12-2009

Relative Performance Comparison and Loss Estimation of Seismically Isolated and Fixed-based Buildings Using PBEE Approach

Prayag J. Sayani
Utah State University

RELATIVE PERFORMANCE COMPARISON AND LOSS ESTIMATION OF SEISMICALLY ISOLATED AND FIXED-BASED BUILDINGS USING PBEE APPROACH

by

Prayag J. Sayani

A dissertation submitted in partial fulfillment
of the requirements for the degree

of

DOCTOR OF PHILOSOPHY

in

Civil and Environmental Engineering

Approved:

Dr. Keri Ryan Major Professor	Dr. Marvin Halling Committee Member
Dr. Paul Barr Committee Member	Dr. James Bay Committee Member
Dr. Wenbin Yu Committee Member	Dr. Byron Burnham Dean of Graduate Studies

UTAH STATE UNIVERSITY
Logan, Utah

2009

ABSTRACT

Relative Performance Comparison and Loss Estimation of Seismically Isolated and Fixed-based Buildings Using PBEE Approach

by

Prayag J. Sayani, Doctor of Philosophy
Utah State University, 2009

Major Professor: Dr. Keri L. Ryan
Department: Civil and Environmental Engineering

Current design codes generally use an equivalent linear approach for preliminary design of a seismic isolation system. The equivalent linear approach is based on effective parameters, rather than physical parameters of the system, and may not accurately account for the nonlinearity of the isolation system. The second chapter evaluates an alternative normalized strength characterization against the equivalent linear characterization. Following considerations for evaluation are included: (1) ability to effectively account for variations in ground motion intensity, (2) ability to effectively describe the energy dissipation capacity of the isolation system, and (3) conducive to developing design equations that can be implemented within a code framework.

Although current code guidelines specify different seismic performance objectives for fixed-base and isolated buildings, the future of performance-based design will allow user-selected performance objectives, motivating the need for a consistent performance comparison of the two systems. Based on response history analysis to a suite of motions, constant ductility spectra are generated for fixed-base and isolated buildings

in chapter three. Both superstructure force (base shear) and deformation demands in base-isolated buildings are lower than in fixed-base buildings responding with identical deformation ductility. To compare the relative performance of many systems or to predict the best system to achieve a given performance objective, a response index is developed and used for rapid prototyping of response as a function of system characteristics. When evaluated for a life safety performance objective, the superstructure design base shear of an isolated building is competitive with that of a fixed-base building with identical ductility, and the isolated building generally has improved response. Isolated buildings can meet a moderate ductility immediate-occupancy objective at low design strengths whereas comparable ductility fixed-base buildings fail to meet the objective.

In chapter four and five, the life cycle performance of code-designed conventional and base-isolated steel frame buildings is evaluated using loss estimation methodologies. The results of hazard and structural response analysis for three-story moment resisting frame buildings are presented in this paper. Three-dimensional models for both buildings are created and seismic response is assessed for three scenario earthquakes. The response history analysis results indicate that the performance of the isolated building is superior to the conventional building in the design event. However, for the Maximum Considered Earthquake, the presence of outliers in the response data reduces confidence that the isolated building provides superior performance to its conventional counterpart. The outliers observed in the response of the isolated building are disconcerting and need careful evaluation in future studies.

(168 pages)

DEDICATION

To my parents

Jagdish N. Sayani and Sarla J. Sayani

and

my loving wife

Reena M. Patel

ACKNOWLEDGMENTS

I would like to express my deep appreciation to my advisor, Professor Keri Ryan, for her encouragement and support throughout the years and for giving me the opportunity to work under her supervision. Working under your supervision was always an inspiration and honor. I must say that I am going to miss the long hour meetings that we had almost every week and the motivation that you have provided me over the years. Professor Ryan, you have taught me to be a good researcher. “Thank you” for everything.

I would also like to express my appreciation to my committee members, Professors Marvin Halling, Paul Barr, James Bay, and Wenbin Yu, for providing assistance through the entire process. Special thanks to Dr. Troy Morgan for providing us design of the buildings and for reading the manuscript. I also wish to thank Professor Stephen Mahin for contributing his technical expertise and offering feedback on the study. Many thanks to Professor Judith Mitrani Reiser who made my stay at Johns Hopkins University very pleasant and provided me valuable assistance for my research.

I would like to acknowledge the National Science Foundation (Grant Number CMMI-0724208) and Utah State University for their financial support for this research. I would also like to especially thank the Graduate Student Senate at Utah State University for providing me travel grants and the Enhancement award, which made my life lot better. I also thank fellow students and colleagues at USU for their help and support. Special thanks to fellow Indian students and dear friends Anurag Srivastava, Prabuddha Ghosh, and Rachna Gollamudi for all their help and great moments that we had. I wish to

thank my dear friends Rushikesh Trivedi, and Gaurang Shah for their support and love all these years.

I would like to specially thank my parents for their unconditional love and support throughout the years. I am truly grateful for the sacrifices they made in their lives to give me the best possible education. I am blessed to have them. I would like to express my deepest gratitude to my best friend, my wife Reena Patel, for being with me at every step of my life and for making me smile every day. Thank you for your true love and support for all these years.

Prayag Sayani

CONTENTS

LIST OF TABLES

LIST OF FIGURES

CHAPTER 1

INTRODUCTION

The principal benefit of seismic isolation for buildings, to offer far superior performance in a design level earthquake, is generally accepted and recognized by structural engineers. With seismic isolation, flexible devices installed at the base lengthen or shift the building's natural period to the low acceleration region of the spectrum. Consequently, an isolated building accommodates the lower design forces elastically, and structural damage is eliminated or greatly reduced relative to a conventional building that accommodates the design forces through inelastic response. However, only 10-20% of the value in a typical U.S. building is apportioned to the structural system, while at least 80% is apportioned to nonstructural components and building contents. Post-earthquake observations suggest that on average, losses in nonstructural components far outweigh the costs of damage to structural elements. Fortunately, lower accelerations experienced in isolated buildings lead to greatly reduced damage in acceleration-sensitive nonstructural components.

The seismic performance objectives implicit in U.S. building codes currently differ for conventional (fixed-base) and base-isolated buildings. As an example, conventional buildings are permitted a force reduction factor R of up to 8, which may allow significant inelastic action in the design basis earthquake and can be interpreted as a "life safety" performance objective. Likewise, isolated buildings are limited to R factors no larger than 2, and remain essentially elastic due to overstrength. The reduced R factor, together with other requirements, may be interpreted as seeking a performance objective

more comparable to “immediate occupancy” or “operational”. Consequently, the superstructure design forces in an isolated building are sometimes larger than in a comparable conventional building. If fixed-base and isolated buildings are compared relative to a consistent performance objective (life safety or continued occupancy), the cost-competitiveness of base isolation may be improved relative to conventional design.

In the U.S., seismic performance objectives, which differ for isolated and conventional systems, are only implicitly embedded in code design standards, and the performance benefits generally are not recognized by building owners and decision makers. The business culture cultivates an emphasis on initial rather than lifetime costs of structural systems. Design performance objectives are rarely discussed with stakeholders, and a typical building owner expects that a code compliant building will retain operability following an earthquake. Even sophisticated owners that initially require or are convinced to choose higher performance are constrained by initial costs. When faced with additional complexities of seismic isolation design, such as analysis procedures, involved device testing requirements, and a lengthy design review process, these owners, in consultation with design professionals, often opt for alternative systems. As a result, seismic isolation has become an expensive technology that in the U.S. and is adopted only for continued operation of essential facilities such as hospitals, emergency response units, and supercomputing centers; or preservation of historical buildings. However, seismic isolation has the potential to be routinely adopted if reliable analysis tools are available to predict economic outcomes, and cultural transformation leads to routine discussion of lifetime economics as a basis for making design decisions.

The objective of the present study is to develop a methodology to systematically

evaluate relative performance of conventional and base-isolated buildings as measured by engineering demand parameters. To compare the relative performance of multiple systems, including conventional and base-isolated buildings, a response index (RI) is developed. The methodology can be used as desired; e.g., to identify the best performing system, to identify the minimum system that meets the performance objective, or to identify a desirable combination of performance and strength. In this study, analysis is restricted to single story (i.e. single degree-of-freedom or SDF) structures with and without an isolation system subjected to a suite of 20 ground motions. Within this scope, the methodology is used to rapidly prototype the response of buildings based on key characteristics such as natural vibration period and design base shear.

Most recently, performance-based seismic design approaches are under development and attracting great interest in the U.S. Performance-based engineering allows owner-selected performance objectives for the structural and non structural building components considering specific seismic events or the aggregate hazard. The new approach, developed by Pacific Earthquake Engineering Research Center (PEER) specifies performance in terms of probabilistic losses (casualties, repair costs, downtime). The consequence analysis is deconstructed into four basic stages: hazard analysis to determine ground motion intensity, structural response analysis to determine engineering demand parameters, damage analysis to determine damage indicators, and loss analysis to determine the decision variables. Considering the intermediate variables at each stage to be discrete random variables, the analyses are combined by integration over each random variable to determine the expected annual losses according to the total probability theorem. The development of fragility and loss functions, which relate losses to

traditional response measures, is an ongoing process. When performance-based engineering matures, designers will be able to employ the latest design and analysis techniques to create efficient designs that meet specified performance objectives, and building owners will be able to comparatively evaluate base isolation and conventional design with reference to a quantitative performance objective.

To our knowledge, conventional and seismic-isolated buildings thus far have not been comparatively evaluated using the PEER loss estimation methodology. The focus of this study is to comparatively evaluate the life cycle performance of code-designed 3-story conventional and base-isolated steel moment resisting frame buildings using the PEER loss estimation methodology. The overall cost versus benefit of seismic isolation will be analyzed through comparison of initial design costs and expected economic losses (repair costs, downtime, etc.) over the life of the buildings. A moment frame has been selected to address whether a similar benefit can be provided by applying isolation to a relatively flexible lateral system compared to an ideal stiff system.

A total probabilistic evaluation of performance inevitably involves the consideration of a wide range of ground motion intensities, including low probability events that exceed the design ground motion. Yielding of the isolated superstructure in extreme events is likely. A key observation is that an isolated structure, upon yielding, accumulates ductility in the superstructure more quickly than a comparable conventional building, and thus the drift demand in the isolated superstructure can in fact be greater than in a comparable conventional building.

CHAPTER 2

EVALUATION OF APPROACHES TO CHARACTERIZE SEISMIC ISOLATION SYSTEMS FOR DESIGN

Abstract

Current design codes generally use an equivalent linear approach for preliminary design of a seismic isolation system. The equivalent linear approach is based on effective parameters, rather than physical parameters of the system, and may not accurately account for the nonlinearity of the isolation system. This paper evaluates an alternative normalized strength characterization against the equivalent linear characterization. Following considerations for evaluation are included: (1) ability to effectively account for variations in ground motion intensity, (2) ability to effectively describe the energy dissipation capacity of the isolation system, and (3) conducive to developing design equations that can be implemented within a code framework.

1. Introduction

Structural design codes such as the International Building Code [ICC, 2006] and ASCE 7-05 [ASCE, 2005] regulate the design of buildings incorporating seismic base isolation systems. The code guidelines allow analysis of the isolated building system by several procedures: the equivalent lateral force method, response spectrum analysis and nonlinear response history analysis. While use of the equivalent lateral force method (i.e. static analysis) for final design has been limited by the codes to a narrow class of structures, static analysis is the logical starting point for the conceptual design phase, and furthermore, the codes require that the response determined from an acceptable dynamic

analysis procedure does not fall below limits determined by static analysis. Thus, accessibility to static equations that can simply and accurately predict important response parameters, such as the deformation demand of the isolation system, is a critical aspect of design.

While isolation devices are available that respond with essentially linear force-deformation behavior (i.e. natural rubber bearings), a typical isolation system utilizes at least one type of device that economically combines flexibility and hysteretic energy dissipation in one compact unit. Examples are lead-rubber bearings, where the energy is dissipated by plastic flow of the lead core, and friction pendulum isolators, where energy is dissipated by sliding on a curved frictional surface. Such devices have significant nonlinearity in their force-deformation relations.

Current codes employ an equivalent linear approach to estimate the deformation demand, or "design displacement" of the isolation system and the design base shear of the structure above. The design values are given by the spectral response using the equivalent linear system properties: effective stiffness (or effective period) and effective damping ratio. Determining the spectral response is an iterative procedure if the specifications of the isolation system are known, whereby initial guesses for the effective period and damping ratio are updated as the design displacement is re-computed at each iteration. Alternatively, the isolation system can be designed for target effective properties and design displacement. The equivalent linear approach conveniently relies on a linear design spectrum with which practitioners are very familiar. However, the equivalent linear properties cannot be related to physical parameters of the isolation

system, and an equivalent linear approach may not accurately represent the typical nonlinear response behavior of isolation devices.

The accuracy of equivalent-linear systems to estimate seismic demands has been documented for general nonlinear systems [Chopra and Goel, 2000; Fajfar, 1999] and specifically for isolation systems [Anderson and Mahin, 1998; Dicleli and Buddaram, 2007; Franchin *et al.*, 2001; Hwang, 1996]. To account for observed inaccuracies in equivalent linear methods for isolation systems, modifications to the effective damping ratio have been proposed [Dicleli and Buddaram, 2006; Hwang *et al.*, 1995; Jara and Casas, 2006; Weitzmann *et al.*, 2006]. Because the equivalent linear approach cannot characterize the isolation system based on its physical parameters, often requires iteration, and potentially suffers from inaccuracy, other approaches to estimate the deformation demand of the isolation system are worth investigation.

Nonlinear response spectrum concepts may be applicable to describe the peak response of a nonlinear system to a given ground acceleration. For instance, relations between the response of a nonlinear single degree-of-freedom (SDOF) system and its corresponding linear system – a system with the same stiffness that remains linear – have been developed in terms of strength (force reduction factor) and ductility. This approach is ineffective for isolation systems because the initial stiffness is not a meaningful parameter of a typical isolation device. Thus, application of nonlinear response spectrum to isolation systems requires selection of appropriate physical parameters to characterize the nonlinear devices. Accounting for ground motion intensity is also important since, unlike a linear system, the peak response does not scale linearly with the intensity of the ground motion.

Several researchers have explored the application of nonlinear response spectrum approaches for isolation systems [Park and Otsuka, 1999; Ryan and Chopra, 2004; Tena-Colunga, 2002; Zhao and Zhang, 2004]. Ryan and Chopra [2004] developed an approach that characterizes the isolation system according to the period corresponding to its post-yield stiffness and the yield strength normalized by peak ground velocity. The procedure was shown to lead to a simple estimate of the peak deformation demand, as well as minimize the statistical variation of the normalized deformation, which was hypothesized to be independent of ground motion intensity and has a simple relation to the actual deformation. As a drawback, the normalized strength is not an effective measure of the energy dissipation capacity of the system. In Park and Otsuka [1999], a method was developed to determine the optimum yield strength of an isolation system based on the absorbed energy and total input energy to the system, which is dependent on ground motion intensity.

The objective of the present study is to comparatively evaluate different approaches to characterize and estimate the deformation demands of a nonlinear isolation system. The approaches are evaluated against three criteria: inherent ability to account for scaling effects of ground motion intensity, existence of a parameter that effectively describes the energy dissipation capacity of the isolation system, and ease in converting the nonlinear response spectra observed for individual motions to simplified design equations or design spectra. Modifications to both the normalized strength characterization [Ryan and Chopra, 2004] and the equivalent linear system characterization are proposed to address deficiencies in meeting the above criteria.

2. System and Governing Equation

2.1. System Considered

The system considered here is a single degree-of-freedom (SDOF) system with a rigid mass mounted on a single isolator, representative of a single story structure on isolators [Fig. 2.1(a)]. The mass m represents the total mass above the isolation system, including both structure mass and additional base mass. The lateral force-deformation relationship of the isolation system is idealized as bilinear, characterized by the post yield stiffness kb, the yield strength Q, and either the initial stiffness ki or yield deformation uy (= 1 cm in this study) [Fig. 2.1(b)]. The lateral force f_b in the isolation system is determined from

$$f_b = k_b u_b + Qz \tag{1}$$

where u_b is the isolator deformation and z is the fraction of the yield strength applied. The function z, which depends on the initial stiffness, deformation, and velocity, equals ±1 on the upper and a lower bounding surface – dashed lines in Fig. 2.1(b) – and varies linearly between these bounding surfaces.

The amplitude dependent effective stiffness and damping are generally characterized according to the peak response of the isolation system. The effective stiffness is the secant stiffness with respect to the peak values of isolator force f_{bo} and deformation u_{bo}, given by:

$$k_{eff} = \frac{f_{bo}}{u_{bo}} \tag{2}$$

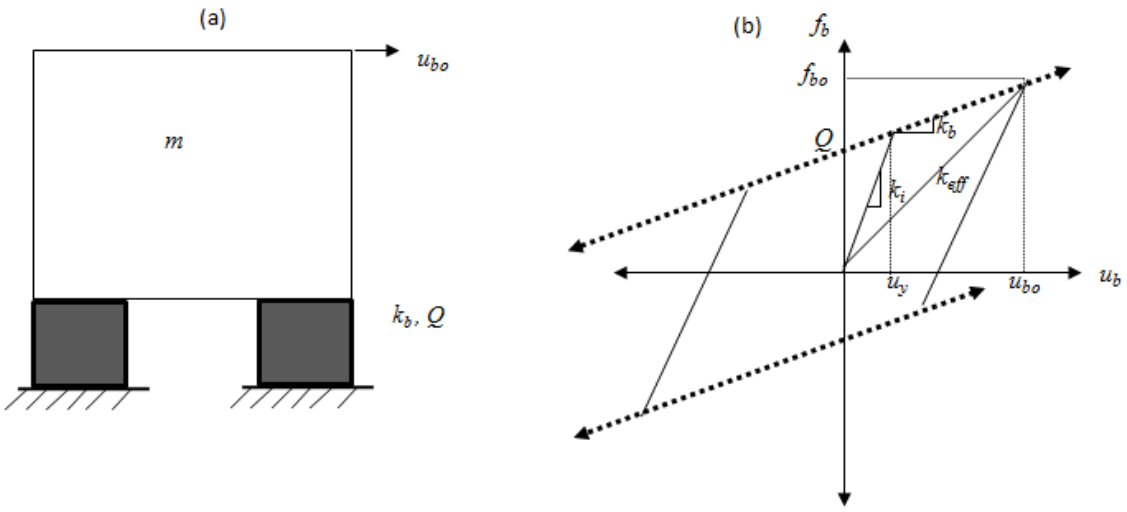

FIGURE 2.1 (a) Single-DOF isolated structure and (b) lateral force–deformation of the isolation system.

The effective period T_{eff} is related to the effective stiffness by $T_{eff} = 2\pi\sqrt{m/k_{eff}}$. The effective damping ratio is determined by equating the hysteretic energy dissipated in a complete cycle at deformation u_{bo} (equivalent to the area enclosed by a complete loop) with the energy dissipated in viscous damping:

$$\zeta_{eff} = \frac{Q\left(u_{bo} - u_y\right)}{\frac{\pi}{2} k_{eff} {u_{bo}}^2} \tag{3}$$

2.2. Equation of Motion

The governing differential equation, or equation of motion, of the rigid mass supported on a single isolator and subjected to a ground acceleration history $\ddot{u}_g(t)$, is given by summing the inertial force and the restoring force of the isolator:

$$\ddot{u}_b(t) + \omega_b^2 u_b(t) + \mu g z(t, k_1, u_b, \dot{u}_b) = -\ddot{u}_g(t) \tag{4}$$

Equation 1 has been divided through by *m*, where $\omega_b = \sqrt{k_b/m}$ is the isolation frequency – or frequency of the structure vibrating in the post-yield range, and $\mu = Q/w$ is the characteristic strength ratio, which quantifies the strength of the system relative to the structure weight *w*. The isolation period $T_b = 2\pi/\omega_b$ may be used in lieu of the isolation frequency.

2.3. Ground Motion Ensembles

The different ground motion ensembles selected for response history analysis in this study are described. The Large Magnitude Small Distance (LMSR) ensemble, described in previous studies by the authors [Ryan and Chopra, 2004], consists of twenty single component motions recorded from four California earthquakes, representative of ground shaking relatively close to fault rupture during a large magnitude earthquake. In addition, several ensembles are selected that were developed originally for the SAC steel project and have been widely used by the structural engineering community [Somerville *et al*., 1998]. These ground motion ensembles represent events with various probability of occurrence at several locations (Los Angeles, Seattle, and Boston) and occurring on firm soil conditions. Selected for this study are the ensembles representing a 2 % in 50 year event, 10 % in 50 year event, and 50 % in 50 year event in Los Angeles as well as a 10 % in 50 year event for Seattle, referred to hereafter as the LA 2 in 50, 10 in 50, 50 in 50 and Seattle 10 in 50 ensembles. Each of the SAC ensembles consists of 10 pairs of orthogonal motions, of which all 20 components are singly applied in this study. The median acceleration spectrum for each ensemble is shown in Fig. 2.2. The selected

ensembles are intended to be representative of broad-frequency band excitation recorded in the non-near field region of the earthquake.

3. Alternative Characterizations of the Isolation System

As discussed earlier, two general approaches are available to develop meaningful parameters to characterize the isolation system for design. The first approach uses an effective natural period and damping ratio, such that the response of the system can be quantified using a linear response or design spectrum. The effective properties depend on the peak response amplitude, such that iteration may be required and the effective parameters have no relation to physically meaningful parameters of the system.

The second approach uses some obtainable properties of the nonlinear isolation system, such as the isolation frequency ω_b (corresponding to the post-yield stiffness k_b) and the characteristic strength μ. Both of these parameters appear in the equation of motion [Eq. (1)] and are physically meaningful parameters of the isolation system. The post-yield stiffness corresponds to the stiffness of rubber in a lead-rubber bearing and is related to the radius of curvature of a friction pendulum isolator. The characteristic strength corresponds to the strength of the lead core in a lead-rubber bearing or to the friction coefficient of the sliding surface of a friction pendulum isolator. Variations of the two approaches are compared next.

3.1. Characterization by Strength Normalization

A linear system leads to a linear relation between system response and ground motion intensity.

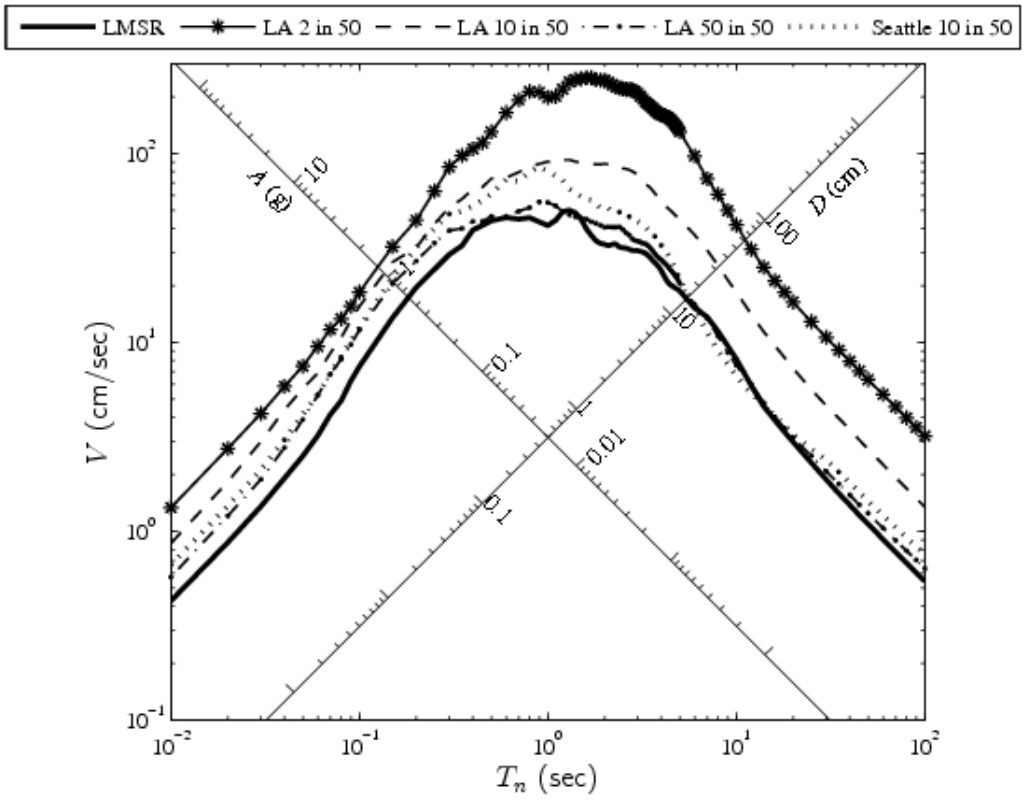

FIGURE 2.2 5% damped median response spectra (4-way log format) for LMSR, LA 2 in 50, LA 10 in 50, LA 50 in 50 and Seattle 10 in 50 ground motion ensembles.

The same cannot be said of a nonlinear system, and in fact the response of a nonlinear system may vary widely with ground motion intensity, and cannot be predicted accurately by a linear design spectrum using only the nonlinear parameters.In this sense, the ground acceleration intensity is an additional parameter that significantly influences the response.

Ryan and Chopra [2004] developed an approach to decrease the effect of intensity. In this approach, the equation of motion is rewritten in terms of a deformation independent normalized deformation, and the physical strength parameter μ is replaced

by a normalized strength. The derivation is briefly outlined as follows. Let $a_y^* = Q/m = \mu g$, equal to the acceleration at yield of a rigid system with strength Q, and

$$u_y^* = \frac{Q}{k_b} = \frac{a_y^*}{\omega_b^2} \tag{5}$$

is a fictitious yield displacement. Dividing Eq. (4) by u_y^* leads to

$$\ddot{\bar{u}}_b + \omega_b^2 \bar{u}_b + \omega_b^2 z = -\omega_b^2 \frac{\ddot{u}_g}{a_y^*} \tag{6}$$

where $\bar{u}_b = u_b / u_y^*$ is the normalized deformation of the system. The normalized strength η is defined as:

$$\eta = \frac{a_y^*}{\omega_d \dot{u}_{go}} \tag{7}$$

where the frequency ω_d corresponds to the period T_d marking the transition from the velocity-sensitive to the displacement-sensitive region of the response or design spectrum, and $\dot{u}_{go}$ is the peak ground velocity (PGV). Incorporating η into the equation of motion [Eq. (6)] results in

$$\ddot{\bar{u}}_b + \omega_b^2 \bar{u}_b + \omega_b^2 z = -\frac{\omega_b^2}{\eta \omega_d} \ddot{\bar{u}}_g \tag{8}$$

where $\ddot{\bar{u}}_g = \ddot{u}_g / \dot{u}_{go}$. That is, the acceleration has been normalized by PGV, and thus the normalized deformation $\bar{u}_b$ is essentially independent of ground motion intensity.

Ryan and Chopra [2004] asserted that normalizing the equation of motion eliminated the effect of ground motion intensity, and limited the variability in normalized deformation to that of a random process. Thus, normalized deformation could be predicted based on only two parameters, isolation period T_b and normalized strength η.

The normalization technique was shown to be effective because the dispersion of the normalized deformation was less than the dispersion of the actual deformation.

However, we make the following observations about this previously proposed normalization technique: (1) selection of PGV as a measure of ground motion intensity is not ideal since the PGV is typically unknown and cannot be determined from a design spectrum; (2) use of the corner frequency ω_d [Eq. (7)], characteristic of isolation systems responding in the medium to long period range, was expected to minimize the discrepancy in response between different ground motion ensembles, but instead contributes to the discrepancy between different ensembles; (3) the normalized strength replaces the familiar damping ratio as a measure of the energy dissipation capacity of the isolation system. To understand the relation between effective damping and normalized strength, the effective damping ratio ζ_{eff} corresponding to different values of normalized strength η is plotted in Fig. 2.3. Here, ζ_{eff} was calculated according to Eq. (3), taking u_{bo} as the median peak deformation of a system with given T_b and η, determined by nonlinear response history analysis of the system to the LMSR ensemble of motions. The observed effective damping ratio as a function of η varies widely across the period range T_b (Fig. 2.3). As a result, the applicable range of η needed to achieve consistent energy dissipation depends on period, making it difficult to select values of η for design. In an attempt to improve the normalization procedure, the next section evaluates alternative definitions for the normalized strength.

3.2. Alternative Normalized Strength Definitions

As a general framework, the following definition of normalized strength is proposed

$$\eta = \frac{a_y^*}{\omega_b I} = \frac{Q}{m\omega_b I} \tag{9}$$

where ω_b has replaced ω_d and the general intensity measure I has replaced $\dot{u}_{go}$ in Eq. (7).

Using the frequency dependent ω_b instead of the fixed value of ω_d will allow the yield strength Q to vary with the isolation frequency for a given normalized strength, which is hypothesized to eliminate the observed variation of effective damping across the period range (Fig. 2.3).

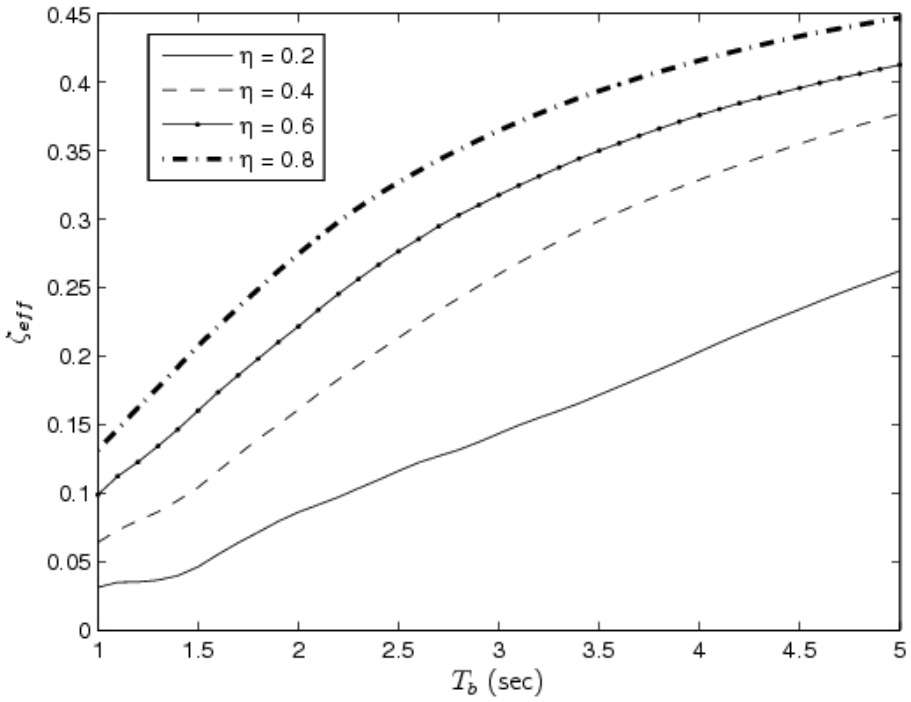

FIGURE 2.3 Observed effective damping ratio ζ_{eff} as a function of normalized strength η for the LMSR.

The following measures are considered for intensity I: (1) PGV $\dot{u}_{go}$, (2) spectral velocity (SV) V obtained from the 5% damped response spectrum, and (3) peak ground displacement (PGD) u_{go}. For the third alternative, $I=\omega_b u_{go}$ such that the normalized strength remains a dimensionless parameter. SV is an attractive alternative for intensity because it can be determined directly from a code design spectrum. PGD may also be a suitable measure of intensity for the increasingly longer period isolation systems that are becoming prevalent in design. Incorporating η from Eq. 9 into the normalized equation of motion [Eq. (6)] results in

$$\ddot{\bar{u}}_{bo} + \omega_b^{\,2}\bar{u}_{bo} + \omega_b^{\,2} z(u_{bo}, \dot{u}_{bo}) = -\omega_b \frac{\ddot{u}_g}{\eta I} \tag{10}$$

The effectiveness of the alternative normalized strength definitions will be assessed, along with parameter characterizations based on the equivalent linear system approach as defined in the next section, according to common criteria.

3.3. Characterization by Equivalent Linear Properties

As discussed previously, the effective stiffness (or effective period) and effective damping ratio depend on the response amplitude. For a given isolation system and ground motion intensity, the effective parameters can be estimated based on the design spectrum. If the isolation system parameters (strength Q and post yield stiffness k_b) are known, the effective parameters are determined from Eqs. (2) and (3) with u_{bo} = design displacement D_D from the design spectrum. Note, however, that this procedure is iterative because of the circular relation between D_D and effective parameters T_{eff} and ζ_{eff} (D_D depends on T_{eff} and ζ_{eff} while T_{eff} and ζ_{eff} depend on D_D). Alternatively, if target values of T_{eff} and ζ_{eff} are

assumed, such as may be done for preliminary design, target values of Q and k_b may be computed by inverting Eqs. (2) and (3) to get:

$$Q = \frac{\frac{\pi}{2} k_{eff} \zeta_{eff} D_D^2}{(D_D - u_y)} \tag{11a}$$

$$k_b = k_{eff} - \frac{Q}{D_D} \tag{11b}$$

While the effective properties can be estimated from the spectral displacement (SD) D_D, the observed peak deformation u_{bo} of the system subjected to ground motions scaled to the design spectrum will deviate from D_D due to the nonlinearity of the isolation system. To draw analogy to the normalization approach from earlier, D_D is hypothesized to be an indirect measure of ground motion intensity. Furthermore, the ratio of nonlinear deformation to design displacement, or deformation ratio $\hat{u}_{bo}$, defined as

$$\hat{u}_{bo} = \frac{u_{bo}}{D_D} \tag{12}$$

is analogous to the normalized deformation $\bar{u}_{bo}$ defined for the strength normalization approach. Since D_D includes intensity information and is determined directly from a design spectrum, a design deformation u_{bo} that accounts for the system nonlinearity can be determined from D_D and u_{bo} based on statistical trends for the deformation ratio $\hat{u}_{bo}$.

4. Evaluation of Alternative System Characterization Approaches

The alternative isolation system characterizations proposed previously are evaluated objectively based on three desirable traits: (1) the ground motion intensity measure successfully represents the variation in response to different ground motions

such that the corresponding normalized response parameter (normalized deformation $\overline{u}_{bo}$ or deformation ratio $\hat{u}_{bo}$) is much less dependent on intensity, (2) the system characterization includes a parameter that effectively describes the energy dissipation capacity of the isolation system, and (3) simplified equations can be developed to predict the peak deformation of the isolation system that can easily be implemented within a design code framework.

4.1 Intensity Measures and Response Dispersion

Dispersion in response is evaluated for the system characterization approaches presented earlier, including the alternative normalized strength characterizations and the equivalent linear characterization. For the normalized strength alternative [Eq. (9)], the three proposed ground motion intensity measures – PGV $\dot{u}_{go}$, SV V, and PGD u_{go} – are each evaluated independently. The characterizations are considered to be effective if the normalized deformation $\overline{u}_{bo}$ or deformation ratio $\hat{u}_{bo}$ [Eq. (12)] is effectively independent of intensity, that is, the observed dispersion in response is reduced compared to the dispersion of the actual deformation. Although the dispersion in response of a system that is totally insensitive to intensity is zero, some dispersion is expected due to inherent variability in the ground motion records.

The general evaluation procedure is described as follows. The median $\tilde{x}$ and dispersion δ of the peak response x over a given ensemble are evaluated according to:

$$\tilde{x} = \exp\left[\frac{\sum_{i=1}^{n} \ln x_i}{n}\right] \qquad \delta = \left[\frac{\sum_{i=1}^{n} \left(\ln x_i - \ln \tilde{x}\right)^2}{n-1}\right]^{1/2} \tag{13}$$

where n is the number of motions in the ensemble. Each observation x_i is the peak response determined by nonlinear response history analysis of the system to a single ground motion in the given ensemble. The dispersion δ in response for each of the alternative characterizations considered is reported separately for the LMSR ensemble, and for the SAC Master ensemble, which is a compilation of the four individual SAC ensembles selected for this study. From preliminary analysis, the dispersion in ground motion intensity was observed to be much smaller for any individual SAC ensembles than for LMSR ensemble. In other words, individual SAC ensembles are uniform with respect to intensity and therefore poor choices to demonstrate the effectiveness of various characterization approaches to reduce or eliminate the effect of intensity. Since each SAC ensemble is representative of a distinct event and thus a distinct measure of intensity, combining the SAC ensembles into a single ensemble comprises a more disparate set of motions with broader intensity variation to effectively evaluate the characterization approaches.

The parameter ranges considered are T_b = 1 to 5 seconds and η = 0.2 to 0.8 for the normalized strength characterization with $I = \dot{u}_{go}$ or V, T_b = 1 to 5 seconds and η = 0.3 to 1.6 for the normalized strength characterization with $I = \omega_b u_{go}$, and T_{eff} = 1 to 5 seconds and ζ_{eff} = 0.05 to 0.30 for the equivalent linear characterization. The range of η for each normalized strength alternative was determined by evaluating an applicable range of Q corresponding to the considered range of T_{eff} and ζ_{eff} and the observed peak response of a linear system to the considered ground motion ensembles [Eq. (11a)], and subsequently evaluating a range for η based on the ranges of Q and the ground motion intensities in the ensemble [Eq. (9)]. Note that for this analysis, the intensity measure I (normalized

strength characterization) or SD D_D (equivalent linear characterization) are evaluated independently for analysis to each ground motion in the various ensembles.

The dispersion of the peak normalized deformation $\overline{u}_{bo}$ and peak deformation u_{bo} for the normalized strength characterization using PGV $\dot{u}_{go}$ is shown in Fig. 2.4. The dispersion of the normalized deformation [Fig. 2.4(b) and (d)] is observed to be consistently lower than the dispersion of the actual deformation [Fig. 2.4(a) and (c)]. For the SAC master ensemble, the dispersion of $\overline{u}_{bo}$ ranges from 0.6 to 0.8 of the dispersion of u_{bo} for different values of η especially over the period range of 2 to 5 seconds [Fig. 2.4(a) and (b)]. Likewise, for the LMSR ensemble, the dispersion of $\overline{u}_{bo}$ ranges from 0.5 to 0.9 of the dispersion of u_{bo} for different values of η over the period range of 2 to 5 seconds [Fig. 2.4(c) and (d)]. Thus, PGV appears to be an acceptable measure of intensity and this normalized strength characterization effectively reduces the dispersion of normalized deformation.

The dispersion of the peak normalized deformation $\overline{u}_{bo}$ compared to peak deformation u_{bo} for the normalized strength characterization using SV V is shown in Fig. 2.5. The dispersion of the peak normalized deformation [Fig. 2.5(b) and (d)] is not reduced significantly compared to the dispersion of the actual deformation [Fig. 2.5(a) and (c)]. For larger values of normalized strength like $\eta = 0.8$, no reduction in dispersion is observed. In general, the dispersion trends are not consistent and vary widely with ground motion ensemble and with isolation period T_b. Thus, SV is not a good measure of intensity and should be eliminated from further consideration.

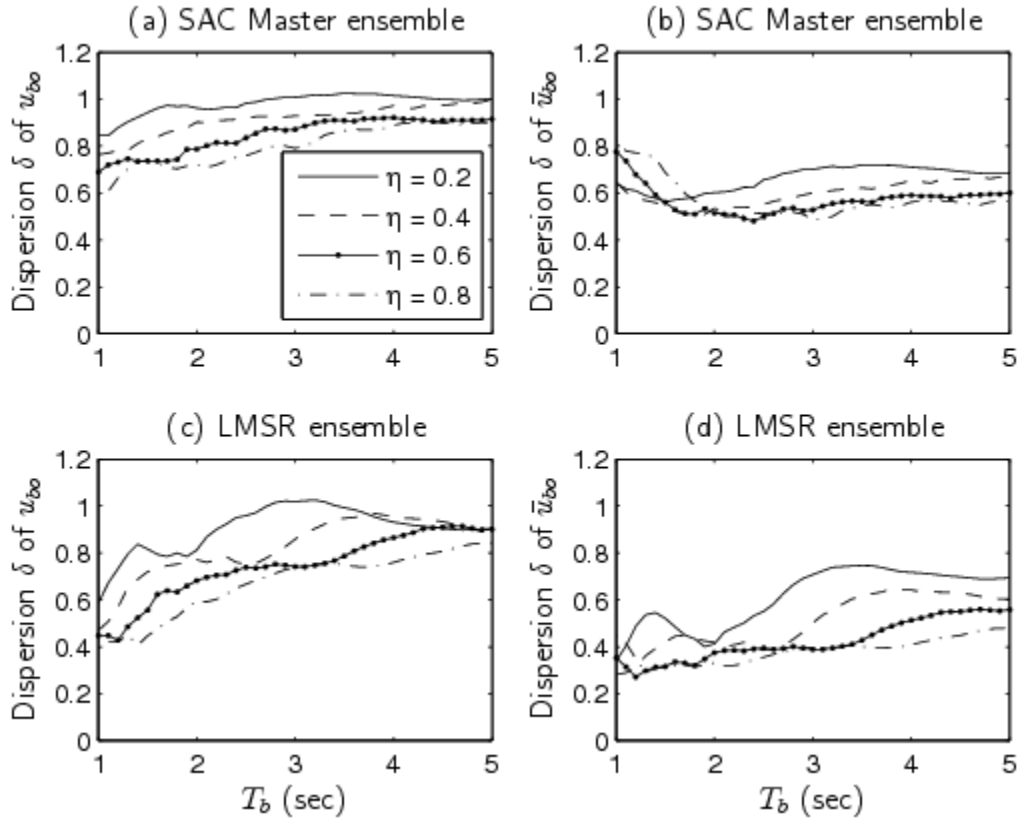

FIGURE 2.4 Dispersion of (a), (c) deformation u_{bo} and (b), (d) normalized deformation $\bar{u}_{bo}$ for ground motion ensembles as indicated, using the normalized strength approach with intensity characterized by PGV.

The dispersion of the peak normalized deformation $\bar{u}_{bo}$ compared to the peak deformation u_{bo} for the normalized strength characterization using PGD u_{go} is presented in Fig. 2.6. The dispersion of the peak normalized deformation [Fig. 2.6(b) and (d)] is actually consistently higher than the dispersion of the peak deformation [Fig. 2.6(a) and (c)] in the short period range (T_b = 1 to 3 seconds for the SAC Master ensemble and 1 to 2 seconds for the LMSR ensemble). This observation is not surprising since the constant displacement, or displacement sensitive region of the spectrum generally does not take effect until periods of at least 2.5 seconds. The dispersion trends are better in the range of T_b = 3 to 5 seconds for the LMSR ensemble [Fig. 2.6(c) vs. (d)], which transitions to the

displacement sensitive region at $T_n \approx 2$ seconds. However, reductions in dispersion are not observed for the SAC Master ensemble over any portion of the period range [Fig. 2.6(a) vs. (b)]. Ultimately, a compelling argument cannot be made that PGD is an effective measure of intensity, even in the longer period range, and thus PGD is eliminated from further consideration.

Finally, the equivalent linear characterization is evaluated by comparing the dispersion of the peak deformation ratio $\hat{u}_{bo}$ to the actual peak deformation u_{bo}, where the system is characterized by effective period T_{eff} and damping ζ_{eff} (Fig. 2.7).

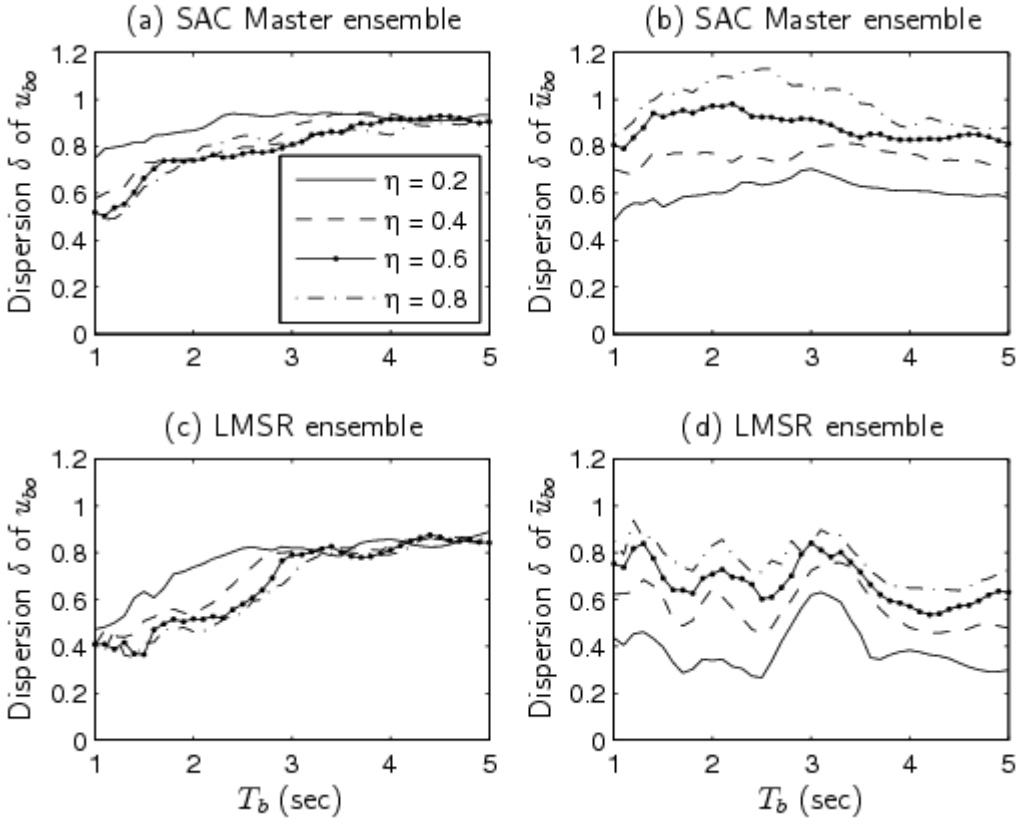

FIGURE 2.5 Dispersion of (a), (c) deformation u_{bo} and (b), (d) normalized deformation $\bar{u}_{bo}$ for ground motion ensembles as indicated, using the normalized strength approach with intensity characterized by SV.

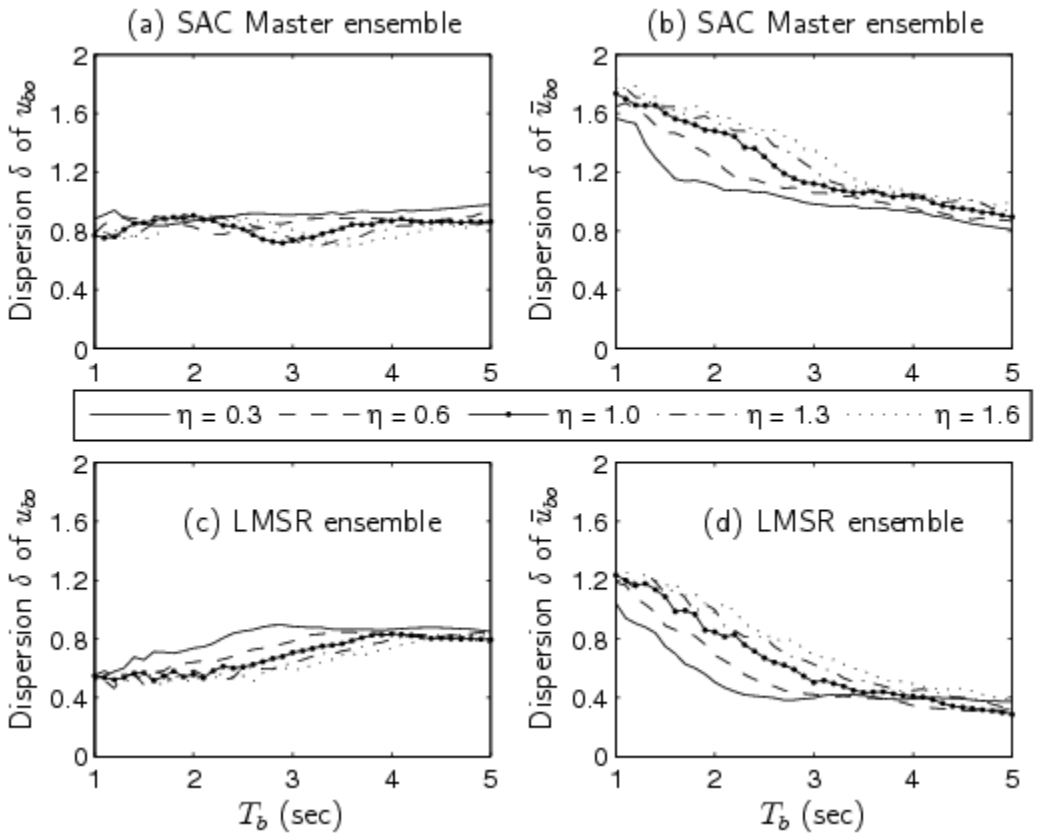

FIGURE 2.6 Dispersion of (a), (c) deformation u_{bo} and (b), (d) normalized deformation $\bar{u}_{bo}$ for ground motion ensembles as indicated, using the normalized strength approach with intensity characterized by PGD.

Recall that the yield force in the isolation system Q and the post-yield stiffness k_b [Eq. (11)] are calculated to match the target effective period T_{eff} and damping ζ_{eff} at the SD D_D for individual ground motions. Figure 2.7 indicates that the dispersion of the deformation ratio $\hat{u}_{bo}$ is significantly lower than dispersion of peak deformation u_{bo} for both the SAC master ensemble [Fig. 2.7(a) vs. (b)] and the LMSR ensemble [Fig. 2.7(c) vs. (d)]. The deformation ratio based on SD of an equivalent linear system has much less variation than the actual deformation and the observed trends for dispersion are consistent across the range of effective period and damping. Theoretically, the deformation u_{bo} of

the nonlinear system approaches the SD D_D, or $\hat{u}_{bo} \to 1$, as $\zeta_{eff} \to 0$, which means that the dispersion in $\hat{u}_{bo}$ must approach 0 as $\zeta_{eff} \to 0$. Thus, as expected, the dispersion in the deformation ratio $\hat{u}_{bo}$ is observed to increase slightly as damping increases (Fig. 2.7). Overall, the SD of a corresponding linear system as employed in the equivalent linear characterization appears to be a very effective measure of intensity such that the dispersion of the deformation ratio $\hat{u}_{bo}$ is consistently and substantially reduced compared to the dispersion of the peak deformation u_{bo}.

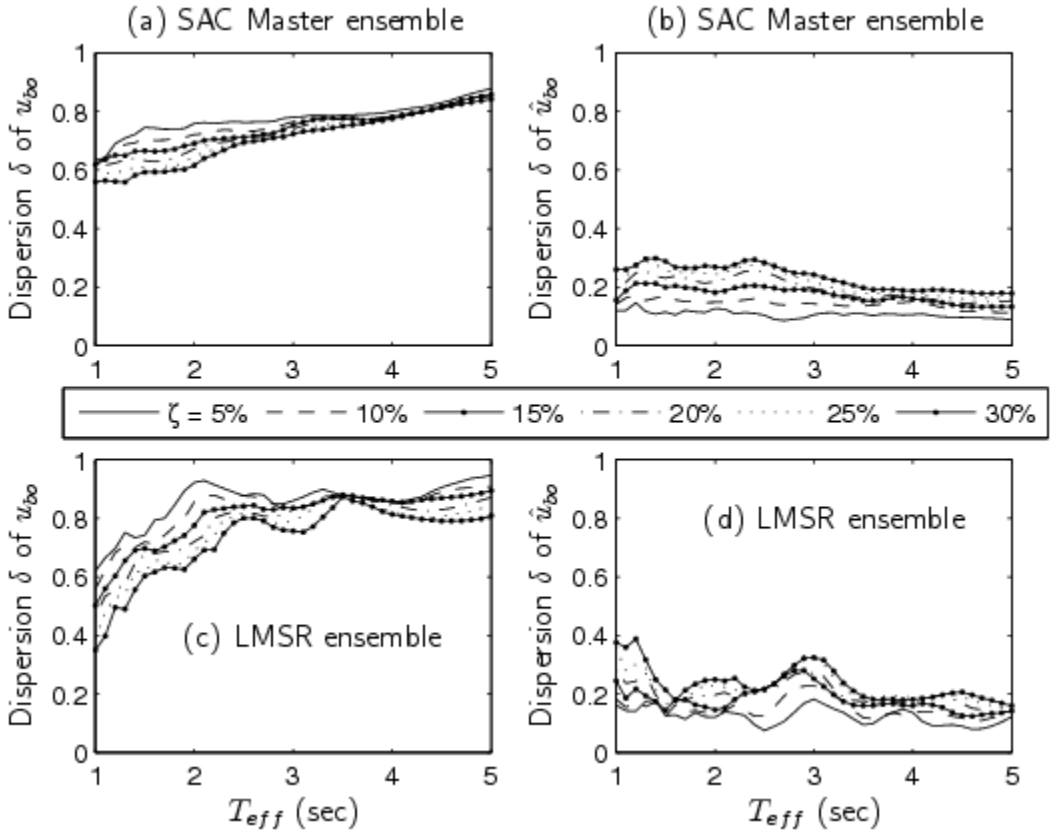

FIGURE 2.7 Dispersion of (a), (c) deformation u_{bo} and (b), (d) deformation ratio $\hat{u}_{bo}$ for ground motion ensembles as indicated, using the equivalent linear approach with intensity characterized by spectral displacement D_D.

4.1.1. Discussion of Results

For the normalized strength characterization of the isolation system, PGV has been observed to be the most effective measure of intensity because the dispersion of the normalized deformation is consistently reduced relative to the dispersion of the actual deformation when $I = \dot{u}_{go}$ in the normalized strength definition [Eq. (9)]. While SV and PGV are similar measures of intensity, PGV is relatively period-independent while SV depends on the period. As such, it is observed that α_v – interpreted as $V(T_b)/\dot{u}_{go}$ for each motion – varies widely, as indicated by the variation of α_v for individual ground motions [Fig. 2.8(a)] and its dispersion over the LMSR ensemble [Fig. 2.8(b)]. Hence, Fig. 2.8 confirms the intuition that PGV is the more stable measure of intensity.

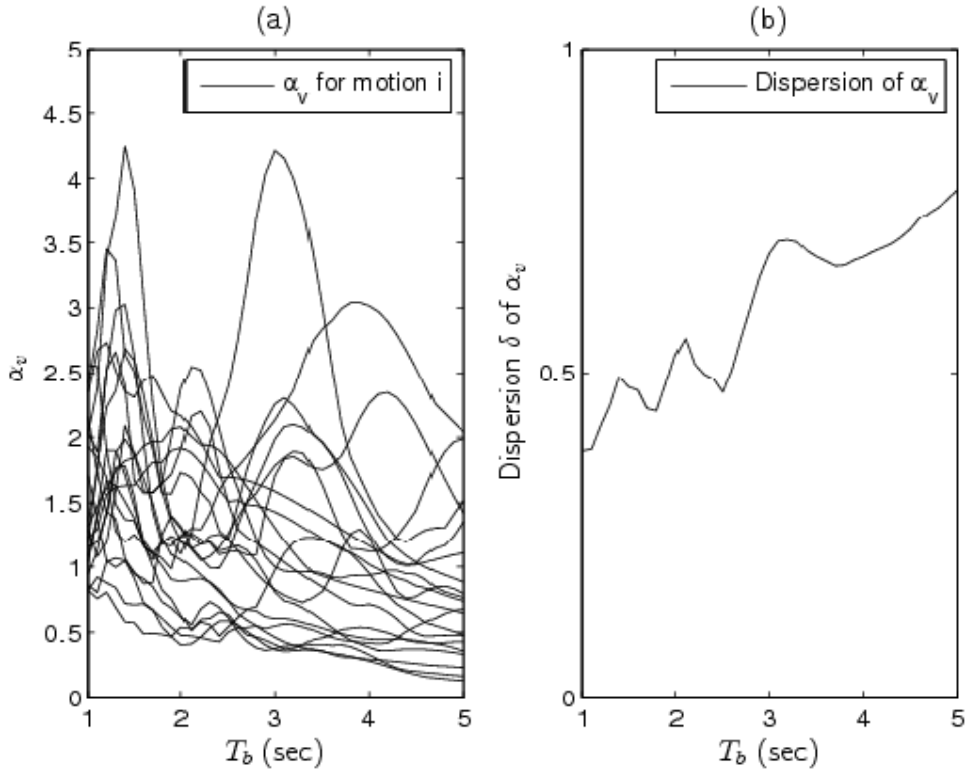

FIGURE 2.8 (a) Value of $\alpha_v = V(T_b)/\dot{u}_{go}$ for individual motions and (b) dispersion of α_v for LMSR ensemble.

From here forward, the normalized strength characterization with ground motion intensity quantified by PGV – since the other two intensity measures were deemed unacceptable – is compared to the equivalent linear characterization with ground motion intensity quantified by SD. Although care should be taken in comparing two approaches that use very different response measures, the equivalent linear characterization appears to be extremely effective in lowering the dispersion of the deformation ratio while the normalized strength characterization is only mildly effective in lowering the dispersion of the normalized deformation. The normalized strength characterization poses a challenge to designers to choose an appropriate target value of the normalized strength η, which has not been used within the context of seismic isolation design, while the equivalent linear characterization uses a familiar damping ratio. This issue is addressed next.

4.2. Energy Dissipation Capacity

The effective damping ratio is a well known parameter that can be interpreted as a measure of the energy dissipation capacity of the isolation system, which is an advantage of the equivalent linear approach used in current design codes. Unfortunately, the effective damping ratio is not easily quantifiable by physically meaningful parameters of the system. In contrast, the normalized strength is easily determined from the yield strength and post-yield stiffness of the system, as well as the design PGV. To quantify the energy dissipation capacity of a system characterized by normalized strength, the corresponding effective damping ratio ζ_{eff} is shown for various ground motion ensembles (Fig. 2.9). The effective damping ratio is determined using Eq. (3) as a function of T_b and η, using the median deformation u_{bo} obtained from nonlinear response history analysis for

each ensemble. The SAC Master ensemble has been decomposed into its individual ensembles to observe the variation of effective damping with ground motion intensity.

Figure 2.9 indicates that the effective damping ratio ζ_{eff} varies from about 0.05 to 0.40 over the range of η considered in the study. The observed ζ_{eff} is somewhat sensitive to the ground motion ensemble, but the variation of ζ_{eff} across ensembles for a given normalized strength is limited to about 0.1 for longer isolation periods T_b where most systems typically fall. Most importantly, the value of ζ_{eff} for a given normalized strength varies only mildly as the isolation period changes from 1 to 5 seconds. This is a significant improvement compared to the original normalized strength characterization proposed by Ryan and Chopra (Fig. 2.3), where effective damping is observed to increase by as much as a factor of 4 over the isolation period range. While the value of ζ_{eff} increases slightly with increasing isolation period for the LA 50 in 50, Seattle 10 in 50, and LMSR ensembles [Fig. 2.9(c), (d), (e)], ζ_{eff} remains nearly constant over the isolation period range for the LA 2 in 50 and LA 10 in 50 ensembles [Fig. 2.9(a), (b)]. Thus, the results are consistent enough to correlate specific values of normalized strength η to energy dissipation in terms of effective damping.

4.3. Simplified Equations to Predict Deformation

Next, the normalized strength characterization and the equivalent linear characterization are evaluated in their ability to facilitate a simple prediction of deformation that is amenable to code implementation. Trends for median peak normalized deformation $\overline{u}_{bo}$ as a function of η (normalized strength characterization)

[Fig. 2.10(a) and (c)] and deformation ratio $\hat{u}_{bo}$ as a function of ζ_{eff} (equivalent linear characterization) [Fig. 2.10(b) and (d)] are compared. The median normalized deformation and deformation ratio were computed by applying Eq. (13) to values obtained by nonlinear response history analysis of individual ground motions in the ensemble as described earlier.

The normalized deformation $\overline{u}_{bo}$ associated with the normalized strength characterization decreases essentially monotonically as a function of isolation period T_b, and a nonlinear relation between normalized deformation and normalized strength η is observed [Fig. 2.10(a) and (c)]. (If the relation were linear, the curves for different values of η would be equally spaced.)

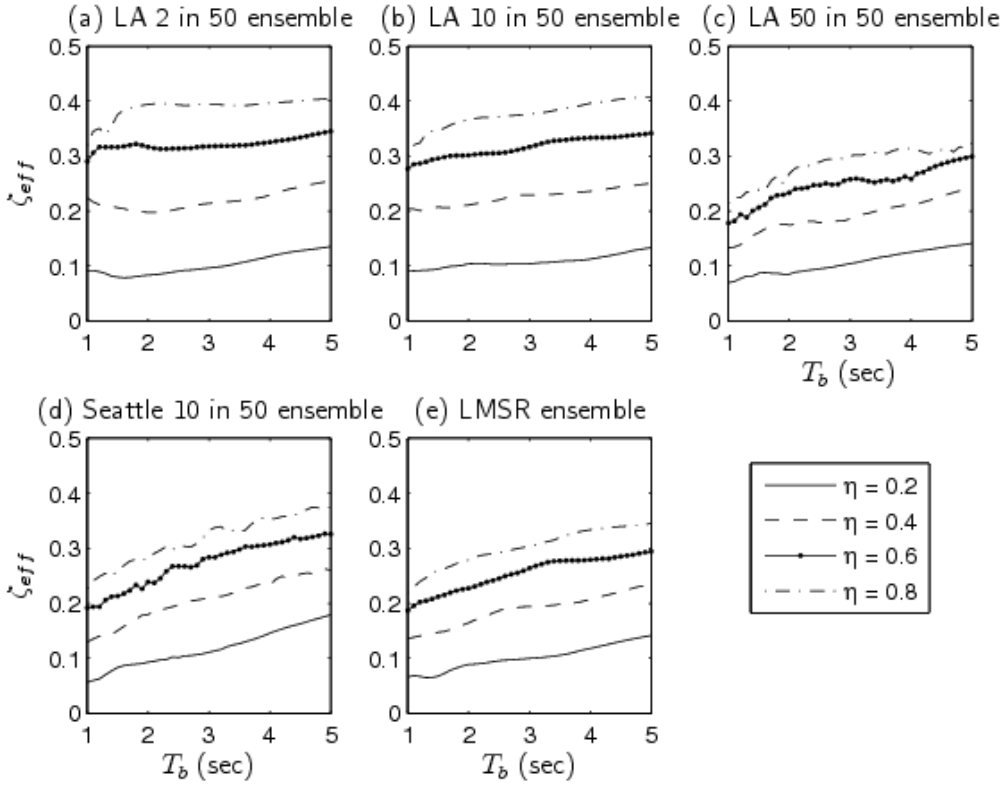

FIGURE 2.9 Effective damping ζ_{eff} as a function of isolation period T_b and normalized strength η for 5 ground motion ensembles.

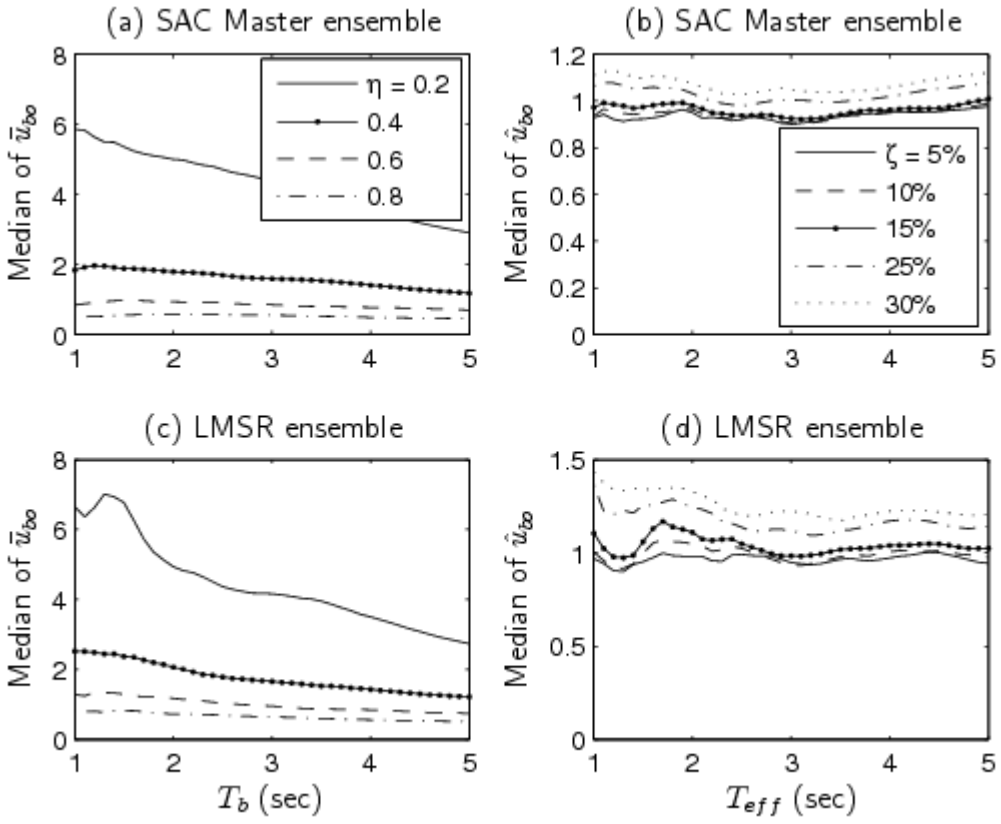

FIGURE 2.10 Median response trends for (a), (c) normalized deformation $\bar{u}_{bo}$ using the normalized strength characterization; and (b), (d) deformation ratio $\hat{u}_{bo}$ using the equivalent linear approach, for the ground motion ensembles indicated.

Consequently, the interaction between T_b and η should be considered when developing an equation to predict the normalized deformation. In the original characterization [Ryan and Chopra, 2004], the relation between normalized deformation and isolation period T_b was linear on a log-log plot. Unfortunately, the simple log-log relation is not applicable here, and at best, the relation between normalized deformation and isolation period T_b may be loosely interpreted as linear on a semilog plot (not shown here). Thus, developing convenient and simple equations to predict the normalized deformation may be difficult.

The deformation ratio associated with the equivalent linear characterization is essentially an invariant function of effective period T_{eff}, aside from slight local variation

[Fig. 2.10(b) and (d)]. Therefore, development of a simple design equation to predict the deformation ratio as a function ζ_{eff}, which could be applied as an amplification factor to the current code SD, seems very feasible. This design equation should adhere to the theoretical limit that the deformation ratio tends to 1 as the effective damping tends to zero. Some variation of the deformation ratio amplitude with ground motion ensemble is observed [Fig. 2.10(b) vs. (d)], and should be explored in more detail. Note that this approach, which uses a deformation ratio or deformation amplification factor for nonlinearity, is only slightly different than the approach proposed by previous researchers [e.g. Dicleli and Buddaram, 2007; Hwang *et al*., 1995] to alter the effective damping ratio in some systematic way.

5. Conclusions

Various approaches to characterize nonlinear isolation systems for design have been evaluated. The normalized strength approach characterizes the isolation system in terms of an isolation frequency, a characteristic strength, and a ground motion intensity measure. The equivalent linear approach characterizes the isolation system in terms of an effective period and effective damping ratio. For both approaches, intensity independent response measures were proposed: normalized deformation for the normalized strength characterization and deformation ratio (peak deformation divided by spectral displacement) for the equivalent linear characterization; and were evaluated in their ability to reduce dispersion compared to the actual deformation. For the normalized strength characterization, three measures of intensity were evaluated: peak ground velocity, spectral velocity, and peak ground displacement; wherein peak ground velocity was judged to be the most effective.

The key considerations in the comparative evaluation are summarized as follows:

- The normalized strength characterization is based on physically meaningful parameters of the isolation system that can be easily determined, while the equivalent linear characterization uses an effective period and effective damping ratio that are generally determined by iteration.
- For the normalized strength characterization, the dispersion of normalized deformation is reduced somewhat compared to the dispersion of the actual deformation, indicating that peak ground velocity is an effective measure of ground motion intensity for this approach. For the equivalent linear characterization, the dispersion of the deformation ratio is reduced substantially compared to the dispersion of the actual deformation, indicating that spectral displacement, which has long been used as the estimated deformation, is an effective starting point to obtain the actual deformation considering system nonlinearity.
- The effective damping ratio in the equivalent characterization is a widely used and meaningful measure of energy dissipation. For the normalized strength characterization, the normalized strength was shown to correlate directly and consistently to the effective damping ratio, indicating that a target range of normalized strength that represents standard energy dissipation can easily be defined.
- For the normalized strength characterization, the median normalized deformation shows relatively smooth variation with isolation period and normalized strength, but interaction between these two parameters may lead to difficulty when

developing a smooth design spectrum. For the equivalent linear characterization, the deformation ratio is essentially constant with effective period, indicating that a simple equation can be developed to estimate the deformation ratio as a function of effective damping.

References

American Society of Civil Engineers (ASCE) [2005] ASCE 7-05 *Minimum Design Loads for Buildings and Other Structures*, Reston, VA.

Anderson, E. and Mahin, S. A. [1998] "Displacement-based design of seismically isolated bridges," *Proc. of the Sixth U.S. National Conference on Earthquake Engineering.* Earthquake Engineering Research Institute, Oakland, California.

Chopra, A. K. and Goel, R. K. [2000] "Evaluation of NSP to estimate seismic deformation: SDF systems," Journal of Structural Engineering 126(4):482-490.

Dicleli, M. and Buddaram, S. [2007] "Comprehensive evaluation of equivalent linear analysis method for seismic-isolated structures represented by SDOF systems," Engineering Structures 29:1653-1663.

Fajfar, P. [1999] "Capacity spectrum method based on inelastic demand spectra," Earthquake Engineering and Structural Dynamics 28(9):979-993.

Franchin, P., Monti, G., and Pinto, P. E. [2001] "On the accuracy of simplified methods for the analysis of isolated bridges," Earthquake Engineering and Structural Dynamics 30:363-382.

Hwang, J. S, Chiou, J. M., and Sheng, L. H. [1995] "Establishment of an equivalent linear model of seismically isolated bridges using a system identification method," *Proc. of the 4th U.S. Conference on Lifeline Earthquake Engineering*, ASCE, New York, pp. 416-423.

Hwang, J. S. [1996] "Evaluation of equivalent linear analysis methods of bridge isolation," Journal of Structural Engineering, 122(8), 972-976.

International Code Council (ICC) [2006] *International Building Code (IBC)*, Falls Church, VA.

Jara, M. and Casas, J. [2006] "A direct displacement-based method for the seismic design of bridges on bi-linear isolation devices," Engineering Structures 28:869-879.

Park, J.G. and Otsuka, H. [1999] "Optimal yield level of bilinear seismic isolation devices," Earthquake Engineering and Structural Dynamics 28:941-955.

Ryan, K. L. and Chopra, A. K. [2004] "Estimation of seismic demands on isolators based on nonlinear analysis," Journal of Structural Engineering 130(3), 392-402.

Somerville, P., Anderson, D., Sun, J., Punyamurthula, S., and Smith, N. [1998] "Generation of ground motion time histories for performance-based seismic engineering," *Proc. of the 6th U.S. National Conf. of Earthquake Engineering*, Seattle, Washington.

Tena-Colunga, A. [2002] "Seismic design of base-isolated structures using constant strength spectra," Journal of Earthquake Engineering 6(4):553-585.

Weitzmann, R., Ohsaki, M., and Nakashima, M. [2006] "Simplified methods for the design of base-isolated structures in the long-period high-damping range," Earthquake Engineering and Structural Dynamics 35:497-515.

Zhao, J. X. and Zhang J. [2004] "Inelastic demand spectra for bi-linear seismic isolation systems based on nonlinear time history analysis," Proc. of the JSSI 10th Anniversary Symposium on Performance of Response Controlled Buildings, Yokohama, Japan.

CHAPTER 3

COMPARATIVE EVALUATION OF BASE-ISOLATED AND FIXED-BASE BUILDINGS USING A COMPREHENSIVE RESPONSE INDEX

Abstract Although current code guidelines specify different seismic performance objectives for fixed-base and isolated buildings, the future of performance-based design will allow user-selected performance objectives, motivating the need for a consistent performance comparison of the two systems. Based on response history analysis to a suite of motions, constant ductility spectra are generated for fixed-base and isolated buildings. Both superstructure force (base shear) and deformation demands in base-isolated buildings are lower than in fixed-base buildings responding with identical deformation ductility. To compare the relative performance of many systems or to predict the best system to achieve a given performance objective, a response index is developed and used for rapid prototyping of response as a function of system characteristics. When evaluated for a life safety performance objective, the superstructure design base shear of an isolated building is competitive with that of a fixed-base building with identical ductility, and the isolated building generally has improved response. Isolated buildings can meet a moderate ductility immediate-occupancy objective at low design strengths whereas comparable ductility fixed-base buildings fail to meet the objective.

Introduction

The seismic performance objectives implicit in U.S. building codes currently differ for fixed-base and base-isolated buildings. As an example, fixed-base buildings are permitted a force reduction factor R of up to 8, which may allow significant inelastic

action in the design basis earthquake and can be interpreted as a "life safety" performance objective. Likewise, isolated buildings are limited to *R* factors no larger than 2, and remain essentially elastic due to overstrength. The reduced *R* factor, together with other requirements, may be interpreted as seeking a performance objective more comparable to "immediate occupancy" or "operational" (SEAOC 1995). Consequently, the superstructure design forces in an isolated building are sometimes larger than in a comparable fixed-base building. Factoring in the added design, material, and testing costs; seismic isolation has become an expensive technology that in the U.S. is adopted only for continued operation of essential facilities such as hospitals, emergency response units, and supercomputing centers; or preservation of historical buildings. If fixed-base and isolated buildings are compared relative to a consistent performance objective (life safety or continued occupancy), the cost-competitiveness of base isolation may be improved relative to fixed-base design.

Cost comparison studies of fixed-base and base-isolated buildings, which included initial design and construction costs, were performed for selected cases where comparative data was available (Mayes *et al.* 1990). Incorporating seismic isolation into a new building was generally found to result in a cost premium in the range of 1-5%, because higher performance standards for isolated buildings did not allow sufficient reductions in the cost of the structural framing system to offset the cost of the isolation system. The cost premium for seismic isolation may have increased since 1990 due to additional requirements in recent codes. In one case, preliminary designs and cost estimates were developed for a fixed-base and isolated building subjected to the same performance criteria, and the isolation design was shown to be 6% less expensive.

Most recently, performance-based seismic design approaches are under development and attracting great interest in the U.S. Performance-based engineering allows owner-selected performance objectives for the structural and non structural building components considering specific seismic events or the aggregate hazard. The new approach, developed by PEER and being adapted for practice by ATC-58 (Miranda and Aslani 2003; Krawinkler 2005; ATC 2007), specifies performance in terms of probabilistic losses (casualties, repair costs, downtime). The development of fragility and loss functions, which relate losses to traditional response measures, is an ongoing process (Porter *et al.* 2007). When performance-based engineering matures, designers will be able to employ the latest design and analysis techniques to create efficient designs that meet specified performance objectives, and building owners will be able to comparatively evaluate base isolation and fixed-base design with reference to a quantitative performance objective.

The concept of designing base-isolated buildings using criteria comparable to fixed-base buildings was previously examined (Lin and Shenton 1992; Shenton and Lin 1994), wherein the performance of fixed-base and base-isolated concrete and steel frames was compared. The reference fixed-base buildings were designed to code standards for fixed-base buildings (ICBO 1991), while the isolated buildings were designed to 100%, 50% and 25% of code base shear for isolated buildings. The study concluded that isolated buildings designed with identical force reduction factors would out-perform fixed-base structures, and future codes could include optional performance requirements for isolated buildings. More recently, Naaseh *et al.* (2002) compared the response of a code compliant 3-story concentric braced frame steel building (ICBO 1997), and a comparable

isolated building with reduced base shear capacity relative to code. The study concluded that isolated buildings designed to reduced forces would meet performance objectives for conventional fixed-base buildings, and yet still see the benefit of substantially reduced floor accelerations.

Several researchers have presented analytical studies that consider yielding in the superstructures of seismic-isolated buildings. Approaches to evaluate inelastic behavior in base-isolated buildings have been presented, such as collapse spectra (Palazzo and Petti 1996) and damage characterization through superstructure hysteretic energy dissipation (Ceccoli *et al.* 1999). Ordonez *et al.* (2003) focused on the comparative demands of yielding superstructures for different types of isolation systems. Kikuchi *et al.* (2008) concluded that yielding isolated structures are more susceptible to damage than fixed-base structures; that is, due to fundamental differences in response damage is self-limiting in fixed-base structures but self-propagating in seismically isolated structures.

Ryan *et al.* (2006) conducted a simple parametric study comparing fixed-base and isolated structures with identical fixed-base periods and responding with identical deformation ductility. Response history analyses demonstrated that base shear, inter-story drift and roof accelerations were reduced in isolated buildings compared to the comparable fixed-base buildings. A comparative performance measure (CPM) was developed to assess relative response – quantified by structural drift and acceleration – of the comparable isolated and fixed-base buildings. A drawback to this approach was that comparison was restricted to structures with identical ductility demands, and did not allow identification of the best design considering both performance objectives and cost considerations.

The objective of the present study is to develop a methodology to systematically evaluate relative performance of fixed-base and base-isolated buildings as measured by engineering demand parameters. To compare the relative performance of multiple systems, including fixed-base and base-isolated buildings, a response index (RI) is developed. The RI is an improvement over the CPM because it facilitates ranking the relative response of many systems rather than comparing a single base-isolated building and its fixed-base counterpart. The methodology can be used as desired; e.g., to identify the best performing system, to identify the minimum system that meets the performance objective, or to identify a desirable combination of performance and strength. In this study, analysis is restricted to single story (i.e. single degree-of-freedom or SDF) structures with and without an isolation system subjected to a suite of 20 ground motions. Within this scope, the methodology is used to rapidly prototype the response of buildings based on key characteristics such as natural vibration period and design base shear. However, the general methodology could be extended to more complex structural systems, and potentially fills a critical gap in the performance-based design process, since the current ATC guidelines do not address how to develop preliminary designs that are likely to meet desired objectives (ATC 2007).

Models for Comparative Analysis

Systems Considered

The system considered is an inelastic single-story fixed-base building and the same building on isolators. The fixed-base building [Fig. 3.1(a)] with mass m responds with elastic-perfectly plastic force-deformation (f_s vs. u_s) [Fig. 3.1(c)] with initial stiffness k and yield force f_y. When isolated [Fig. 3.1(b)], the single story superstructure

sits on a base mass m_b supported on an isolation system. Because the superstructure is modeled as an SDF system higher mode effects are not accounted for. The force f_b in the isolation system is determined from a bilinear force-deformation relationship [Fig. 3.1(d)], represented by the following equation:

$$f_b = k_b u_b + Qz\left(k_i, u_b, \dot{u}_b\right) \tag{1}$$

where u_b and $\dot{u}_b$ are the deformation and velocity of the isolation system; the initial stiffness k_i, post-yield stiffness k_b, and y-intercept yield strength Q control the response of the isolation system; and z is a dimensionless number from -1 to 1 that represents the fraction of the yield strength applied (Ryan and Chopra 2004). The initial stiffness k_i is determined by the yield deformation u_{by}, which is assumed as 1 cm in this study.

The characteristic natural vibration frequencies and periods of the fixed-base building (ω_s, T_s) and the isolated building (ω_b, T_b) are given by:

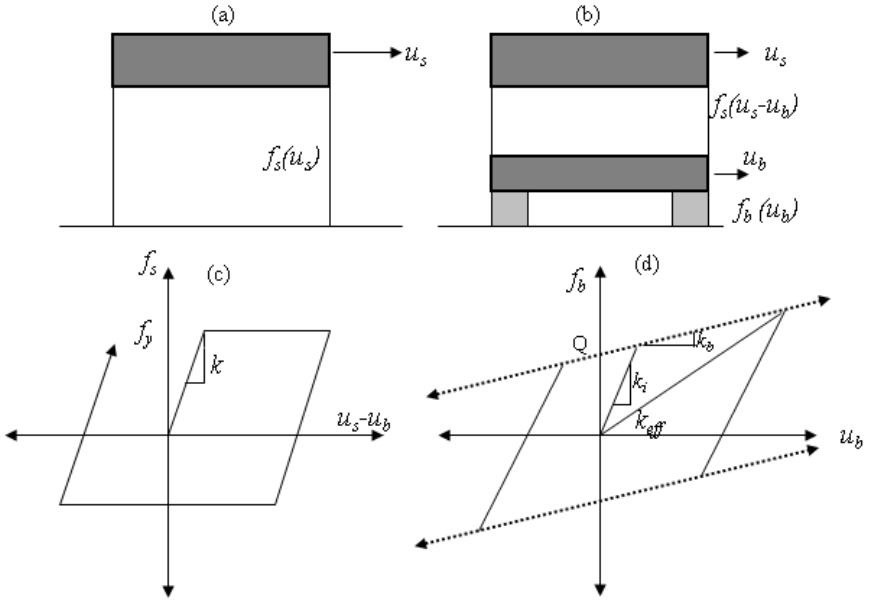

Fig. 3.1. (a) Single-story fixed-base building, (b) building on base isolation system, (c) elasto-plastic force-deformation relation of superstructure or fixed-base structure, and (d) bilinear force–deformation relation of isolation system.

$$\omega_s = \sqrt{\frac{k}{m}} \qquad T_s = \frac{2\pi}{\omega_s} \tag{2a}$$

$$\omega_b = \sqrt{\frac{k_b}{m+m_b}} \quad T_b = \frac{2\pi}{\omega_b} \tag{2b}$$

The fixed-base natural period is characterized by the initial stiffness of the superstructure because ductile systems are presumed to vibrate predominantly in the elastic range with minor inelastic excursions. The natural period of the isolated building (assuming a rigid structure), or isolation period, is characterized by the post-yield stiffness of the isolation system, which is expected to cycle with large inelastic excursions. The parameter T_{shift} indicates the separation between the isolation period and the superstructure period:

$$T_{shift} = T_b - T_s \tag{3}$$

Although period separation has often been described in terms of a frequency or period ratio (ω_b/ω_s or T_b/T_s), such an approach is ineffective when the superstructure or isolation period are varied over a large range. Unlike a frequency ratio, the additive period shift defined here is meaningful for both short period (T_s = 0.01 sec) and long period superstructures (T_s = 2 sec). For a given superstructure period, the isolation period increases as the period shift increases. Thus, a larger period shift is synonymous with a more effective isolation system. In the present study, values of T_{shift} from 1.5 to 4 are considered.

Equations of Motion

The equations governing the motion of the isolated building [Fig. 3.1(b)], in matrix form, are

$$\begin{bmatrix} m_b + m & m \\ m & m \end{bmatrix} \begin{Bmatrix} \ddot{u}_b \\ \ddot{u}_s - \ddot{u}_b \end{Bmatrix} + \begin{Bmatrix} 0 \\ c_s \cdot (\dot{u}_s - \dot{u}_b) \end{Bmatrix} + \begin{Bmatrix} f_b(u_b) \\ f_s(u_s - u_b) \end{Bmatrix} = -\begin{Bmatrix} m_b + m \\ m \end{Bmatrix} \ddot{u}_g \qquad \begin{matrix} (4a) \\ (4b) \end{matrix}$$

where f_b is given by Eq. (1), f_s is determined according to Fig. 3.1(c), and $\ddot{u}_g$ is the ground acceleration. Although the inertia terms are coupled, Eq. (4a) approximately governs the deformation u_b of the isolation system, while Eq. (4b) approximately governs the relative deformation (u_s-u_b), or drift, of the superstructure. Equation (4b) includes superstructure viscous damping, proportional to the relative superstructure velocity by constant c_s. The damping in the isolation system is hysteretic, and quantified by the normalized strength parameter η defined in the next section. Setting $u_b = \dot{u}_b = \ddot{u}_b = 0$ in Eq. (4b) leads to the equation of motion for the fixed-base building:

$$m\ddot{u}_s + c_s\dot{u}_s + f_s(u_s) = -m\ddot{u}_g \tag{5}$$

Ground Motions Considered

The design of the isolation system is closely related to intensity of the ground motions to which it is to be subjected. The probabilistic spectral maps recently developed by the USGS provide a first order site-specific estimate of response spectra for use in design. However, performance-based evaluation requires a detailed specification of input ground motions, namely ground motion acceleration histories. As part of the SAC steel project, ground shaking estimates were developed for Boston, Seattle, and Los Angeles, corresponding to UBC Seismic Zones 2, 3 and 4 respectively (ICBO 1997; Somerville *et al.* 1998). Among the data developed for each location were suites of time histories at variable probabilities of occurrence for firm soil conditions. Because they represent a uniform intensity event, characterized by the probability of occurrence, the acceleration

histories for the 10% in 50 year event in Los Angeles are selected for this study, referred to hereafter as the SAC-LA 10 in 50 suite. The suite consists of 10 pairs of orthogonal motions, of which all 20 components are singly applied in this study. The components have been altered in the frequency domain to match desired site characteristics, and rotated 45 degrees from fault-normal, fault-parallel orientation. Although the SAC-LA suite is not meant to be explicitly characteristic of near-fault motions, several of the motions were recorded within 10 km of the fault. Essential characteristics of the recorded motions are listed in Table 3.1, including the site, the earthquake and magnitude, the closest distance to fault rupture *H*, the amplitude scale factor, and the peak ground acceleration (PGA) for each component after scaling. The 5% damped median response spectrum for the motions is shown in Fig. 3.2.

Effective Characterization of the Isolation System

For the purpose of characterizing the isolation system, suppose that the superstructure is rigid $(u_s - u_b = 0)$. Applying this assumption to Eq. (4a) leads to the following equation for the deformation of the isolation system:

$$\left(m + m_b\right)\ddot{u}_b + f_b(k_1, u_b, \dot{u}_b) = -\left(m + m_b\right)\ddot{u}_g \tag{6}$$

Introducing Eq. (1) for f_b into Eq. (6), and dividing by the total mass $m + m_b$ leads to

$$\ddot{u}_b + \omega_b^2 u_b + \frac{Q}{W} gz\left(k_i, u_b, \dot{u}_b\right) = -\ddot{u}_g \tag{7}$$

where *g* is the acceleration due to gravity. The characteristic strength ratio *Q/W* quantifies the isolation system strength relative to the structure weight *W*. Typically, the strength *Q* of the isolation system is selected based on target ranges of *Q/W*.

Table 3.1. Characteristics of Ground Motions in the SAC-LA 10 in 50 Suite

Number	Site	Earthquake	Magnitude M_w	H (km)	Scale Factor	Comp. 1 *PGA* (g)	Comp. 2 *PGA* (g)
1, 2	El Centro	1940 Imperial Valley	6.9	10	2.01	0.460	0.675
3, 4	El Centro Array #5	1979 Imperial Valley	6.5	4.1	1.01	0.393	0.487
5, 6	El Centro Array #6	1979 Imperial Valley	6.5	1.2	0.84	0.301	0.234
7, 8	Barstow Vineyard	1992 Landers	7.3	36	3.20	0.421	0.425
9, 10	Yermo Fire Sta.	1992 Landers	7.3	25	2.17	0.519	0.360
11, 12	Gilroy Array #3	1989 Loma Prieta	7.0	12	1.79	0.665	0.968
13, 14	Newhall – Fire Sta.	1994 Northridge	6.7	6.7	1.03	0.677	0.656
15, 16	Rinaldi Rec. Sta.	1994 Northridge	6.7	7.5	0.79	0.533	0.579
17, 18	Sylmar – Olive View	1994 Northridge	6.7	6.4	0.99	0.569	0.816
19, 20		1986 North Palm Springs	6.0	6.7	2.97	1.018	0.985

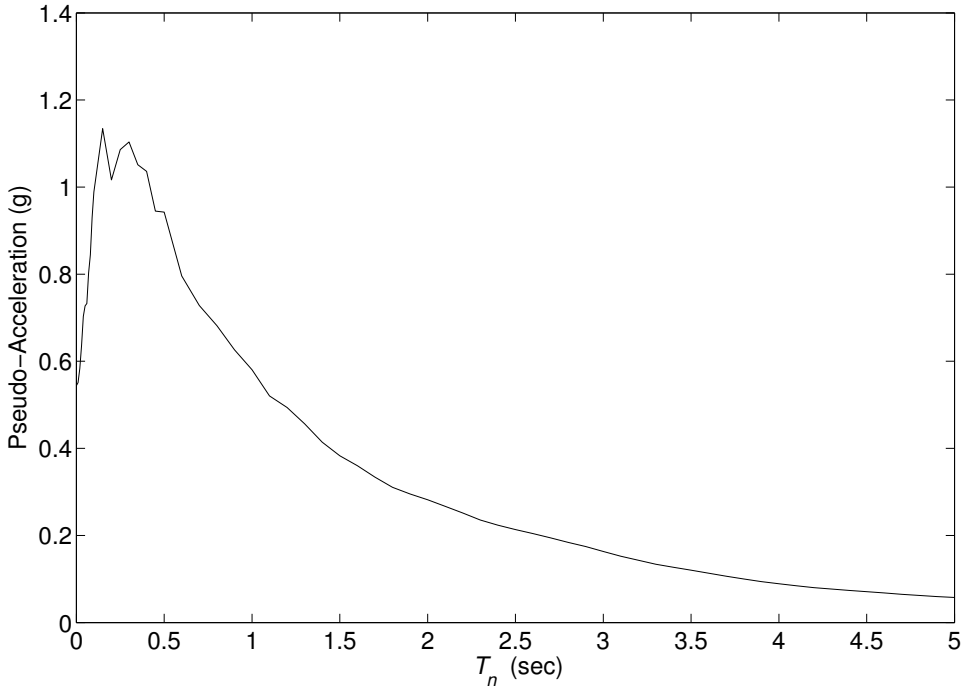

Fig. 3.2. 5% damped median linear response spectrum for the SAC-LA 10 in 50 suite; PGA = 0.54 g; PGV = 77.1 cm/s.

However, the deformation u_b is sensitive to ground motion intensity [Eq. (7)], suggesting that the ideal design strength varies according to intensity.

Development of an effective characterization of the isolation system has been the subject of ongoing research (Ryan and Chopra 2004; see Chapter 2). Such characterization leads to appropriate selection of the nonlinear parameters of the isolation system considering the intensity of the ground motion. Sayani and Ryan (see Chapter 2) have proposed that the isolation system be characterized by the isolation period T_b and normalized strength η, defined as:

$$\eta = \frac{Q}{m\omega_b \dot{u}_{go}} \tag{8}$$

where $\dot{u}_{go}$ is the peak ground velocity (PGV). This normalized strength [Eq. (8)] has been shown to be an effective measure of the energy dissipation capacity of the isolation system that is practically independent of the isolation period (Chapter 2). In addition, when Eq. (7) is written in normalized form (details in Ryan and Chopra 2004; Chapter 2), the response is shown to depend only on T_b and η and be independent of ground motion intensity. Thus, the design of the isolation system is determined by suitable ranges of T_b and η, and the strength coefficient Q/W is determined from target values of these parameters according to:

$$\frac{Q}{W} = \frac{Q}{mg} = \frac{\eta\omega_b \dot{u}_{go}}{g} \tag{9}$$

Note that an appropriate range of Q/W varies with the isolation period T_b.

At representative ground motion intensities, η is recommended to range from 0.2 to 0.8 (Chapter 2). Using the median value of $\dot{u}_{go} = 77.1\,\text{cm/s}$ for the SAC-LA 10 in 50

suite (Fig. 2), *Q/W* ranges from 0.05 to 0.2 for T_b = 2 seconds and from 0.025 to 0.1 for T_b = 4 seconds. The range of *Q/W* could vary with differing peak ground velocity for other ground motion suites.

Superstructure Strength and Ductility

Deformation ductility μ and force reduction factor *R* are mathematically defined and interpreted for meaningful comparative response analysis of fixed-base structures and isolated superstructures. Equation (4b), repeated here for convenience:

$$m\ddot{u}_b + m\cdot(\ddot{u}_s - \ddot{u}_b) + c_s\cdot(\dot{u}_s - \dot{u}_b) + f_s\left(u_s - u_b\right) = -m\ddot{u}_g \tag{10}$$

governs the relative deformation u_s-u_b between the roof and base mass of the isolated building, or the absolute deformation u_s of the fixed-base building (where u_b, $\dot{u}_b$ and $\ddot{u}_b$ are zero). Dividing Eq. (10) by the structure mass *m* leads to

$$\ddot{u}_s + 2\xi\omega_s\cdot\left(\dot{u}_s - \dot{u}_b\right) + \frac{f_s(u_s - u_b)}{m} = -\ddot{u}_g \tag{11}$$

where $\xi = c_s/2m\omega_s$ is the damping ratio of the superstructure vibrating within its linearly elastic range. Dividing Equation (11) by the yield deformation u_y leads to

$$\frac{\ddot{u}_s}{u_y} + 2\xi\omega_s\frac{\left(\dot{u}_s - \dot{u}_b\right)}{u_y} + \frac{\omega_s^2}{k}\frac{f_s\left(u_s - u_b\right)}{u_y} = -\frac{\ddot{u}_g}{u_y} \tag{12}$$

where ω_s^2/k has been substituted for 1/*m*. Deformation ductility is defined as the ratio of the deformation to the yield deformation of the system:

$$\mu = \frac{(u_s - u_b)}{u_y} \tag{13}$$

and is a useful measure of the damage in a building. Ductility is constrained to be less than 1 in systems that remain elastic, and has peak values exceeding 1 in systems

deforming into the inelastic range. Equation (12) is rewritten in terms of μ, which leads to

$$\frac{\ddot{u}_s}{u_y} + 2\xi\omega_s\dot{\mu} + \omega_s^2 \frac{f_s(u_s - u_b)}{f_y} = -\omega_s^2 \frac{\ddot{u}_g}{A_y} \tag{14}$$

where ku_y has been replaced by f_y and $A_y = f_y/m$ is the pseudo-acceleration associated with the yield force f_y (Chopra 2007). Ductility can be limited by minimizing the relative intensity ratio $\ddot{u}_g/A_y$, which quantifies the intensity of the ground motion relative to the strength of the structure.

An alternative and more commonly used intensity to strength measure is the previously mentioned force reduction factor *R*, relevant only for inelastic systems:

$$R = \frac{f_o}{f_y} \tag{15}$$

where f_o is the peak force if the superstructure were to remain elastic. The value of *R* is considered to be 1 for linearly elastic systems and greater than 1 for inelastic systems. Because the force-deformation relation is elastic-perfectly plastic, overstrength has been neglected and the *R* referred to in this study reflects only the ductility-based R_μ. In general, designing to a larger force reduction factor *R* allows larger ductility demand and greater damage in the building. Current codes prescribe upper bound *R* values for various structural systems. Prescribed *R* values are lower for isolated buildings compared to fixed-base buildings, which limits superstructure ductility but leads to larger base shear demands. In this study, the design yield acceleration A_y and the relative response of fixed-base and isolated buildings responding with the same ductility are compared.

Comparative Analysis Results

Constant Ductility Spectra

Median constant ductility spectra – responses at specified values of ductility – are generated for both fixed-base and isolated systems. Comparison of these spectra gives insight to the relative cost and overall performance of systems that sustain similar levels of structural damage. To identify one point on a constant ductility spectrum, spectral response must be determined repeatedly for different R until the response converges to the desired ductility. This process is repeated for various values of ductility and natural period. For n observed response values x_i in a suite of ground motions, the median over the suite is

$$\hat{x} = \exp\left[\frac{\sum_{i=1}^{n} \ln x_i}{n}\right] \tag{16}$$

The parameter ranges considered in this study are as follows: T_s = 0 to 2 seconds, ductility μ = {1, 1.5, 2, 3, 4, 6, and 8}, T_{shift} = {1.5, 2, 3, and 4}, and normalized strength η = {0.2, 0.4, 0.6, and 0.8}. To ensure that the period shift is sufficient to lead to an effective isolation system, the range of T_s for isolated buildings is constrained by the requirement

$$\frac{T_s}{T_b} \leq 0.4 \tag{17}$$

Thus, for T_{shift} of 1.5 and 2, T_s is limited to 1.0 and 1.33 seconds, respectively, in all subsequent results. Furthermore, although exceptions may occur in practice, an upper bound superstructure period of T_s = 2 seconds has been selected for application of seismic isolation, because providing an adequate period shift is difficult beyond this.

Median constant ductility spectra – over the SAC-LA 10 in 50 suite – for the force reduction factor R and yield acceleration A_y as a function of superstructure period T_s are shown in Fig. 3.3 for fixed-base and isolated buildings with T_{shift} =2. The strength Q/W has been computed assuming η=0.4 [Eq. (9)]. Observe that to achieve the same ductility; force reduction factors R in isolated buildings are much smaller than those in fixed-base buildings. In the superstructure natural period range of greatest interest ($T_s < 1$ second), R for isolated buildings exceeds 2 only for the largest values of ductility [Fig. 3.3(b)]. In contrast, force reduction factors are much larger for fixed-base buildings, and the well-known long period equal displacement rule (Chopra 2007), which implies that $R = \mu$, is observed to hold approximately [Fig. 3.3(a)]. These results imply that force reduction factors must be limited in isolated buildings to constrain ductilities to reasonable values. Lower permitted force reduction factors suggest that the potential benefit of allowing base-isolated superstructures to respond inelastically may be less than expected. Relative to an elastic structure ($\mu = 1$), the reduction in yield acceleration A_y (i.e., design base shear) for increasing values of ductility is large for fixed-base buildings [Fig. 3.3(c)], and comparatively much smaller for isolated buildings [Fig. 3.3(d)].

Figures 3.4 and 3.5 demonstrate the influence of the period shift T_{shift} and the normalized strength η on force reduction factors R and total yield acceleration A_y, respectively, for isolated buildings. The force reduction factor R, which indicates relative force demands in elastic and inelastic superstructures, decreases as the period shift increases [Fig. 3.4(a)-(b)]. In other words, selecting a long isolation period limits the additional benefit of reduced design forces that can be achieved by allowing superstructure inelasticity. However, the influence of T_{shift} on R is small; for a given

period T_s the change in R over the considered range of T_{shift} is limited to about 15%.

The actual yield acceleration A_y incorporates the effects of both elastic demand and inelastic force reduction, and therefore allows an assessment of total strength demand for different systems. The yield acceleration of both elastic and inelastic superstructures drops markedly as T_{shift} increases [see Fig. 3.5(a), (c) and (e) or Fig. 3.5(b), (d) and (f)], which is expected since increasing the fundamental period should reduce overall force demands. Although R factors are smaller for larger values of T_{shift}, considerable benefit is still seen by increasing T_{shift} for isolated structures responding inelastically.

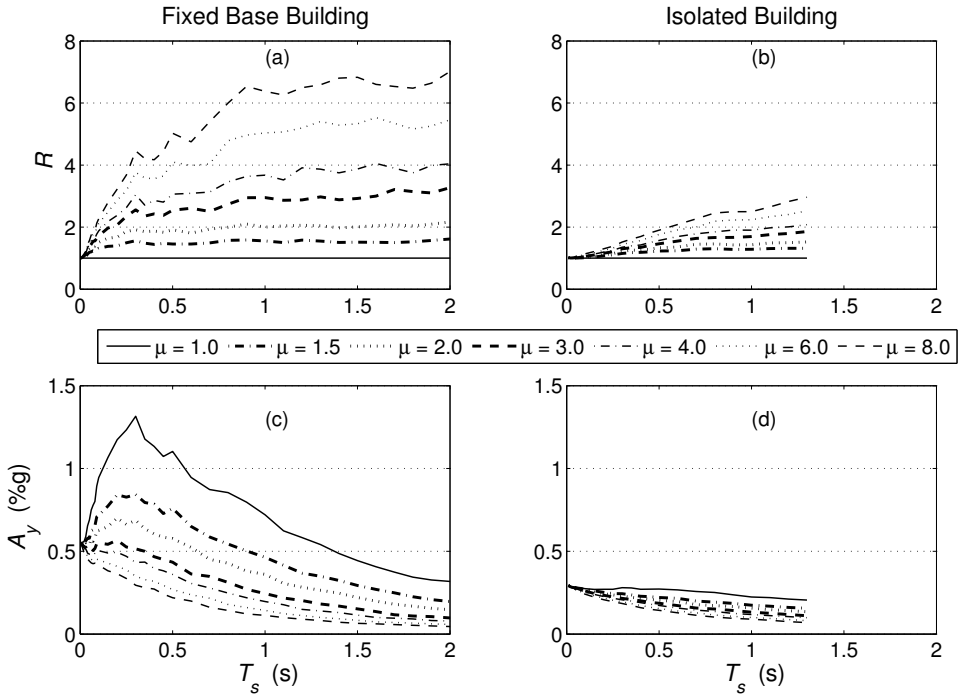

Fig. 3.3. Constant ductility spectra for (a)-(b) force reduction factor R and (c)-(d) yield acceleration spectra A_y. Spectra are shown for fixed-base buildings and base-isolated buildings with T_{shift} =2 and η=0.4.

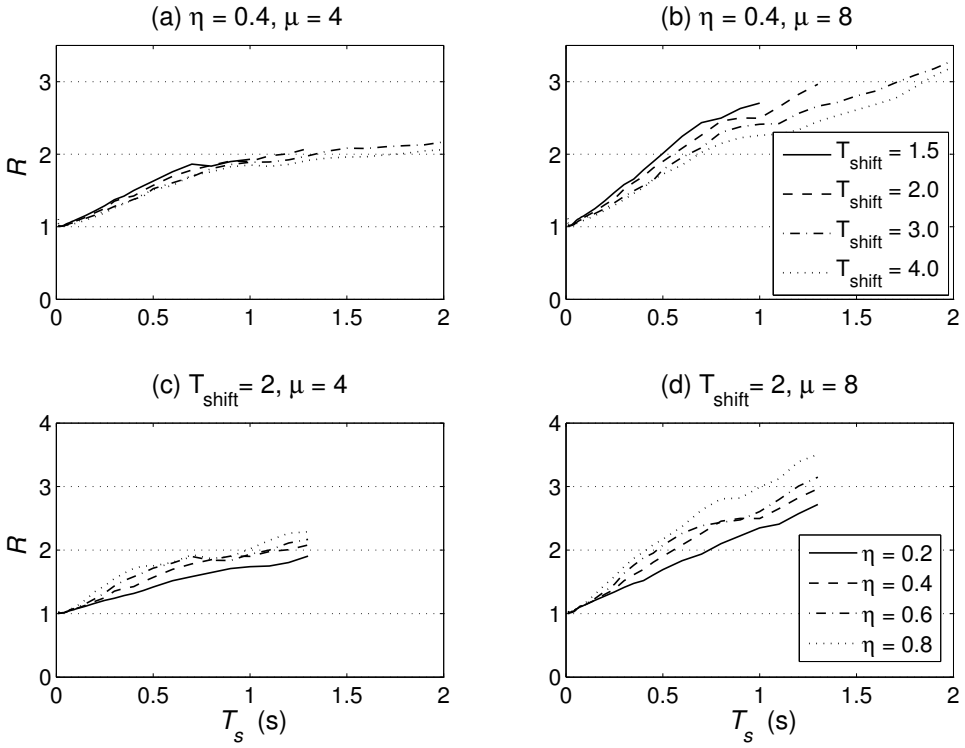

Fig. 3.4. Influence of T_{shift} on R for (a) $\mu = 4$ and (b) $\mu = 8$; and influence of η on R for (c) $\mu = 4$ and (d) $\mu = 8$.

For constant ductility, the force reduction factor R increases as the normalized strength η of the isolation system increases [Fig. 3.4(c)-(d)]. In design, the normalized strength or effective damping is often increased to limit the deformation demand on the isolation system, but at the expense of larger base shear demand on the superstructure. However, the trend observed here indicates that the larger superstructure force demands associated with increased η can be somewhat counteracted if moderate superstructure inelasticity is allowed, since the force reduction factor associated with a given damage state is larger. Figure 3.5, which compares A_y for η=0.4 [Fig. 3.5(a), (c) and (e)] and 0.8 [Fig. 3.5(b), (d) and (f)], supports this observation. In particular, the disparity in elastic acceleration spectra (μ=1) for strengths η=0.4 and 0.8 is large, but the disparity in yield

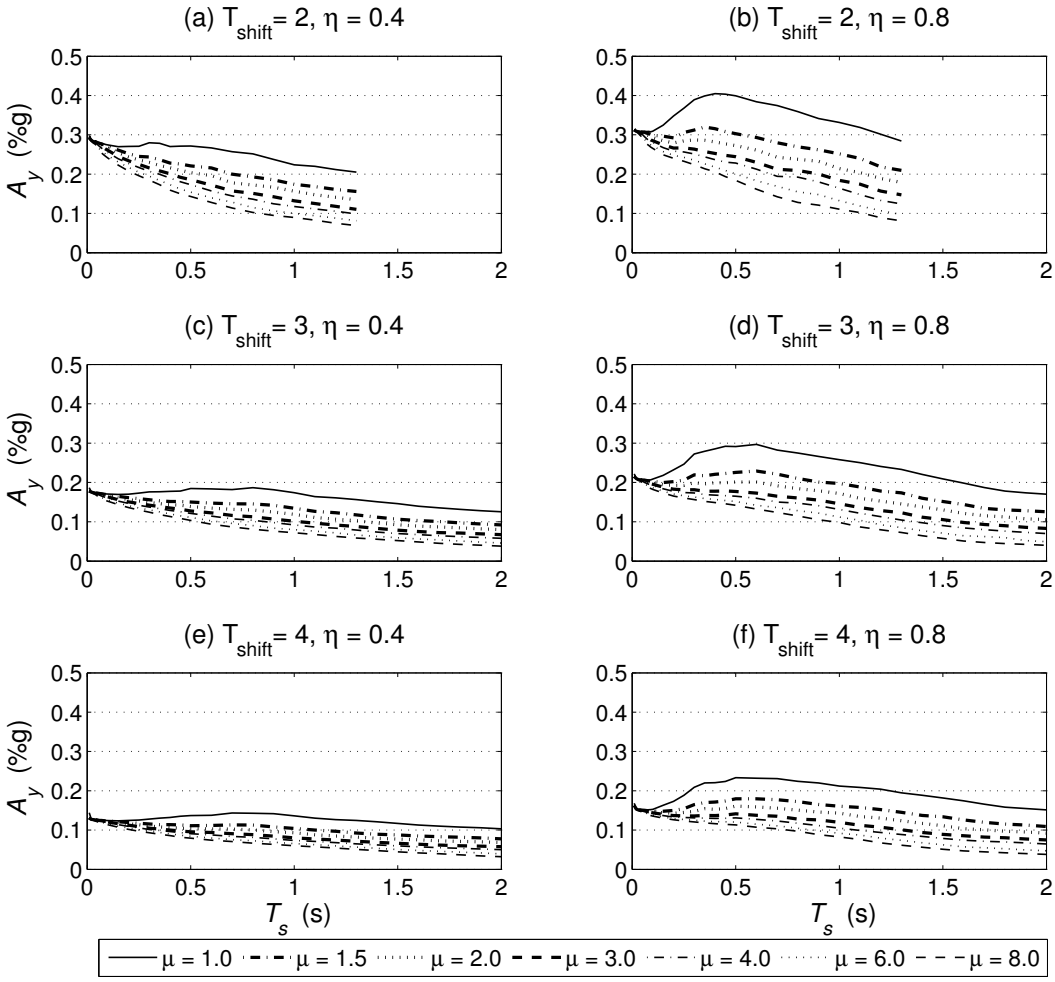

Fig. 3.5. Yield acceleration spectra A_y for isolated buildings with η=0.4 and (a) T_{shift} =2.0, (c) T_{shift} =3.0, (e) T_{shift} =4.0, and with η=0.8 and (b) T_{shift} =2.0, (d) T_{shift} =3.0, (f) T_{shift} =4.0.

acceleration spectra (especially μ=4 to 8) for η=0.4 and 0.8 is comparatively much smaller. On a side note, larger isolation system strength ($\eta = 0.8$) may have other detrimental effects, such as attracting higher mode response in the superstructure, which have not been analyzed here.

Performance Measures

Relative performance can be inferred by comparing various response quantities or engineering demand parameters of the fixed-base and the isolated building. Comparative

response quantities of interest are hereafter referred to as performance measures. Besides ductility, the performance measures selected here are peak structural deformation u_m and peak total acceleration a^t of the structure mass (i.e. roof acceleration). Structural deformation u_m is expected to indicate damage to structural elements and drift-sensitive nonstructural elements while roof acceleration a^t is expected to indicate damage to acceleration-sensitive nonstructural elements and contents.

Median values of these performance measures are again compared for fixed-base and isolated buildings (Fig. 3.6). Superstructure deformation u_m for fixed-base buildings is consistently larger than for isolated buildings [Fig. 3.6(a)-(b)]. For instance, at short superstructure periods (say 0.5 seconds) and small ductilities, u_m in fixed-base buildings is more than twice that in isolated buildings. The discrepancy is not as large as ductility μ increases, because u_m tends to taper off with increasing ductility in fixed-base buildings due to the equal displacement rule [Fig. 3.6(a)], but grows consistently with increasing ductility across the entire period range in isolated buildings [Fig. 3.6(b)].

From the comparative total acceleration spectra [Fig. 3.6(c)-(d)], the roof acceleration in isolated buildings is much lower than in fixed-base buildings, indicating that isolation may offer the benefit of reduced acceleration relative to a fixed-base building even when ductility, and hence structural damage, is comparable. Roof acceleration values are observed to be similar to the previously reported yield accelerations [Fig. 3.3(d) vs. 3.6(d)], which is reasonable since spectral acceleration and total acceleration are identical in undamped SDF systems (Chopra 2007). However, for the relatively simple system considered in this study, numerical results (not depicted graphically) indicated that the roof acceleration a^t ranges from 2 to 30% larger than the

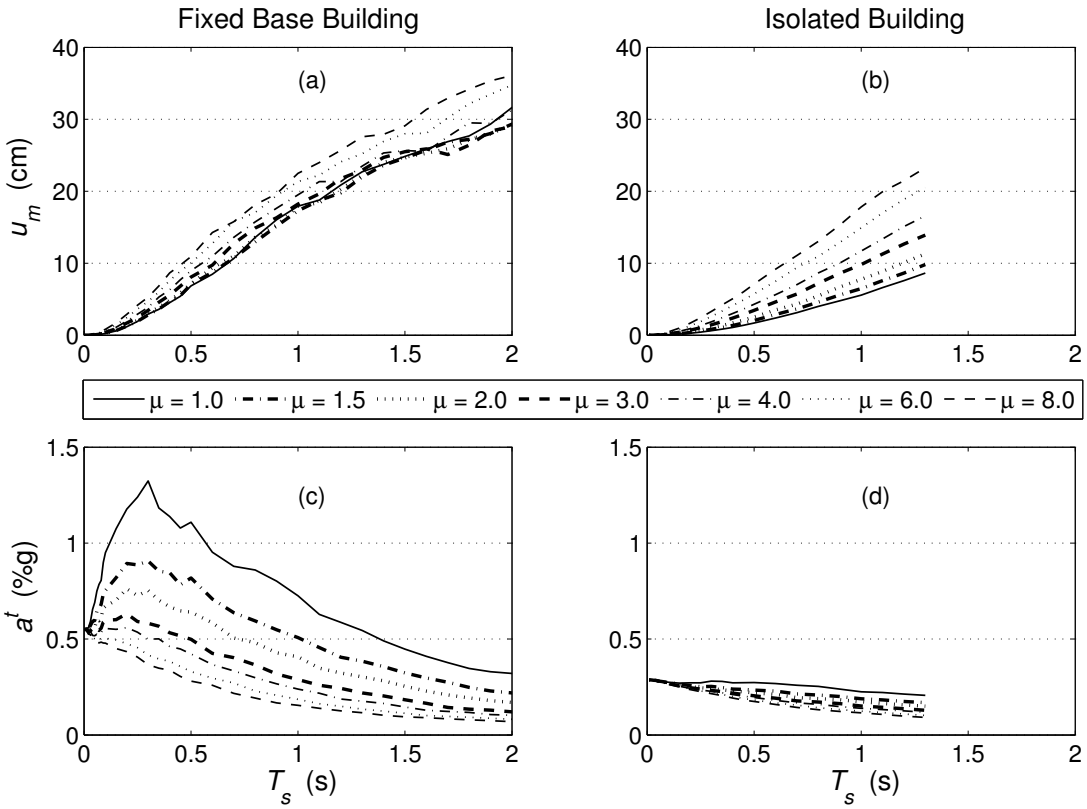

Fig. 3.6. (a) - (b) Peak inelastic deformation u_m and (c) - (d) absolute acceleration a^t of fixed-base buildings and isolated buildings ($T_{shift} = 2$ and $\eta = 0.4$), respectively.

yield acceleration A_y, and the discrepancy is greater with increasing ductility. Peak floor accelerations may increase further in multi-story building models that can better capture complex dynamic and higher mode effects.

The effect of isolation system properties T_{shift} and η on the deformation u_m and roof acceleration a^t is shown in Fig. 3.7 for two values of ductility (μ=4 and 8). As expected, the peak deformation u_m increases with decreasing period shift T_{shift} and increasing normalized strength η (representative of higher damping) [Fig. 3.7(a)-(b)]. The trends are the same for both values of ductility but peak deformation is consistently larger for a ductility of 8 [Fig. 3.7(b)].

The influence of η and T_{shift} is observed to be similar for the roof acceleration a^t

[Fig. 3.7(c)-(d)]. For both deformation and roof acceleration, the variation in period shift (ΔT_{shift}=2) results in greater variation in response than the variation in strength ($\Delta\eta$=0.4). Furthermore, the deformation response in longer period superstructures and the roof acceleration response in shorter period superstructures are most sensitive to the isolation system properties. In summary, increasing the isolation period shift and decreasing the strength, or energy dissipation, of the isolation system within reasonable limits helps to minimize the performance measures of the superstructure responding inelastically, similar to if it had remained elastic.

In a previous study, a comparative performance measure was proposed (Ryan *et al.* 2006) to assess the response of an isolated building relative to a fixed-base building. This combined performance measure (CPM) was defined as:

$$CPM\,(\%) = 100 * \left[\frac{1}{2}\left(\frac{\Delta_{iso} - \Delta_{FB}}{\Delta_{FB}} \right) + \frac{1}{2}\left(\frac{a^t{}_{iso} - a^t{}_{FB}}{a^t{}_{FB}} \right) \right] \tag{18}$$

where $(\Delta_{iso}, a^t{}_{iso})$ and $(\Delta_{FB}, a^t{}_{FB})$ are the peak story drift and peak roof acceleration in isolated and fixed-base buildings, respectively, with identical superstructure periods T_s and responding with identical ductilities. A negative CPM indicates an average percent reduction in response of the base-isolated superstructure relative to the fixed-base structure. Limitations of the CPM are: (1) it cannot compare the response of many fixed-base and isolated structures with different strengths and/or responding with different ductilities, and (2) it cannot indicate whether the systems under consideration meet a desired performance objective.

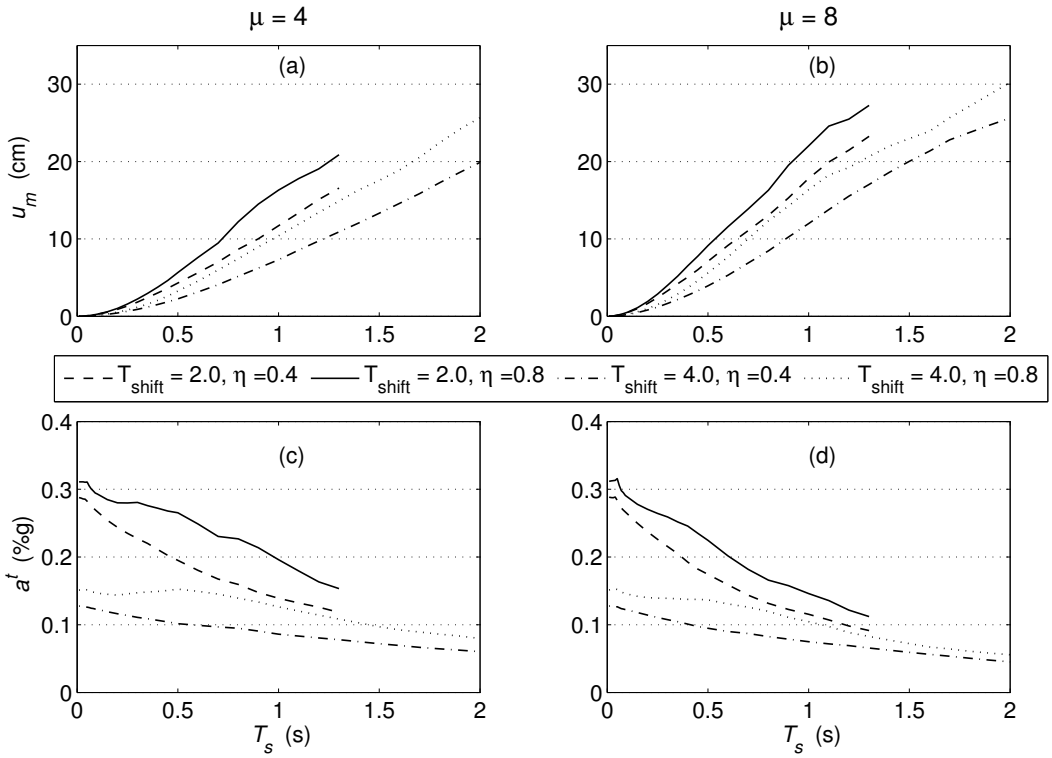

Fig. 3.7. (a) - (b) Peak inelastic deformation u_m and (c) - (d) absolute acceleration a^t of isolated buildings for μ=4 and 8, respectively.

A new comparative measure is introduced here that can remedy these deficiencies. The response index (RI) is defined as:

$$RI = \sum_i \left[w_i \frac{f_i}{f_{i,target}} H\left(f_{i,target} - f_i\right) + H\left(f_i - f_{i,target}\right) \right] \tag{19}$$

where w_i are weight factors assigned to each performance measure, such that the sum of the weight factors equals one ($\sum w_i = 1$); f_i and $f_{i,target}$ are the observed value and target value of the i^{th} performance measure, respectively; and $H(\ )$ represents the Heaviside step function, where

$$H(f_i - f_{i,target}) = \begin{cases} 1 \text{ if } (f_i - f_{i,target}) > 0 \\ 0 \text{ if } (f_i - f_{i,target}) < 0 \end{cases} \tag{20}$$

If a given performance measure meets its target value, then $H(f_{i,target} - f_i) = 1$ and the

first term in Eq. (19) contributes, adding to RI a weighted ratio of the observed to target performance measure. If the performance measure exceeds its target value, then $H(f_i - f_{i,target}) = 1$ and the second term in Eq. (19) contributes, adding 1 to RI.

Thus, when all target performance measures are met, RI < 1, and its value reflects the average improvement in observed response relative to the performance objective. RI > 1 indicates not only that the performance objective is not met but also in how many measures it fails, since 1 is added to RI for each performance measure exceeding the target value (i.e., 1 < RI < 2 indicates failure in one measure, 2 < RI < 3 indicates failure in two measures, and so on).

In this study, the performance measures are ductility μ, peak deformation u_m and roof acceleration a^t, and Eq. (19) specializes to:

$$RI = \frac{1}{3}\frac{\mu}{\mu_{target}} H(\mu_{target} - \mu) + \frac{1}{3}\frac{u_m}{u_{m,target}} H(u_{m,target} - u_m) + \frac{1}{3}\frac{a^t}{a^t_{target}} H(a^t_{target} - a^t) + H(\mu - \mu_{target}) \quad + H(u_m - u_{m,target}) \quad + H(a^t - a^t_{target}) \tag{21}$$

Here identical weights of 1/3 have been assigned to each performance measure, but the weights can be varied to place greater emphasis on some measures over others.

Trends for RI

Next, the RI for fixed-base and isolated buildings, computed by Eq. (21), is analyzed for life safety and immediate occupancy performance objectives. Target values of ductility μ, peak deformation u_m (in terms of story drift Δ) and roof acceleration a^t for each performance objective are listed in Table 3.2. Available information relating target performance measures to performance objectives is sparse, and guidance to assist owners

in the selection of loss-based performance objectives, as envisioned for the future of performance-based engineering, is yet to be developed (ATC 2007). Thus, the values chosen in this study are approximate and demonstrative of the comparative process.

An intermediate ductility of 6 has been selected as the target for life safety based on the known relation between ductility and the code-specified force reduction factor R. The target ductility for immediate occupancy has been adjusted accordingly. Target deformation is specified in terms of drift, using provisions in FEMA 356 for life safety and immediate occupancy. Here, the percent story drift is estimated from the peak deformation based on empirical relations between superstructure period and total height: $\Delta = 100u_m / hN$, where h is an approximate story height of 381 cm (12.5 ft), and N is the number of stories, which is estimated from $T_s = 0.2N$. Roof acceleration is especially difficult to quantify. Accelerations obtained from four instrumented building shaken in the Loma Prieta and Northridge earthquakes ranged from 0.24 to 1.5g (Miranda and Taghavi 2005). Accordingly, the target acceleration for immediate occupancy has been set close to the lower bound value, while the target acceleration for life safety has been set slightly higher. This rather strict acceleration criterion helps to emphasize the difference between fixed-base and isolated building performance.

For the two performance objectives, Fig. 3.8 illustrates RI for several fixed-base and corresponding isolated buildings, computed from the median responses over the SAC-LA 10 in 50 suite. For the life safety objective [Fig. 3.8(a), (c) and (e)], isolated buildings show markedly improved performance compared to fixed-base buildings over the range of acceptable ductility. Isolated buildings fail to meet the objective only when $\mu = 8$, which exceeds the target ductility of 6.

Table 3.2. Target Values of Performance Measures for Different Performance Objectives

Performance objective	Target Δ	Target a^t	Target μ
Life safety	2.5%	0.5g	6
Immediate occupancy	0.7%	0.3g	4

Fixed-base buildings, even those designed to remain elastic, frequently fail to meet the target roof acceleration in the period range of interest (T_s = 0 to 1 seconds), where RI is observed to be between 1 and 2. Relative to the life safety objective, an elastic isolated building has the best performance, but the margin of improvement over an isolated building with a ductility of 4 is small, and the designs with ductilities of 4 or 6 may be more economical [Fig. 3.8(c) and (e)]. Fixed-base buildings are unable to meet the immediate occupancy objective; that is RI > 1 for all values of ductility, and even an elastic building fails to meet the drift requirement over much of the period range [Fig. 3.8(b)]. For ductilities up to the target ductility of 4, isolated buildings easily meet the immediate occupancy objective [Fig. 3.8(d) and (f)]. Isolated buildings with $\mu > 4$ fail to meet target ductility (RI > 1) and sometimes fail to meet target drift as well (RI > 2). At the same ductility, isolated buildings have lower yield accelerations A_y than fixed-base buildings, and are thus able to achieve much lower drifts and roof accelerations. As T_{shift} increases [Fig. 3.8(c),(e) and (d),(f)], RI decreases, which is consistent with earlier observations that increasing the period shift leads to reduced deformations and accelerations.

Strength and Performance Comparison Examples

Next, examples are presented that simultaneously compare required design strength and performance in fixed-base and isolated buildings. Tabulated results compare

the yield acceleration A_y and RI for life safety and immediate occupancy objectives in fixed-base and isolated buildings with T_{shift} =2 or 4 and $\eta = 0.4$. The yield acceleration, indicative of the design yield strength or base shear coefficient, can be loosely correlated to the superstructure design cost, although many other factors contribute to the overall project cost. Comparisons are presented for $T_s = 0.5$ seconds (Table 3.3) and T_s =1 second (Table 3.4), consistent with data in Figs. 3.3(c), 3.5(a), 3.5(c), and 3.8. These comparisons, which assume the same natural period of the building with and without isolators, neglect the likely differences in superstructure design for a fixed-base building and the same building on isolators.

Isolated buildings designed by the current code standards essentially remain elastic when overstrength contributes. For an isolated structure with T_s = 0.5 seconds and T_{shift} = 2 (Table 3.3), the force in the superstructure remaining elastic (A_y = 0.27 g) is the same as in the fixed-base building with μ = 6, which corresponds to a life safety performance objective. The response improvement of the isolated building (RI = 0.26) over the fixed-base building (RI = 0.69) is substantial, but may be overlooked when minimal life safety performance is desired. Since both building types meet the performance objective (RI < 1), motivation to select isolation system is lacking as the added costs associated with the design of the isolation system (e.g. devices, testing and displacement gap) are substantial.

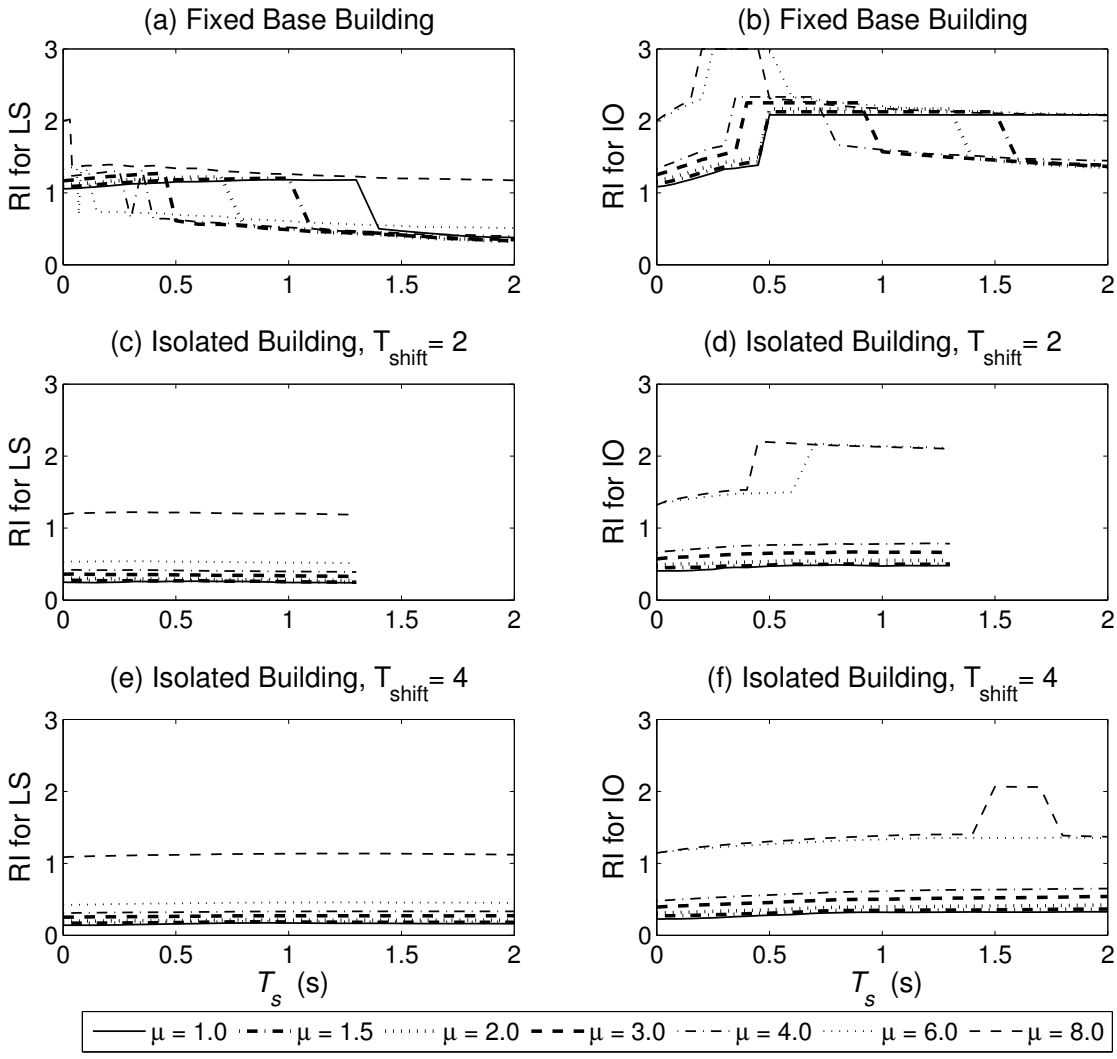

Fig. 3.8. Response index (RI) for fixed-base and isolated buildings with T_{shift} = 2 and T_{shift} = 4 ($\eta = 0.4$) for (a), (c), (e) life safety performance objective, and (b), (d), (f) immediate occupancy performance objective.

Table 3.3. Yield Acceleration A_y (= Yield Force Coefficient f_y/w) and RI for Life Safety (RI-LS) and Immediate Occupancy (RI-IO) Performance Objectives for Specified Ductility μ; T_s =0.5 sec and η=0.4

	Fixed Base			T_{shift}=2			T_{shift}=4		
	A_y (%g)	RI-LS	RI-IO	A_y (%g)	RI-LS	RI-IO	A_y (%g)	RI-LS	RI-IO
μ =1	1.10	1.15	2.08	0.27	0.26	0.47	0.14	0.16	0.28
μ =4	0.36	0.63	2.33	0.17	0.41	0.77	0.101	0.32	0.56
μ =6	0.27	0.69	3.0	0.14	0.54	1.49	0.097	0.44	1.27

Table 3.4. Yield Acceleration A_y (= Yield Force Coefficient f_y/w) and RI for Life Safety (RI-LS) and Immediate Occupancy (RI-IO) Performance Objectives for Specified Ductility μ; T_s = 1 sec and η=0.4

	Fixed Base			T_{shift} = 2			T_{shift} = 4		
	A_y (%g)	RI-LS	RI-IO	A_y (%g)	RI-LS	RI-IO	A_y (%g)	RI-LS	RI-IO
μ =1	0.72	1.18	2.08	0.22	0.25	0.47	0.14	0.17	0.32
μ =4	0.19	0.52	1.6	0.12	0.40	0.78	0.086	0.33	0.61
μ =6	0.14	0.61	2.21	0.08	0.52	2.14	0.079	0.45	1.33

Alternatively, suppose that the only stipulation on the isolation system design is that it meets the performance objective, and design alternatives are evaluated based on combined strength demand and performance. The lowest strength fixed-base building to meet the life safety objective (μ = 6) has A_y = 0.27g and RI = 0.69, while isolation solutions such as T_{shift} = 2 (A_y = 0.14g and RI = 0.54) and T_{shift} = 4 (A_y = 0.08g and RI = 0.44) are possible. Although the design strength is on the order of 2 to 3 times smaller, the performance of the isolated buildings as measured by RI still exceeds that of the fixed-base building. Even the immediate occupancy objective (μ = 4) can be satisfied in an isolated building with only a small increase in design strength (A_y = 0.17g).

Similar observations are made for a building with a 1 second superstructure period (Table 3.4). At identical ductilities (μ = 6), A_y = 0.14g and RI = 0.61 for the fixed-base building while A_y = 0.08g and RI = 0.52 for the isolated building with T_{shift} = 2. The isolated building therefore outperforms the fixed-base building at just over half of the superstructure design force. Increasing T_{shift} to 4 has only a small influence on design strength (A_y = 0.07g) and performance (RI = 0.45). Again, an isolated building that meets the immediate occupancy objective (μ = 4) has lower superstructure design strength (A_y = 0.12g for T_{shift} = 2, or A_y = 0.07g for T_{shift} = 4) than a fixed-base building that meets life safety (A_y = 0.14g).

Conclusions

The possibility of allowing the superstructures of isolated buildings to respond inelastically – with deformation ductilities comparable to those of fixed-base buildings – has been investigated. Response history analysis results have demonstrated that given comparable ductility, force reduction factors *R* in base-isolated buildings are smaller than in fixed base buildings, but superstructure design forces in isolated buildings can still be reduced considerably. Also, at the same superstructure ductility, isolated buildings showed greatly enhanced performance with respect to superstructure deformation and total acceleration demands. Thus, isolated buildings designed to reduced strength, which is expected to correlate to reduced design costs, still outperform fixed-base buildings.

Force reduction factors for isolated buildings tend to decrease with increasing isolation period shift, which limits the benefit of reducing forces by allowing superstructure inelasticity, but increase with increasing isolation system strength, which somewhat counteracts the larger superstructure force demands associated with increased strength. In general, the inelastic superstructure response is less sensitive to the isolation system properties than an elastic superstructure.

A response index (RI) has been developed to allow relative response evaluation of fixed-base and isolated buildings, and to allow different designs to be evaluated against a quantifiable performance objective, such as life safety and immediate occupancy. The performance objective is quantified in terms of target values of performance measures (e.g. ductility, drift and acceleration). The RI can be used to identify the best performing system, the minimum strength system that meets performance requirements, or the system that is an ideal combination of both considerations.

When evaluated for a life safety performance objective, the superstructure design strength of an isolated building is less than that of a fixed-base building with identical ductility, and the isolated building generally has improved performance as quantified by RI. Target ductility is a pivotal factor controlling the immediate occupancy objective, since isolated buildings typically meet target drift and acceleration criteria easily. If moderate ductility can be allowed in an immediate occupancy objective, isolation systems can meet this objective with low superstructure design forces whereas comparable ductility fixed-base buildings will fail.

The analysis in this study has allowed for rapid prototyping of fixed-base and isolated building response based on basic superstructure and isolation system properties. Further research is needed to extend the concepts developed here to be used within the envisioned loss-based performance objective framework. As limitations on the current study, the systems examined in this paper do not recognize the relationship between superstructure strength and stiffness that may constrain the relative parameters. Further, more work is needed to verify that the trends observed in this study, especially with respect to roof acceleration response, are applicable to more dynamically complex multi-story systems. Finally, the susceptibility of base-isolated buildings to rapid displacement pulses with dominant frequencies in the longer period range remains a legitimate concern, and should be explored rigorously for isolated buildings with inelastic superstructures.

References

Applied Technology Council (ATC) (2007). "Guidelines for seismic performance assessment of buildings 35% Complete.", *Draft prepared for the Department of Homeland Security,* Washington, D.C.

Ceccoli, C., Mazzotti, C., and Savoia, M. (1999). "Non-linear seismic analysis of base-isolated RC frame structures." Earthquake Engineering and Structural Dynamics, 28(6):633-653.

Chopra, A. K. (2007). *Dynamics of Structures: Theory and applications to earthquake engineering*, 3rd Ed., Prentice-Hall, Inc., Upper Saddle River, N.J.

International Conference of Building Officials (ICBO) (1991). *Uniform Building Code*, Whittier, Calif.

International Conference of Building Official (ICBO) (1997). *Uniform Building Code*, Volume 2, Whittier, Calif.

Kikuchi, M., Black, C. J., and Aiken, I. D. (2008). "On the response of yielding seismically isolated structures." *Earthquake Engineering and Structural Dynamics*, 37(5), 659-679.

Krawinkler, H. (ed.) (2005). "Van Nuys hotel building testbed report: exercising seismic performance assessment." *PEER 2005-11*. Pacific Earthquake Engineering Research Center, University of California, Berkeley, Calif.

Lin, A. N., and Shenton, H. W., III. (1992). "Seismic performance of fixed-base and base-isolated steel frames." *J. Eng. Mech.*, 118(5), 921-941.

Mayes, R.L., Jones, L.R., and Kelly, T.E. (1990). "The economics of seismic isolation in buildings." *Earthquake Spectra,* 6(2), 245-263.

Miranda, E., and Aslani, H. (2003). "Probabilistic response assessment for building specific loss estimation." *PEER 2003-03*. Pacific Earthquake Engineering Research Center, Univ. of California, Berkeley, Calif.

Miranda, E., and Taghavi, S. (2005). "Approximate floor acceleration demands in multi-story buildings. II: Application." *J. Struct. Eng.,* 131(2), 212–220.

Naaseh, S., Morgan, T. A., and Walters, M. T. (2002). "A critical evaluation of current U.S. building code provisions and FEMA guidelines for the design of seismic isolated structures, *Proc., ATC 17-2 Seminar on Seismic Isolation, Passive Energy Dissipation and Active Control*, Applied Technology Council, Los Angeles, CA.

Ordonez, D., Foti, D. and Bozzo, L. (2003). "Comparative study of the inelastic response of base isolated buildings." Earthquake Engineering and Structural Dynamics, 32(1):151-164.

Palazzo, B., and Petti, L. (1996). "Reduction factors for base isolated structures." *Computers and Structures,* 60(6):945-956.

Porter, K., Kennedy, R., and Bachman, R. (2007). "Creating fragility functions for performance-based earthquake engineering." *Earthquake Spectra*, 23(2), 471-489.

Ryan, K. L., and Chopra, A. K. (2004). "Estimation of seismic demands on isolators based on nonlinear analysis." *J. Struct. Eng*., 130(3), 392-402.

Ryan, K. L., Morgan, T. A., and Sayani, P. (2006). "Consistent performance comparison of seismic-isolated and fixed-base buildings." *Proc. 8th U.S. National Conf. of Earth-quake Engineering*, San Francisco, Calif, Paper No. 1617.

SEAOC (1995). Vision 2000 – Performance *based seismic engineering of buildings*, Vol I, II, Structural Engineers Association of California,Vision 2000Committee. Sacramento, Calif.

Shenton, H. W., III, and Lin, A. N. (1994). "Relative performance of fixed-base and base-isolated concrete frames." *J. Struct. Eng.,* 119(10), 2952-2968.

Somerville, P., Anderson, D., Sun, J., Punyamurthula, S., and Smith, N. (1998). "Generation of ground motion time histories for performance-based seismic engineering." *Proc. 6th U.S. National Conf. of Earthquake Engineering*, Seattle, Washington.

CHAPTER 4

COMPARATIVE PERFORMANCE OF LOW-RISE BASE-ISOLATED AND CONVENTIONAL STEEL MOMENT RESISTING FRAME BUILDINGS FOR LOSS ESTIMATION

Abstract In this study, the life cycle performance of code-designed conventional and base-isolated steel frame buildings is evaluated using loss estimation methodologies. The results of hazard and structural response analysis for three-story moment resisting frame buildings are presented in this paper. Three dimensional models for both buildings are created and seismic response is assessed for three scenario earthquakes. The response history analysis results indicate that the performance of the isolated building is superior to the conventional building in the design event. However, for the Maximum Considered Earthquake, the presence of outliers in the response data reduces confidence that the isolated building provides superior performance to its conventional counterpart. The outliers observed in the response of the isolated building are disconcerting and need careful evaluation in future studies.

Introduction

The principal benefit of seismic isolation for buildings, to offer far superior performance in a design level earthquake, is generally accepted and recognized by structural engineers. With seismic isolation, flexible devices installed at the base lengthen or shift the building's natural period to the low acceleration region of the spectrum. Consequently, an isolated building accommodates the lower design forces elastically, and structural damage is eliminated or greatly reduced relative to a conventional building that

accommodates the design forces through inelastic response. However, only 10-20% of the value in a typical U.S. building is apportioned to the structural system, while at least 80% is apportioned to nonstructural components and building contents (ATC 2008a; Taghavi and Miranda 2003). Post-earthquake observations (Kircher *et al.* 1997; Porter *et al*. 2002; Comerio and Stallmeyer 2002) suggest that on average, losses in nonstructural components far outweigh the costs of damage to structural elements. Fortunately, lower accelerations experienced in isolated buildings lead to greatly reduced damage in acceleration-sensitive nonstructural components.

In the U.S., seismic performance objectives, which differ for isolated and conventional systems, are only implicitly embedded in code design standards (BSSC 2004; ASCE 2005; ICC 2006), and the performance benefits generally are not recognized by building owners and decision makers. The business culture cultivates an emphasis on initial rather than lifetime costs of structural systems. Design performance objectives are rarely discussed with stakeholders, and a typical building owner expects that a code compliant building will retain operability following an earthquake. Even sophisticated owners that initially require or are convinced to choose higher performance are constrained by initial costs. When faced with additional complexities of seismic isolation design, such as analysis procedures, involved device testing requirements, and a lengthy design review process, these owners, in consultation with design professionals, often opt for alternative systems. However, performance approaches based on stiffening, strengthening, or even energy dissipation, are not nearly as effective as seismic isolation in eliminating acceleration related damage. Seismic isolation has the potential to be routinely adopted if reliable analysis tools are available to predict economic outcomes,

and cultural transformation leads to routine discussion of lifetime economics as a basis for making design decisions.

Methodologies for performance evaluation and life cycle cost estimation have been under development for many years, with major investment by the earthquake engineering research centers (Moehle and Deierlein 2007; MAE 2009). Several comprehensive, structure specific examples have been developed that demonstrate alternative details in carrying out the methodology (Comerio 2005; Krawinkler 2005; Haselton *et al.* 2007). The Pacific Earthquake Engineering Research (PEER) Center approach is currently being adapted for practice by ATC-58, wherein partial guidelines (ATC 2007) and a loss estimation tool have been released. The PEER approach measures performance in terms of probabilistic decision variables, such as repair costs, downtime, indirect profit loss, and casualties (Miranda and Aslani 2003). The consequence analysis is deconstructed into four basic stages: hazard analysis to determine ground motion intensity, structural response analysis to determine engineering demand parameters, damage analysis to determine damage indicators, and loss analysis to determine the decision variables. Considering the intermediate variables at each stage to be discrete random variables, the analyses are combined by integration over each random variable to determine the expected annual losses according to the total probability theorem.

To our knowledge, conventional and seismic-isolated buildings thus far have not been comparatively evaluated using the PEER loss estimation methodology. However, closely related techniques have been applied to evaluate seismic protection strategies applied to buildings (Bruno and Valente 2002) and bridges (Hahm *et al*. 2004). A number of studies have developed fragility functions – probabilistic functions relating damage

measures to metrics of response or ground motion intensity – for isolated structures (Karim and Yamazaki 2007; Mezzi and Comodini 2008; Zhang and Huo 2009), but stopped short of predicting economic consequences. Comparative assessments of isolated and conventional buildings strictly limited to responses are numerous (Shenton and Lin, 1994; Lin and Shenton 1992; Hall and Ryan 2000; Dolce and Cardone 2003; Hamidi *et al*. 2003; Agarwal *et al*. 2007; Dolce *et al*. 2007).

A total probabilistic evaluation of performance inevitably involves the consideration of a wide range of ground motion intensities, including low probability events that exceed the design ground motion. Yielding of the isolated superstructure in extreme events is likely and the associated response trends have been examined by many (Pinto and Vanzi 1992; Palazzo and Petti 1996; Ceccoli *et al*. 1999; Naaseh *et al*. 2002; Ordonez *et al*. 2003; Politopoulos and Sollogoub 2005; Kikuchi *et al*. 2008; see Chapter 3). A key observation is that an isolated structure, upon yielding, accumulates ductility in the superstructure more quickly than a comparable conventional building, and thus the drift demand in the isolated superstructure can in fact be greater than in a comparable conventional building. Furthermore, ATC-63 (ATC 2008b) concluded that, when designed by current code standards, conventional and seismic isolated RC buildings have about the same probability of collapse in the Maximum Considered Earthquake (MCE).

The overarching objective of our study is to comparatively evaluate the life cycle performance of code-designed 3-story conventional and base-isolated steel moment resisting frame buildings using the PEER loss estimation methodology. The overall cost versus benefit of seismic isolation will be analyzed through comparison of initial design costs and expected economic losses (repair costs, downtime, etc.) over the life of the

buildings. A moment frame has been selected to address whether a similar benefit can be provided by applying isolation to a relatively flexible lateral system compared to an ideal stiff system. Post-Northridge moment resisting frames are attractive, providing reliable seismic performance and allowing for flexibility of architectural design. A number of mid-rise steel moment frame isolated buildings are in various phases of the design and construction process in California.

Using a two-phase presentation, the hazard analysis and structural response analysis results are presented here, while the actual cost/benefit study, including initial and life cycle cost estimation through damage analysis and loss analysis will be presented in a follow-up paper. For our complete study, ground motions are selected for nine discrete earthquake scenarios representing various annual probabilities of exceedance on the seismic hazard curve. Response measures for three of the nine scenarios are presented and analyzed here.

Design and Modeling Assumptions for the Buildings

Design Assumptions

Hypothetical three-story conventional and base-isolated moment resisting frame buildings were designed by Forell/Elsesser Engineers Inc. for use in this study. These office buildings (occupancy category II and importance factor I = 1.0) were designed by the *Equivalent Lateral Force Method* based on 2006 International Building Code (ICC 2006), ASCE 7-05 (ASCE 2005), and AISC 341-05 (AISC 2005). The buildings were designed for Los Angeles, CA location (Latitude: 34.50 N, Longitude: 118.2 W) on stiff soil (site class D with reference shear wave velocity = 180 to 360 m/s). The mapped

spectral accelerations for this location are $S_s = 2.2g$ for short periods and $S_1 = 0.74g$ for a 1 second period (g = acceleration due to gravity).

The conventional building was detailed for high ductility as a special moment resisting frame (SMRF), and uses reduced beam section (RBS or "dogbone") connections, which are the only pre-qualified welded connections permitted by AISC 341-05 (AISC 2005). However, the isolated building, which has lower ductility requirements, was detailed as an intermediate moment resisting frame (IMRF) utilizing welded unreinforced flange, welded web (WUF-W) beam-column connections. As such, design force reduction factors were $R = 8$ for the SMRF and $R_I = 1.67$ for the isolated IMRF – assuming a design yield strength of 345 MPa (50 ksi) for structural steel – while design drift limits were 2.5% for the SMRF and 1.5% for the isolated IMRF. The design of both buildings was drift controlled.

The building configurations are based on the plan layout for the 3-story SAC steel buildings (FEMA 2000a) with modifications (Fig. 4.1). The buildings are 55 m by 36.6 m (180 ft by 120 ft) in plan, with story heights of 4.57 m (15 ft) and column spacing of 9.15 m (30 ft) in each direction. Lateral resistance is provided by two 5-bay perimeter moment frames in the X-direction, and two 3-bay perimeter and two 2-bay interior moment frames in the Y-direction; moment-resisting bays are indicated by bold lines in Fig. 4.1. The steel sections selected for the moment-resisting frame members are listed in Table 4.1. Floor slabs are composed of 82.5 m (3.25 in) thick lightweight concrete over 50.8 mm (2 in) thick steel deck.

Seismic mass properties were calculated from anticipated gravity loads on the floors and roof, which in addition to the weight of the structural frame members,

includes: floor/roof dead loads computed from slabs = 2.01 kPa (42 psf), super-imposed floor dead load = 1.1 kPa (23 psf), super-imposed roof dead load = 1.2 kPa (25 psf), and exterior cladding load = 0.96 kPa (20 psf). For the conventional building, the seismic weights of each story were computed as 8561 kN (1924 kips), 8532 kN (1918 kips), and 8922 kN (2005 kips) at the first, second and roof floor, respectively. For the isolated building, the seismic weights of each story were computed as 7765 kN (1745 kips), 8085 kN (1817 kips), 8063 kN (1812 kips) and 8728 kN (1962 kips) at the base, first, second, and roof floors, respectively.

The design displacement D_D of the isolators in the design earthquake and the maximum displacement D_M in the MCE at the center of rigidity are computed as (ASCE 2005):

$$D_D = \frac{gS_{D1}T_D}{4\pi^2 B_D} \quad , \quad D_M = \frac{gS_{M1}T_M}{4\pi^2 B_M} \tag{1}$$

where T_D, T_M are effective isolation periods; B_D, B_M are coefficients that modify the spectrum for damping; and S_{D1}, S_{M1} are the 1 second spectral accelerations for the corresponding events. Target values of T_M = 3.07 sec and effective damping ratio β_M = 16% were chosen for the MCE, while design values T_D and β_D were determined by iteration (Table 4.2).

Table 4.1. Member Sizes for the Conventional SMRF and Isolated IMRF

Frame	Story	Columns	Beams
SMRF	Roof	W14x211	W27x102
	2	W14x370	W33x130
	1	W14x370	W33x141
IMRF	Roof	W14x109	W18x60
	2	W14x176	W24x76
	1	W14x176	W24x84

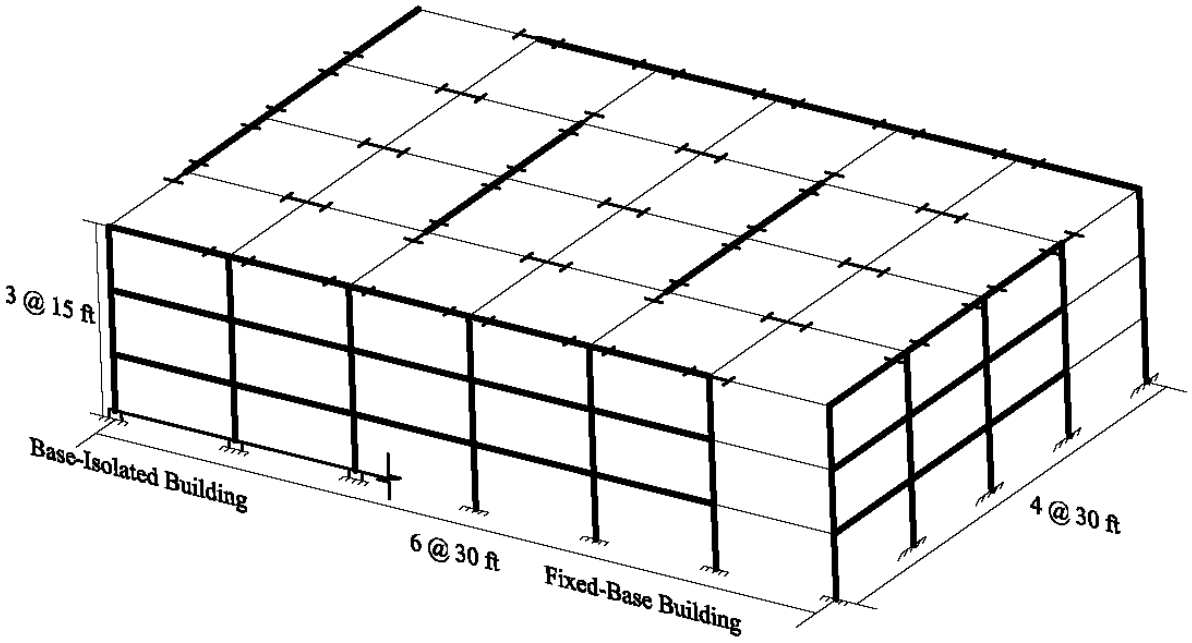

Fig. 4.1. 3D view of the building elevation and plan layout.

The total isolator displacement in Table 4.2 accounts for displacement amplification due to accidental torsion (Eq. 17.5-5 and 17.5-6 of ASCE, 2005). The isolation devices have not been designed in detail so as to keep the study neutral with respect to isolation system. Note that the isolated building does not qualify for design exclusively by the equivalent lateral force method because $S_1 > 0.6g$ and the Maximum Considered Earthquake (MCE) effective period $T_M > 3.0$ seconds (ASCE 2005). However, use of typical response spectrum or response history analysis procedures would likely reduce the peak forces and isolator displacements to be used in design.

Modeling Assumptions

Models for evaluation were based on both ASCE 7 (ASCE 2005) for design of new buildings and ASCE 41 (ASCE 2007) for evaluation of existing buildings.

Table 4.2. Design Parameters for the Isolation Systems

Isolator Properties	DBE	MCE
Effective Period	T_D = 2.77 sec	T_M = 3.07 sec
Effective Damping	B_D = 24.2 %	B_M = 15.8 %
Isolator Displacement	D_D = 32.1 cm (12.7 in.)	D_M = 61.7 cm (24.3 in.)
Total Displacement	D_{TD} = 38.8 cm (15.3 in.)	D_{TM} = 74.6 cm (29.4 in.)

Detailed three dimensional (3D) numerical models of both buildings were developed in the OpenSees computational environment. Although the buildings are symmetric about both axes, the mass centers were shifted by 5% of the longest plan dimension in both directions to account for accidental torsion, as required by ASCE 7 for dynamic analysis (ASCE 2005). Equivalent mass and rotational inertia were lumped at the center of mass. Slab action was accounted for through a rigid diaphragm constraint, except at the base level of the isolated IMRF, where slabs were explicitly modeled with shell elements to enhance the rigidity of the model against local isolator uplift.

Member capacities were based on the expected yield strength of structural steel f_{ye} = 379 MPa (55 ksi) rather than the nominal design strength (ASCE 2007). All columns and moment resisting beams were modeled using force-based nonlinear beam-column elements that combine finite length "plastic hinge" regions at the element ends with an interior elastic region (Scott and Fenves 2006). The nonlinear constitutive relationship in the plastic hinge regions can be defined using either stress-resultant models or fiber sections. All columns were modeled using *fiber* sections that inherently account for moment-axial force interaction at each analysis step. However, stress resultant models were chosen for the moment resisting beam elements, since fiber sections may be influenced by axial loads artificially generated to satisfy the rigid diaphragm constraint. The steel stress-strain relationship for fiber sections and moment-curvature relationship

for stress resultant models were both assumed to be bilinear with a strain hardening ratio of 3%. Gravity beams were modeled using elastic frame elements with moment releases at both ends. In the conventional SMRF, moment resisting and gravity columns were fixed and pinned at the base, respectively; while in the isolated OCBF, fixed connections were assumed at all beam-column joints at the base level.

Energy dissipation was applied to the conventional structure and the isolated superstructure using stiffness proportional damping calibrated to give 2.5% damping at their respective first mode frequencies. Stiffness proportional damping was selected since Rayleigh damping has been observed to artificially suppress the first mode of an isolated building even compared to a rigid structure approximation (Ryan and Polanco 2008). Stiffness proportional damping in conventional buildings might be expected to suppress higher mode response; however, damping comparison studies dismissed that concern for this particular building. The damping matrix was set proportional to the tangent stiffness matrix rather than the initial stiffness matrix to prevent the damping forces from becoming unrealistically large compared to the element forces after the superstructure yields (Hall 2006; Charney 2008).

Three analytical models were developed to quantify the effect of various analytical details on the dynamic properties of the buildings. The first is a basic centerline model of the moment resisting frame that neglects panel zone flexibility, referred to as M1. Although widely used in practice, the centerline model can overestimate both moments and inter-story drift if the difference between clear and centerline lengths of the beams and the columns is significant (Gupta and Krawinkler 1999). The second model, referred to as M2, incorporates rotational springs to model panel zone behavior and rigid

end offsets to account for clear length dimensions of beams and columns (FEMA 2000a). ASCE 7 prescribes that panel zone deformation shall be included to evaluate story drifts for steel moment frames (Sec. 12.7.3 of ASCE 2005). The last of three models (M3) applies to the conventional SMRF only, and in addition to panel zone springs incorporates a multi-element approach to simulate the behavior of RBS.

Panel Zone Flexibility

Panel zones exhibit desirable hysteretic behavior characterized by considerable strain hardening following yielding and stable hysteresis loops. Yielding propagates from the center of the panel zone and toward the four corners resulting in a parallelogram shape (Krawinkler 1978). Several mathematical models for panel zone shear force-shear strain (V-γ) relationships have been proposed (Krawinkler 1978; Lu *et al.* 1988; Tsai and Popov 1988; Kim and Engelhardt 2002). This study utilizes rotational springs that simulate tri-linear force-strain behavior (Fig. 2) (Krawinkler 1978; FEMA 2000a). The control values for yield force V_y, plastic force V_p, yield stain γ_y, and plastic strain γ_p, are given by:

$$V_y = 0.55 f_{ye} d_c t_w \qquad V_p = V_y \left(1 + \frac{3 b_{cf} t_{cf}^{\,2}}{d_b d_c t_w} \right) \tag{2a}$$

$$\gamma_y = \frac{f_{ye}}{\sqrt{3} G} \qquad \gamma_p = 4 \gamma_y \tag{2b}$$

where d_c = column depth, b_{cf} = column flange width, d_b = beam depth, t_w = web thickness, t_{cf} = column flange thickness, and G = shear modulus. The elastic stiffness K_e and the postyield stiffness K_p are calculated as the slopes from 0 to yield force V_y, and from V_y to the plastic capacity V_p, respectively. Beyond the plastic capacity, mild hardening is represented by a slope of αK_p with $\alpha = 0.03$ (Fig. 4.2).

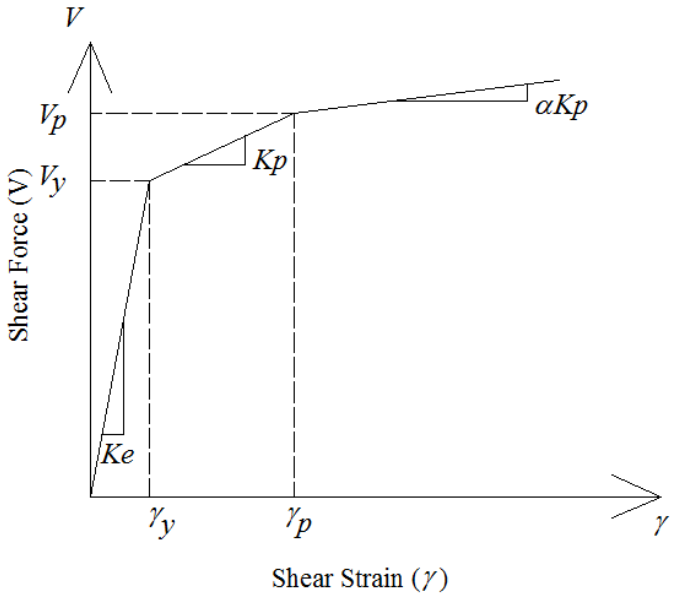

Fig. 4.2. Panel zone force-deformation behavior.

To implement the rotational springs, the shear strain γ = the rotation angle and the panel zone shear V is related to ΔM (the net moment transferred to the connection) according to:

$$V = \frac{\Delta M}{d_b} \tag{3}$$

Reduced Beam Section

The RBS approach was developed as an improved approach following the unexpected brittle failures of steel moment frame connections in the Northridge Earthquake, and is now used extensively (FEMA 2000b; Foutch and Yun 2002). In the RBS configuration, portions of the beam flanges at a section away from the beam end are tapered. This approach was observed to effectively eliminate the brittle failure mode by transferring the zone of plasticity away from the column (FEMA 2000b; Lee and Foutch

2002), as well as improve the overall ductility capacity of the beam-to-column assembly (Shen *et al*. 2000).

The typical geometry of a circular RBS is depicted in Fig. 4.3(a), where only half of the beam is drawn due to symmetry. The flange is tapered starting $3b_f/4$ (b_f = beam flange width) from the face of the column over a length of $3d_b/4$, with a peak reduction of 50% of the flange width in the middle of the taper. Beams incorporating RBS were modeled with three elements. Elastic frame elements were assigned at the beam ends with lengths L_1 equal to the distance between the column face and the center of the taper [Fig. 4.3(b)]. A nonlinear beam-column element with total length L_2 was assigned over the remaining interior, with plastic hinge regions of length equal to half of the total taper at both ends. Although the section properties change throughout the tapered region, both the moment capacity and the stiffness of the model were assumed to equal the minimum values – computed via section moment-curvature analysis at the midpoint of the taper – over the plastic hinge region [Fig. 4.3(b)].

Isolator Model

A model was developed for the behavior of isolation devices that incorporates a composite force-deformation relation in each direction that could represent either elastomeric or friction pendulum devices. An elastic column element and an elastic-perfectly plastic spring were assembled in parallel [Fig. 4.4(a)] to obtain the composite bilinear lateral force-deformation behavior for a single isolator as shown in Fig. 4.4(b). The column element ensures transfer of the moments that arise due to the lateral deformation of the isolator [Fig. 4.4(a)]. The elastic-perfectly plastic spring is a bidirectionally coupled element with a circular yield surface that exhibits identical

resistance in any direction in the *x*-*y* plane. Likewise, the column's vertical stiffness acts in parallel with compression only stiffness [represented by a vertical spring in Fig. 4.4(a)] to obtain the composite vertical force-deformation behavior shown in Fig. 4.4(c).

Isolators were modeled as independent elements, one beneath each column. The characteristic yield strength Q, postyield stiffness k_b, and yield displacement u_y of the isolators [Fig. 4.4(b)] determine the lateral force-deformation relation. Assuming u_y = 1 cm, Q and k_b were determined by matching the secant stiffness k_M and hysteretic energy dissipated to the equivalent period T_M = 3.07s and damping ratio β_M = 15.8% at the MCE displacement D_M = 62 cm (24.3 in) (Table 4.2) according to:

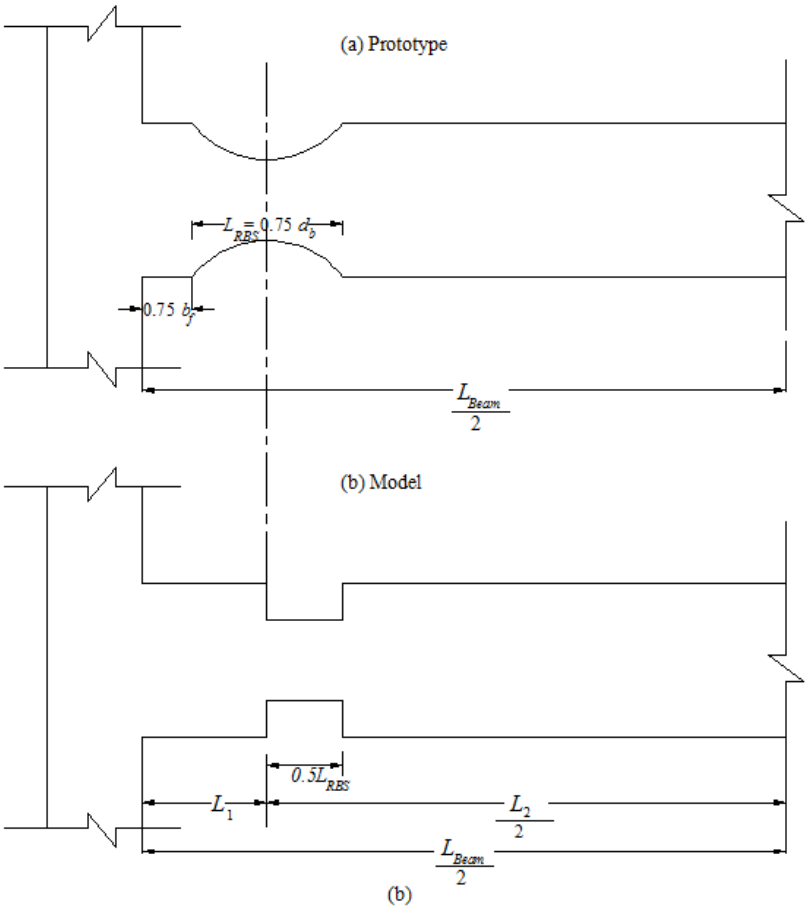

Fig. 4.3. For RBS, (a) plan view with typical geometry, and (b) 3-element frame model.

$$Q = \frac{\pi k_M \beta_M D_M^{\,2}}{2(D_M - u_y)} \tag{4}$$

$$k_b = k_M - \frac{Q}{D_M} \tag{5}$$

The compressive stiffness of the isolators was computed assuming a vertical frequency of 10 Hz. Since typical friction bearings have no resistance to tension, and typical elastomeric bearings cavitate (form bubbles in the rubber matrix) at low tensile forces, the tensile stiffness was assumed to be 1% of the value of the compressive stiffness. The energy dissipation in the isolator model is provided by hysteresis in the lateral directions and viscous damping in the vertical direction (using a damping coefficient of 5% at the vertical frequency of 10 Hz).

Fundamental Properties

Eigenvalue analysis was carried out on the various building models to evaluate their elastic dynamic properties. For eigen value analysis, the isolators were modeled as linear springs with stiffness corresponding to the design period T_D = 2.77 sec. The first three elastic periods and the corresponding deformation modes of each model are listed in Table 4.3. Both the panel zone springs (M2) and the RBS model (M3) add additional flexibility to the conventional building, which lengthens its fundamental periods. Since the first three natural periods of the isolated building are dominated by the isolation system flexibility, these periods are not affected by including the panel zone model. The moderate lengthening of the fundamental period of the isolated building relative to T_D suggests that structural participation in the fundamental mode is non-negligible.

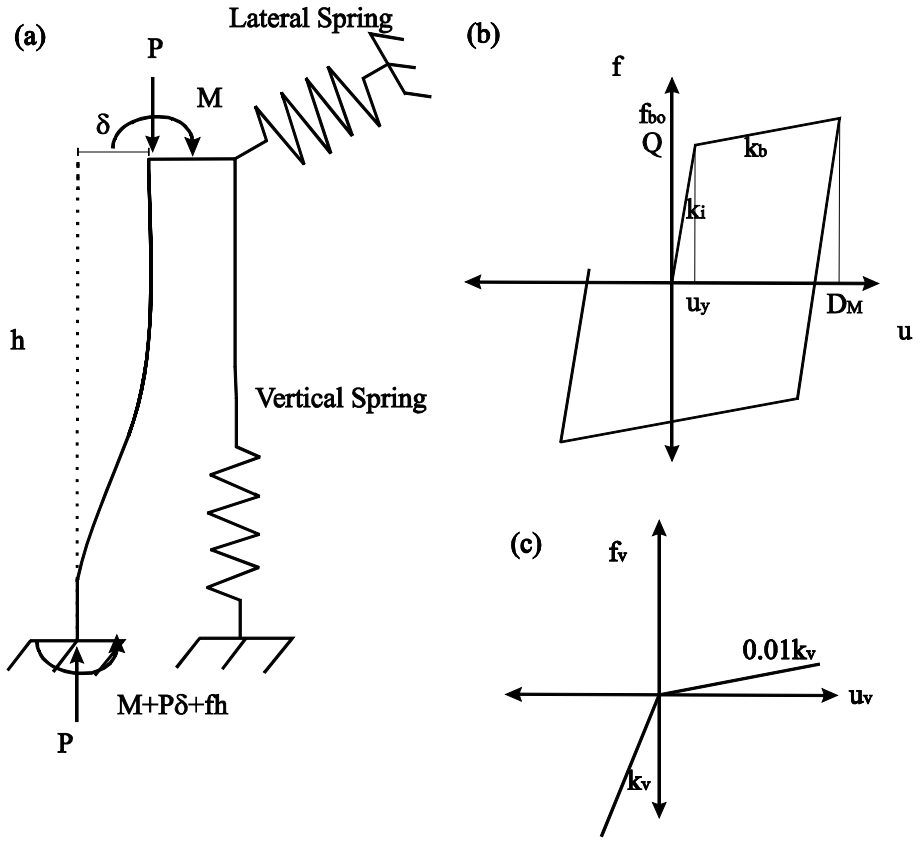

Fig. 4.4. (a) Isolator model composed of an elastic column element in parallel with lateral and vertical springs; (b) lateral force-deformation and (c) vertical force-deformation in the isolation devices

The fundamental period for the superstructure of the isolated building, obtained from a model of the IMRF in a fixed-base condition, was found to be around 1.5 seconds, and thus isolation lengthens the period by less than a factor of 2.

Nonlinear static analysis (or pushover analysis) was carried out under an inverted triangle load pattern to determine the base shear capacity and post-yield behavior based on the various building models. Capacity curves for both the conventional SMRF and superstructure of IMRF (without isolators) are plotted in Fig. 4.5. The added flexibility of panel zone springs (M2 model) and RBS (M3 model) also leads to reduced base shear

capacity. The conventional SMRF has a base shear capacity V ≈ 0.65W (M3 model), while the isolated IMRF has a base shear capacity V ≈ 0.25W (M2 model). Thus, the conventional SMRF is computed to be more than twice as strong as the isolated IMRF. While the SMRF model has positive incremental stiffness out to large deformation limits, the IMRF capacity curve essentially flattens after complete yielding. Thus, the isolated IMRF may be more prone to large inelastic excursions in yielding events.

Note that the required minimum design strength coefficients for the SMRF and isolated IMRF were computed as:

$$C_{s,SMRF} = \frac{S_{D1}}{TR} \qquad C_{s,IMRF} = \frac{V_s}{W_s} = \frac{k_D D_D}{R_I W_s} \tag{6}$$

$C_{s,SMRF}$ = 0.113, based on a natural period of T = 0.82 sec, which is the upper bound period for this steel moment frame permitted by ASCE 7; and $C_{s,IMRF}$ = 0.135, based on design base shear V_s = 790.4 kip and structural weight above the base level W_s = 5858 kip. Thus, although both buildings have similar strength requirements, the capacity of the conventional SMRF exceeds its required strength by a much larger factor. Although the allowable drift is larger in the SMRF than the isolated IMRF, the drift in the SMRF is carried entirely by the lateral moment system, which led to the selection of much larger member sizes.

Table 4.3. Fundamental Periods of Each Model

	Conventional (SMRF)				Base-isolated (IMRF)	
Period (sec)	M1	M2	M3	Mode	M1 & M2	Mode
T1	0.76	0.86	0.89	Lateral torsional	3.23	Lateral torsional
T2	0.74	0.84	0.86	Bidirectional lateral	3.02	Bidirectional Lateral
T3	0.49	0.56	0.57	Torsional	2.60	Torsional

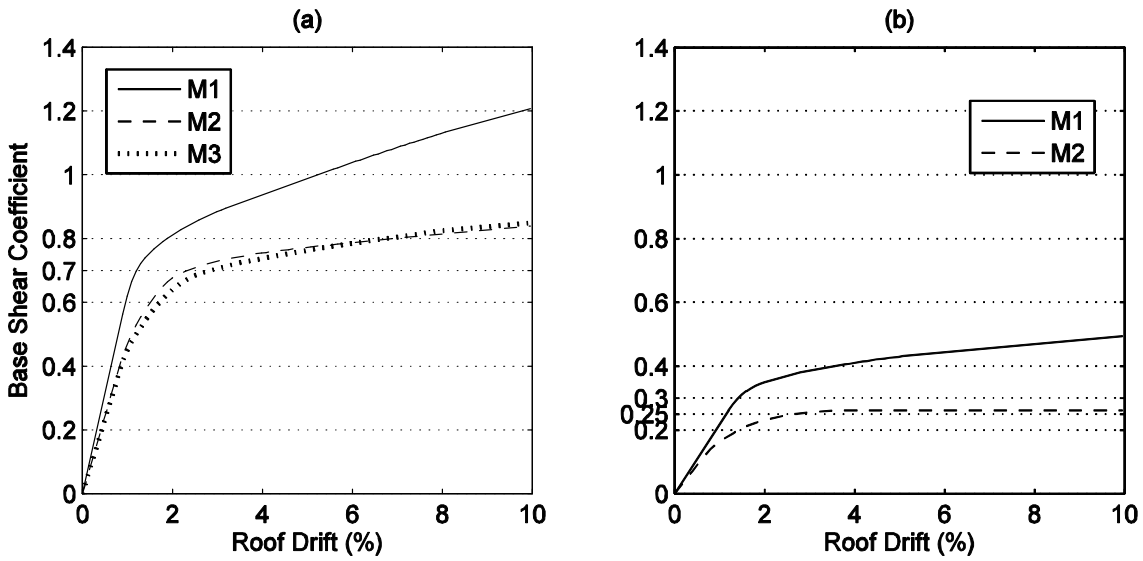

Fig. 4.5. Capacity curve for (a) conventional and (b) base-isolated building.

Ground Motions

The following general procedure was used to select ground motions for loss estimation (ATC 2007). First, a hazard curve was defined that quantifies ground motion intensity versus frequency of occurrence. Individual points along the hazard curve represent various earthquake scenarios ranging from frequent small events to large rare events. For several distinct earthquake scenarios, target spectra were generated and ground motions were selected and amplitude scaled to best match the target spectra.

The response analysis presented here, a subset of the information to be used for loss estimation, is limited to three discrete ground motion scenarios. USGS national seismic hazard maps (Frankel *et al*. 2000) were consulted to generate uniform hazard spectra (target spectra) for the three selected events: 50% probability of exceedance (PE) in 50 years (50/50), 10% PE in 50 years (10/50), and 2% PE in 50 years (2/50), which correspond to 72 year, 475 year, and 2475 year return periods, respectively. The target

spectra list spectral ordinates at periods T=0.1, 0.2, 0.3, 0.5, 1.0 and 2.0 sec. Values at 0.2 sec and 1.0 sec for the 2/50 event correspond to S_S and S_1 values for the MCE.

The target spectra are based on a reference shear wave velocity V_s = 760 m/s (2493 ft/s), and were thus modified to reflect the assumed site conditions – site class D with V_s from 180 to 360 m/s (591 to 1181 ft/s). To modify the target spectra, spectral site modification factors that depend on both ground motion intensity and period were developed from next generation attenuation (NGA) relations (e.g. Campbell and Bozorgnia 2008; Chiou and Youngs 2008). This approach is consistent with site modification factors F_a and F_v used in building codes, but reflects the additional periods accounted for in the target spectra. Specifically, site factors were computed as the ratios of spectral acceleration at 760 m/s (2493 ft/s) and 270 m/s (886 ft/s), with all other factors held constant. Site factors for a given spectral intensity were observed to be basically independent of the particular attenuation relation used and the assumed earthquake magnitude and distance. Site factors were restricted not to fall below 1.0 even in the short period range. The target spectra for each event are plotted in Fig. 4.6.

Using USGS seismic deaggregation data (Frankel *et al*. 2000), ground motions were selected according to the percentage contribution of magnitude and distance pairs to the seismic hazard for a given scenario. The percentage contribution of distance-magnitude pairs was determined by averaging the deaggregation data, which is provided at various periods. For each hazard level, 20 recorded natural ground motions that conform to the magnitude, distance and site class were selected from the PEER NGA database (Chiou *et al*. 2008). When the number of available motions exceeded the number desired, motions were selected randomly. Each pair of records was amplitude

scaled by a common factor that minimized the difference of the mean spectrum of the components and the target spectrum in the least square sense from $T = 0$ to 3 sec.

The selection and scaling procedures were based on a range of periods rather than a single period since the motions were applied to buildings with significantly different fundamental periods. For the 2/50 and 10/50 hazard levels, the median spectra of the initial 20 pairs of ground motions selected and scaled as described above were observed to fall well short of the target spectra, particularly in the long period range. While using recorded ground motions was considered to be ideal, we replaced some of the recorded motions with frequency modified motions to obtain a better match between the target hazard spectra and the median response spectra in the long period range. Hence, 10 pairs of ground motions at the 2/50 and 10/50 hazard levels were replaced by the corresponding SAC steel project – Los Angeles (SAC-LA) ground motion sets. These SAC motions were originally selected for similar location and site conditions, and frequency modified to match the target spectra (Somerville *et al*. 1998).

The ground motions selected for the nonlinear response history analyses, for the 50/50, 10/50 and 2/50 events, respectively, are listed on the NEES TIPS project website (NEES TIPS 2009). Figure 6 compares the target and median response spectra for the 20 pairs of scaled ground motions for each hazard level. For all hazard levels, the median spectrum falls somewhat short of the target spectrum beyond $T = 1.5$ sec despite the introduction of frequency modified motions.

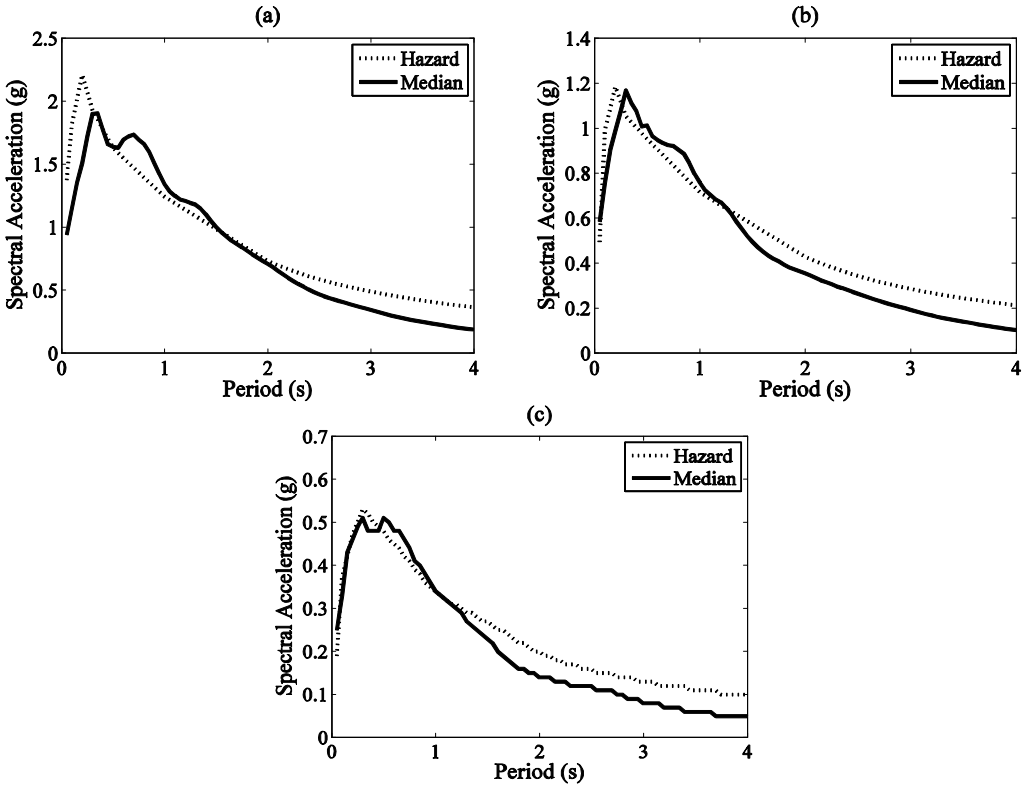

Fig. 4.6. Target hazard spectra and median response spectra of the scaled motions for (a) 2/50, (b) 10/50, and (c) 50/50 year earthquake scenario.

Comparative Results of Nonlinear Response History Analysis

Nonlinear response history analyses (RHA) were carried out to comparatively evaluate the structural response of the conventional SMRF and isolated IMRF when subjected to the ground motion suites described previously. Model M3 for the conventional SMRF and model M2 for the isolated IMRF were used. The statistical distribution of various response quantities for 2/50, 10/50, and 50/50 year events are presented. The selected response quantities include peak and residual story drift, peak total floor acceleration, local element (beam, column, and panel zone) plastic rotations, and isolator deformations (lateral and vertical). Story drift, defined here as the ratio of maximum (or residual) displacement to the story height, indicates damage to structural

elements and drift-sensitive nonstructural components. Large story drifts are also associated with the development of P-Δ instability. Floor acceleration, expressed in *g*, indicates damage in acceleration sensitive nonstructural components and contents. Plastic rotation demands of individual elements can more precisely indicate local damage. Residual drift criteria determine the threshold between restoring and demolishing a damaged building.

Seismic responses, when sampled over many ground motions, are widely accepted to be lognormally distributed. As such, the median $\hat{x}$ and dispersion δ of the lognormal data were generally used to describe the central tendencies and variability of the response quantities for different ground motion sets. They were computed as:

$$\hat{x} = \exp\left[\frac{\sum_{i=1}^{n} \ln x_i}{n}\right] \qquad \delta = \left[\frac{\sum_{i=1}^{n} (\ln x_i - \ln \hat{x})^2}{n-1}\right]^{\frac{1}{2}} \tag{7}$$

However, statistical evaluation based on lognormal distribution [Eq. (7)] is not valid when the sampling set contains zeros, as is the case for plastic rotations. Thus, arithmetic mean μ and standard deviation σ:

$$\mu = \frac{\sum_{i} x_i}{n} \qquad \sigma = \sqrt{\frac{\sum_{i} (x_i - \hat{x})^2}{n-1}} \tag{8}$$

valid for a normal distribution, were used to describe central tendency and variability of the plastic rotation demands. The 84th percentile values were computed as $\hat{x}\exp(\delta)$ when used with Eq. (7) and $\mu + \sigma$ when used with Eq. (8).

To summarize, the aforementioned statistics are presented in Fig. 4.7 for peak story drift, Fig. 4.8 for peak floor acceleration, and Figs. 4.9 and 4.10 for plastic rotations

in beams/panel zones and columns, respectively. To quantify the significance of outliers in the 2/50 year event, selected responses for individual ground motions are presented in Fig. 4.11. Residual drifts and isolator deformations are shown for the 2/50 year event [Fig. 4.11(c), 4.11(f)], and were negligible in the other events. Statistics on various isolator deformation demands are presented in Table 4.4. Story drifts were evaluated separately in each direction as the maximum at any of the four corners of the building. Total floor acceleration at the center of mass and isolator deformations (maximum over all devices) were evaluated as the vector sums of the demands in the X and Y directions. The local plastic rotation demands were evaluated as the maximum over all pertinent elements at the given level. When multiple locations or elements were considered, statistics reflect the median (mean) of the local maxima, which may occur at different locations/elements for different ground motions.

Response in Design (10/50 Year) and Frequent (50/50 Year) Events

Although not explicitly identified in building codes, typical design objectives for an isolated building are to suppress yielding and attenuate accelerations to well below the peak ground acceleration (PGA) in the design (10/50 year) event. Using approximate design principles, yield story drifts Δ_y were evaluated as:

$$\Delta_y = \frac{\varepsilon_y h}{3}\left(\frac{\alpha h}{d_c} + \frac{L_{Beam}}{d_b}\right) \tag{9}$$

where ε_y= yield strain, α = reduction factor of 0.8, and h = height of the story, which led to yield drift values of 1.2% in the conventional SMRF and 1.5% in the isolated IMRF. Accordingly, for both frequent (50/50 year) and design events, the story drift demands in the isolated IMRF are generally below the yield limit of 1.5% [Fig. 4.7(a)-(b), 4.7(d)-(e)],

and beam and column plastic rotation demands are essentially zero [Fig. 4.9(a)-(b), 4.10(a)]. However, the conventional SMRF tends to yield in the design event, with median story drift demands around 2% in stories 2 and 3 [Fig. 4.7(b), 4.7(e)], and median beam plastic rotation demands from 0.01 to 0.015 rad in floors 1 and 2 [Fig. 4.9(b)]. In the frequent event, the conventional SMRF is on the verge of yielding, with story drifts around 1.2% [Fig. 4.7(a)] and accumulated beam plastic rotations around 0.004 rad.

With respect to accelerations, the median roof acceleration in the isolated IMRF is attenuated by a factor of almost two (PGA = 0.61g and roof acceleration = 0.33g) in the design event [Fig. 4.8(b)]. However, the median roof acceleration demand in the conventional SMRF is amplified to 1.15g for the same event. Note that the accelerations at level 0 (ground) designate PGA and the accelerations between 0 and 1 designate accelerations just above the isolators (Fig. 4.8). Based on these results, the design objectives appear to have been met.

In further observation of yielding, column plastic rotation demands in the frequent event were zero everywhere in both buildings and hence are not plotted. Nonzero plastic rotation demands occur only at the base of the ground story columns in the conventional SMRF in the design and larger events (Fig. 4.10). Thus, the strong column-weak beam capacity design concept effectively prevents column yielding and soft story mechanisms. Minor panel zone yielding is observed in the isolated SMRF for the design and even frequent events [Fig. 4.9(d)-(e)].

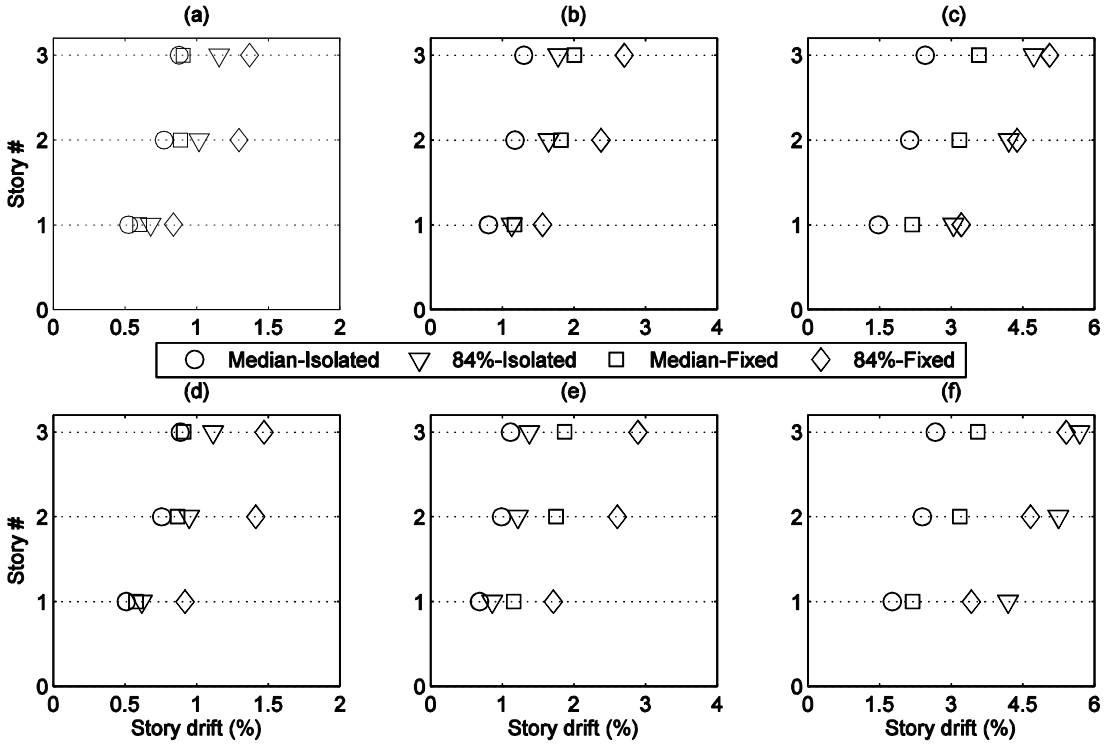

Fig. 4.7. Story drift ratio demands for: (a)-(c) 50/50, 10/50, and 2/50 year events, respectively, in X-direction; and (d)-(f) 50/50, 10/50, and 2/50 year events, respectively, in Y-direction.

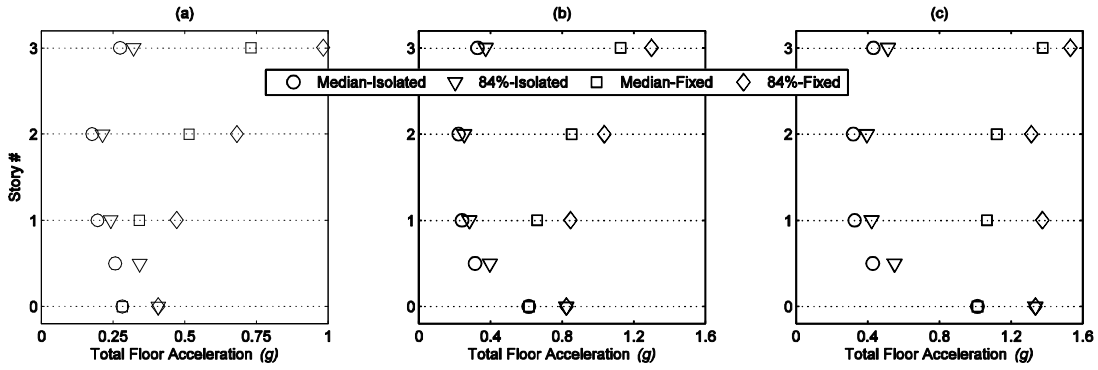

Fig. 4.8. Total floor acceleration demands for (a) 50/50, (b) 10/50, and (c) 2/50 year events.

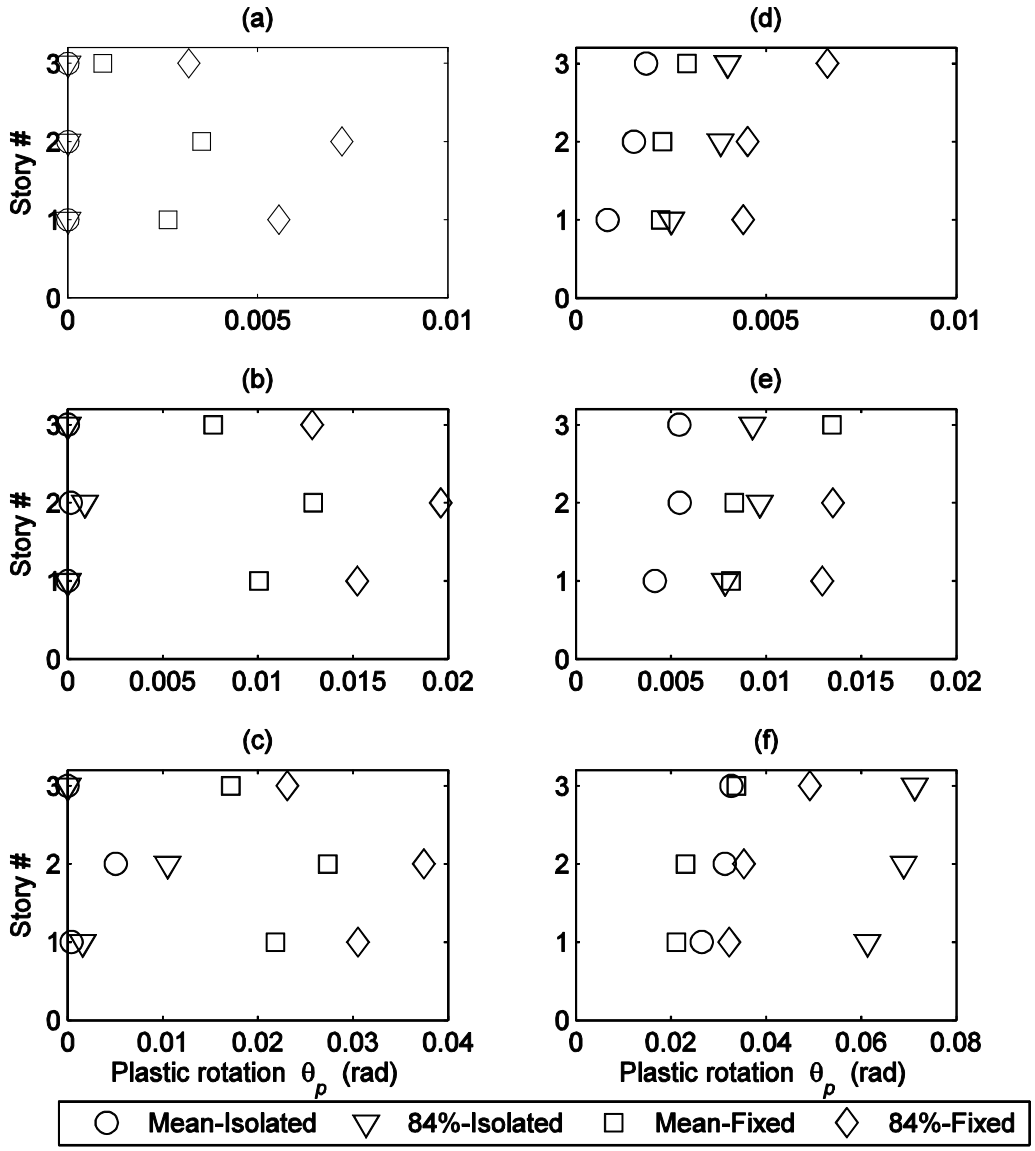

Fig. 4.9. Beam plastic rotation demands for (a) 50/50, (b) 10/50, and (c) 2/50 year events, and panel zone plastic rotation demands for (d) 50/50, (e) 10/50, and (f) 2/50 year events.

For the design and frequent events, the demands in the isolated building can be predicted with high confidence as the dispersions (reflected in the difference between median and 84th percentile responses) in story drifts and especially total floor accelerations are quite small [Fig. 4.7(a)-(b), 4.7(d)-(e), 8(a)-(b)]. As discussed previously, the isolated IMRF does not appear to yield, and since it responds elastically

the dispersion in story drift is limited relative to the conventional SMRF. Regarding floor accelerations, extreme values (high or low) of PGA are observed not to correlate well with extreme values of roof acceleration in the isolated IMRF, as shown plotted for each ground motion [Fig. 4.11(b)] for the 2/50 year event (MCE), where limited dispersion was also displayed [Fig. 4.8(c)]. One possible explanation for the small dispersion in acceleration is that period lengthening generally has a smoothing effect on spectral accelerations, which are correlated to floor accelerations. Another possible explanation is that isolation leads to increased relative attenuation with increasing PGA, such that the overall dispersion in floor acceleration tightens relative to the dispersion in PGA.

Although the benefits of seismic isolation are definitely apparent, story drift reduction is somewhat suppressed compared to ideal applications due to the flexibility of the moment frame. For the design event, median story drift demands in the isolated IMRF are reduced on the order of 33-50% relative to the conventional SMRF [Fig. 4.7(b), 7(e)]. Pedagogical explanations of the concept of seismic isolation (e.g., Kelly 1997) tend to assert that structural drifts are reduced by large factors, and comparative studies may assume that the conventional and isolated superstructure have the same natural period (e.g. Sayani and Ryan 2009). However, here the IMRF without isolators is substantially more flexible than the conventional SMRF. Furthermore, the effective isolation period (T_D = 2.77 sec) exceeds the superstructure natural period (T = 1.5 sec) by less than a factor of 2 when the isolation system is excited comparable to its design displacement. Therefore, significant structural participation in the first mode, leading to moderate story drift demands, is unsurprising. Although structural yielding is prevented,

damage in drift sensitive non-structural components is not eliminated in the design event by seismic isolation. For example, damage to interior partition walls is predicted at median drifts as low as 0.25% (ATC 2007).

The relative drift reduction is even smaller for the frequent event compared to the design event, wherein median story drift demands are reduced only slightly relative to the conventional SMRF [Fig. 4.7(a), 4.7(d)]. To interpret, the isolation system becomes less effective for earthquake intensities lower than the design event because it is not fully activated [median deformation = 11.35 cm (4.47 in) (Table 4.4)], resulting in a higher effective stiffness and a smaller period separation compared to the superstructure. This behavior has limited significance when the superstructure is stiff, but has greater importance when the superstructure is flexible, as observed here for the moment frame. Reduced activation of the isolation system also affects the accelerations, which are barely attenuated below the PGA in the frequent event [Fig. 4.8(a)].

Response in MCE (2/50 Year Event)

While story drifts for the isolated IMRF are generally reduced in the MCE (2/50 year event) relative to the conventional SMRF, the same confidence in the superior performance of isolation in a design event cannot be extended to the MCE. For example, the median peak story drift is reduced from about 3.6% for the conventional SMRF to about 2.7% for the isolated IMRF, but the 84^{th} percentile story drift demands are comparable in both [Fig. 4.7(c), 4.7(f)]. The increase in the 84^{th} percentile drift is the result of outliers; for example, two motions induce peak drift demands on the order of 15-16% in the isolated SMRF [Fig. 4.11(a)].

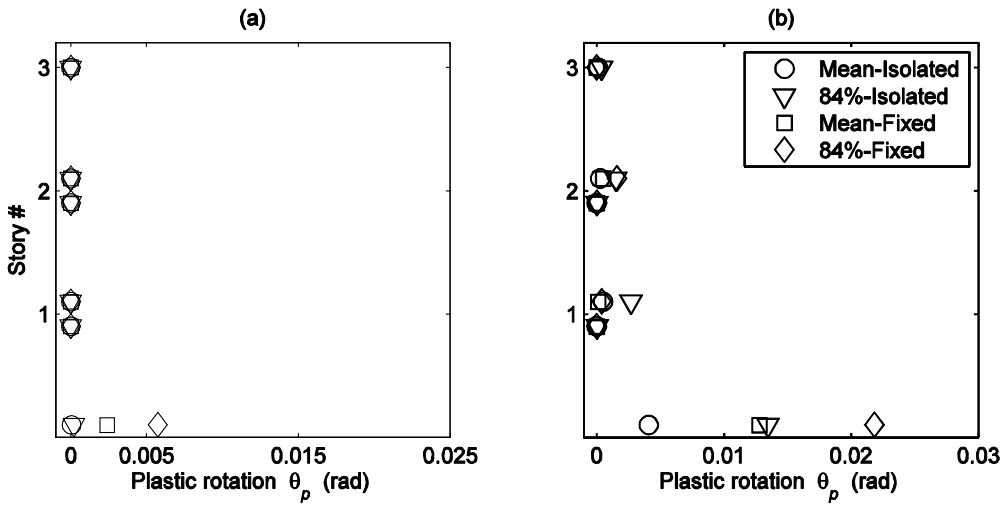

Fig. 4.10. Column plastic rotation demands for (a) 10/50 and (b) 2/50 year events.

In one motion, residual story drift in the isolated IMRF is predicted to be on the order of 11% [Fig. 4.11(c)], which would almost certainly lead to collapse. Similar outliers are not observed for the conventional SMRF, as several motions induce peak story drifts on the order of 5-8% [Fig. 4.11(a)] and residual drifts on the order of 1-2% [Fig. 4.11(c)].

Several studies have drawn conclusions that explain why the outliers occur, e.g. yielding is self-limiting in conventional structures but self-propagating in isolated structures (Kikuchi *et al*. 2008), ductility demands are larger in isolated buildings than conventional buildings for comparable force reduction factors (Chapter 3), and isolated buildings are more sensitive than conventional buildings to statistically reasonable uncertainties in ground motions (Politopoulos and Sollogoub 2005). Furthermore, the observed flattening of the capacity curve of the isolated IMRF beyond the ultimate strength likely amplifies large yield excursions compared to the conventional SMRF that continues to strain harden at large drifts [Fig. 4.5(b)]. Through the simple force balance concept, structural yielding helps to limit acceleration demands. Thus, occurrence of acceleration outliers [Fig. 4.11(b)] or increased dispersion in acceleration [Fig. 4.8(c)] is

not observed for the isolated IMRF in the MCE. The isolation system is very effective in limiting total floor accelerations to levels well below the PGA [Fig. 4.8(c)].

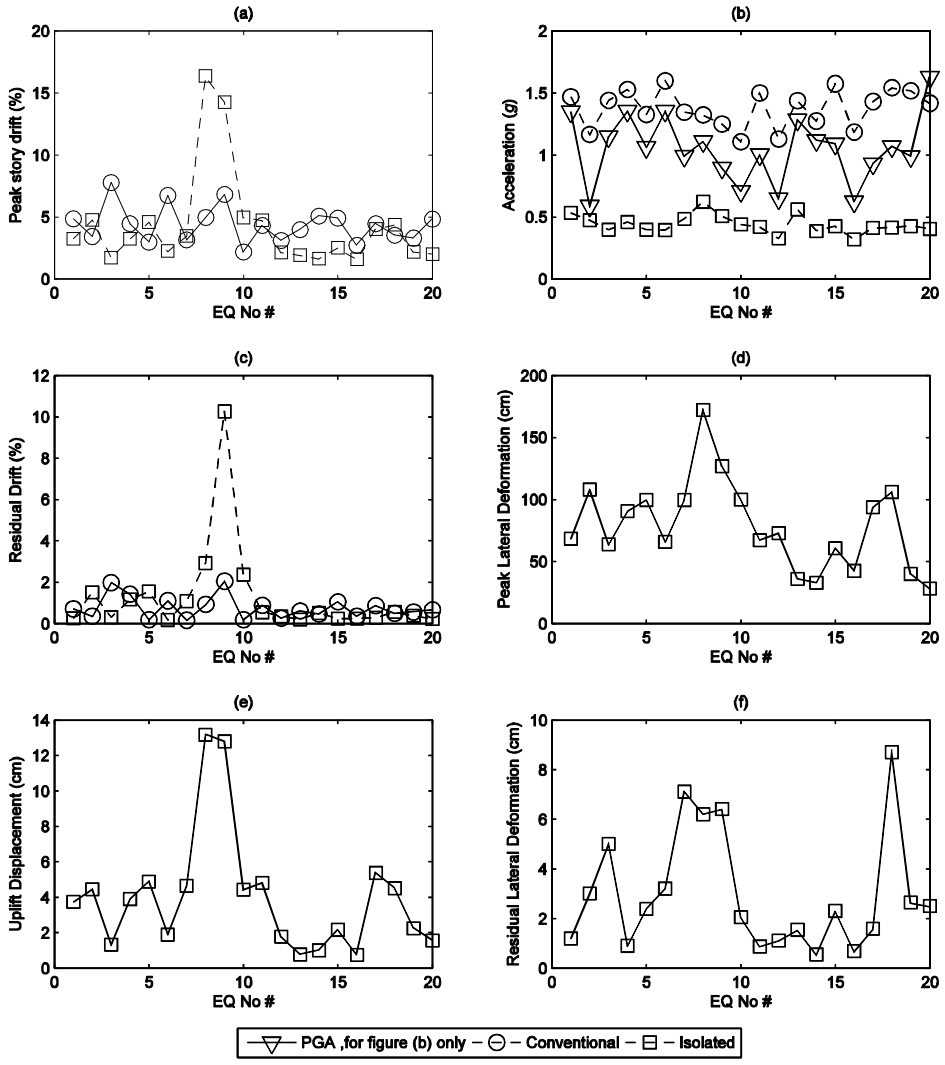

Fig. 4.11. (a) Peak story drift (%), (b) PGA and roof acceleration, (c) maximum residual drift, (d) peak lateral deformation, (e) maximum uplift displacement, and (f) maximum residual lateral deformation demands in the isolation system sampled for individual motions in the 2/50 year event.

With stable post-yield behavior and inability to capture phenomena such as fracture, buckling, etc., the models do not predict collapse nor should conclusions be drawn about the threshold drifts at which collapse occur. However, several additional observations taken all together imply that the probability of collapse or functional failure of the isolated IMRF in the MCE is non-negligible. The median isolator deformation of 70.76 cm (27.86 in) (Table 4.4) exceeds the MCE displacement D_M = 61.7 cm (24.3 in) (Table 4.2), and the 84th percentile deformation of 116.13 cm (45.72 in) (Table 4.4) exceeds D_{TM} = 74.6 cm (29.4 in) (Table 4.2). Furthermore, the peak isolator deformation exceeds D_{TM} for 9 of 20 ground motions [Fig. 4.11(d)]. Since the seismic gap length and moat wall location are at the designer's discretion, the potential collision with a moat wall was *not* simulated in this study. However, under reasonable design practices, collisions with the outer moat wall would be expected for some of the ground motions considered, and would transmit high frequency waves up through the superstructure.

The uplift displacement demands in isolators, sampled for individual ground motions in Fig. 11(e), are also of concern. The average uplift is around 2.5 cm (1 in), which would probably be acceptable in design, but exceeds 12.5 cm (5 in) for two of the ground motions. In reality, different isolation devices manage uplift in a variety of ways that are not well captured here.

Residual drift demands in both buildings are usually below 1%, but demands above 2% are induced by a couple of motions for the conventional SMRF and several motions for the isolated IMRF, including one outlier that has already been discussed [Fig. 11(c)]. Residual isolator deformations are generally below 2.5 cm (1 in), but are predicted to be as high as 12 cm (4.7 in) [Fig. 11(f)]. Further investigation is needed to

Table 4.4. Peak and Residual Isolator Displacement Demands

Scenario	Statistics	Peak isolator displacement (cm)	Residual isolator displacement (cm)
50 in 50	Median	11.35 (4.47 in.)	1.90 (0.75 in.)
	84%	20.22 (7.96 in.)	3.07 (1.21 in.)
10 in 50	Median	35.56 (14.0 in.)	1.68 (0.66 in.)
	84%	54.46 (21.44 in.)	3.07 (1.21 in.)
2 in 50	Median	70.76 (27.86 in.)	2.41 (0.95 in.)
	84%	116.13 (45.72 in.)	5.87 (2.31 in.)

identify drift repair limits.

As observed previously, drift demands are somewhat comparable in both buildings [Fig. 4.7(c), 4.7(f)]. Beam plastic rotations are the source of large drifts for the conventional SMRF [Fig. 4.9(c)], while panel zone plastic rotations are the source of large drifts for the isolated IMRF [Fig. 4.9(f)]. Beam rotations are larger for the conventional SMRF because the RBS model reduces the beam capacity relative to the panel zone capacity. Even though the relative beam versus panel zone plastic rotations are known to be sensitive to the modeling assumptions, the high panel zone rotation demands in the isolated IMRF, on the order of 0.06 – 0.07 rad (6-7%) at the 84^{th} percentile, are disconcerting. The ductility capacity of the WUF-W connection used in the IMRF is expected to be lower than the RBS connection used in the SMRF, perhaps putting the isolated IMRF at risk of weld fractures in the MCE.

Conclusions

The seismic performance of code compliant 3-story low rise steel moment frame buildings – both conventional SMRF and base-isolated IMRF – has been compared. The reported effort is part of a larger cost-benefit study of seismic-isolated steel buildings,

and the purpose of this paper is to evaluate seismic response, i.e., engineering demand parameters (story drifts, total floor accelerations, member plastic rotation demands), to be used in life cycle loss estimation. Synthesis of the seismic response of the two buildings has led to the following conclusions:

- The design objectives for the isolated IMRF have been met, i.e., structural yielding is eliminated for both the design (10/50 year) and frequent (50/50 year) events and floor accelerations are reduced considerably – by factors of 3 or 4 – relative to the conventional SMRF.
- Demands in an isolated building can be predicted with high confidence for ground motion intensities at or below the design intensity, as the dispersions in response parameters are reduced to a fraction of those in the conventional building.
- The flexibility of the moment frame leads to non-negligible structural participation in the first modes of the isolated IMRF, and larger relative story drifts compared to idealized (stiff) structural systems. This phenomenon is exacerbated in a frequent/small event where the isolation system is not fully activated. Even though the isolated IMRF does not yield in the design event, damage to drift-sensitive nonstructural components would not be prevented. However, steel moment frames provides reliable, stable performance, and floor accelerations are attenuated to values that would unequivocally safeguard acceleration sensitive nonstructural components and contents.
- In the MCE (2/50 year event), the presence of significant outliers in the response data reduces the confidence that the isolated IMRF will provide superior performance, even though its median story drifts are lower than those of the

conventional SMRF. Outliers tend to occur when an isolated building yields, because ductility demands accumulate faster in an isolated building than in a conventional building.

- Collapse of an isolated IMRF in an MCE event is possible if the motion induces an outlier response, but cannot be predicted due to effects that were not modeled. Sources of uncertainty include collision of the building with an outer moat wall, uplift in the isolators, and large panel zone ductility demands leading to weld fractures.

Given these conclusions, a knowledgeable stakeholder must determine whether protecting a steel moment-resisting frame building with seismic isolation is a good decision, knowing that performance might not be improved in the MCE. However, the composite probability that (a) an event like the MCE is experienced over the life of the building, and (b) the event induce an outlier response that puts the building in danger of collapse, is extremely small. In our judgment, from the perspective of performance, choosing seismic isolation for a moment frame is still a wise investment, if it can be shown to effectively limit losses and interruptions in design events, which remains to be seen in the complete loss estimation study.

References

Agarwal, V. K., Niedzwecki, J. M., and van de Lindt, J. W. (2007). "Earthquake induced pounding in friction varying base isolated buildings.", Engineering Structures, 29(11):2825-2832.

American Institute of Steel Construction (AISC) (2005). *AISC 341-05 Seismic Provisions for Structural Steel Buildings*, Chicago, Ill.

American Society of Civil Engineers (ASCE) (2005). ASCE 7-05 Minimum Design Loads for Buildings and Other Structures, Reston, Va.

American Society of Civil Engineers (ASCE) (2007). ASCE 41, Seismic Rehabilitation of Existing Buildings, Reston, Va.

Applied Technology Council (ATC) (2007). "Guidelines for Seismic Performance Assessment of Buildings 35% Complete" *Draft prepared for Department of Homeland Security*, Washington, D.C.

Applied Technology Council (ATC) (2008a). Reducing the Risks of Nonstructural Earthquake Damage, ATC-69 Project Report – State of the Art and Practice. Prepared for Federal Emergency Management Agency, Washington, D.C.

Applied Technology Council (ATC) (2008b). Quantification of Building Seismic Performance Factors, ATC-63 Project Report – 90% Draft prepared for Federal Emergency Management Agency, Washington, D.C.

Bruno, S., and Valente, C. (2002). "Comparative response analysis of conventional and innovative seismic protection strategies." Earthquake Engineering and Structural Dynamics, 31(5):1067-1092.

Building Seismic Safety Council (BSSC) (2004). FEMA 450, NEHRP Recommended Provisions and Commentary for Seismic Regulations for New Buildings and Other Structures, Washington, D.C.

Campbell, K. W., and Bozorgnia, Y. (2008). "NGA ground motion model for the geometric mean horizontal component of PGA, PGV, PGD and 5% damped linear elastic response spectra for periods ranging from 0.01 to 10 s", Earthquake Spectra, 24(1):139-171.

Ceccoli, C., Mazzotti, C., and Savoia M. (1999). Non-linear seismic analysis of base-isolated RC frame structures. Earthquake Engineering and Structural Dynamics, 28:633-653.

Charney, F. A. (2008). "Unintended consequences of modeling damping in structures." J. Struct. Eng., 134(4), 581-592.

Chiou, B. S. J., and Youngs, R. S. (2008). "An NGA model for the average horizontal component of peak ground motion and response spectra." Earthquake Spectra, 24(1):173-216.

Chiou, B., Darragh, R., Gregor, N., and Silva, W. (2008). "NGA project strong-motion database." Earthquake Spectra, 24(1):23-44.

Comerio, M. C. (ed.) (2005). "PEER testbed study on a laboratory building: exercising seismic performance assessment." *PEER Report No. 2005/12*, Pacific Earthquake Engineering Research Center, University of California at Berkeley, Calif.

Comerio, M. C., and Stallmeyer, J. C. (2002). "Nonstructural loss estimation: the UC Berkeley case study." *PEER Report No. 2002/01*, Pacific Earthquake Engineering

Research Center, University of California at Berkeley, Calif.

Dolce, M., and Cardone, D. (2003). "Seismic protection of light secondary systems through different base isolation systems." Journal of Earthquake Engineering, 7(2):223-250.

Dolce, M., Cardone, D., and Ponzo, F. C. (2007). "Shaking-table tests on reinforced concrete frames with different isolation systems." Earthquake Engineering and Structural Dynamics, 36(5):573-596.

Federal Emergency Management Agency (FEMA) (2000a) FEMA 355-C State of the Art Report on Systems Performance of Steel Moment Frames Subjected to Earthquake Ground Shaking, Washington, D.C.

Federal Emergency Management Agency (FEMA) (2000b) FEMA 355-D State of the Art Report on Connection Performance, Washington, D.C.

Foutch, D. A. and Yun, S. (2002). "Modeling of steel moment frames for seismic loads." Journal of Constructional Steel Research, 58(5-8):529-564.

Frankel, A. D., Mueller, C.S., Barnhard, T.P., Leyendecker, E.V, and Wesson, R.L. (2000). "USGS national seismic hazard maps." Earthquake Spectra, 16(1):1-19.

Gupta, A. and Krawinkler, H. (1999). "Seismic demands for performance evaluation of steel moment resisting frame structures." Report No. 132. The John A. Blume Earthquake Engineering Center, Stanford University, Calif., USA.

Hahm, D., Koh, H-M., Shin, J-H., and Park, Y.-S. (2004). "Life cycle cost analysis for the seismic isolation of bridges in a region of low to moderate seismicity", *Proc. 13th World Conference on Earthquake Engineering*, Paper No. 2844, Vancouver, Canada, August 1-6.

Hall, J. F. (2006). "Problems encountered from the use (or misuse) of Rayleigh damping." Earthquake Engineering and Structural Dynamics, 35(5):525-545.

Hall, J. F. and Ryan, K. L. (2000). "Isolated buildings and the 1997 UBC near-source factors." Earthquake Spectra, 16(2):393-412.

Hamidi, M., El Naggar, M. H., and Vafai, A. (2003). "Response of structures supported on SCF isolation systems." Earthquake Engineering and Structural Dynamics, 32(10):1555-1584.

Haselton, C. B., Goulet, C.A., Mitrani-Reiser, J., and beck, J.L. (2007). "An assessment to benchmark the seismic performance of a code-conforming reinforced concrete moment frame building." *PEER Report 2007/12*, Pacific Earthquake Engineering Research Center, University of California at Berkeley, 360 pages.

International Code Council (ICC) (2006). *International building code (IBC)*, Falls

Church, Va.

Karim, K. Z. and Yamazaki, F. (2007). "Effect of isolation on fragility curves of highway bridges based on simplified approach." Soil Dynamics and Earthquake Engineering, 27(5):414-426.

Kelly, J. M. (1997). Earthquake-Resistant Design with Rubber, Springer-Verlag, 2nd Edition.

Kikuchi, M., Black, C. J., and Aiken, I. D. (2008). "On the response of yielding seismically isolated structures." Earthquake Engineering and Structural Dynamics, 37(5):659-679.

Kim, K. D., and Engelhardt, M. D. (2002). "Modeling of steel moment frames for seismic loads." Journal of Constructional Steel Research, 58(5-8):605-635

Kircher, C., Reitherman, R., Whitman, R. and Arnold, C. (1997). "Estimation of earthquake losses to buildings." Earthquake Spectra, 13(4):703-720.

Krawinkler, H. (1978). "Shear design of steel frame joints." Engineering Journal, AISC, 15 (3).

Krawinkler, H. (ed.) (2005). "Van Nuys hotel building testbed report: exercising seismic performance assessment." *PEER Report No. 2005/11*, Pacific Earthquake Engineering Research Center, University of California at Berkeley, Calif.

Lee, K., and Foutch, D. (2002). "Performance evaluation of new steel frame buildings for seismic loads." Earthquake Engineering and Structural Dynamics, 31:653-670.

Lin, A. N., and Shenton III, H. W. (1992). "Seismic performance of fixed-base and base-isolated steel frames." Journal of Engineering Mechanics, ASCE, 118(5):921-941.

Lu, L. W., Wang, S. J., and Lee, S. J. (1988). "Cyclic behavior of steel and composite joints with panel zone deformation," Proceedings of the 9th World Conference on Earthquake Engineering, Vol. IV, Tokyo-Kyoto, Japan.

Mezzi, M., and Comodini, F. (2008). "Comparative economic assessment of R/C buildings with innovative seismic protection systems." Proc: 14th World Conference on Earthquake Engineering, Innovation Practice Safety, Paper No. 10-0017, Beijing, China, October 12-17.

Mid America Earthquake Center (MAE) (2009). "Research projects and goals." http://mae.cee.uiuc.edu/projects/research_projects.html [Feb. 6, 2009]

Miranda, E., and Aslani, H. (2003). "Probabilistic response assessment for building specific loss estimation." *PEER Report No. 2003-03*. Pacific Earthquake Engineering Research Center, Univ. of California, Berkeley, Calif.

Moehle, J. P., and Deierlein, G. G. (2007) "The Pacific Earthquake Engineering Research Center, a 10 year perspective." Final Report 2007, http://peer.berkeley.edu/publications/ annual_report.html [Feb. 6, 2009].

Naaseh, S., Morgan, T. A., and Walters, M. T. (2002). "A critical evaluation of current US building code provisions and FEMA guidelines for the design of seismic isolated structures." *Proc., ATC 17-2 Seminar on Seismic Isolation, Passive Energy Dissipation and Active Control*, Applied Technology Council, Los Angeles, Calif.

NEES TIPS: Tools for Isolation and Protective Systems (2009). http://www.neng.usu.edu/cee/faculty/kryan/NEESTIPS/PBEE_study.html [13 July, 2009].

Ordonez, D., Foti, D., and Bozzo, L. (2003). "Comparative study of the inelastic response of base isolated buildings." Earthquake Engineering and Structural Dynamics, 32:151-164.

Palazzo, B., and Petti, L. (1996). "Reduction factors for base isolated structures." Computers and Structures, 60(6):945-956.

Pinto, P.E., and Vanzi, I. (1992). "Base isolation: reliability for different design criteria." *Proc. 10th World Conference on Earthquake Engineering*, pp. 2033-2038, Balkema, Rotterdam.

Politopoulos, I., and Sollogoub, P. (2005) "Vulnerability of elastomeric bearing isolated buildings and their equipment." Journal of Earthquake Engineering, 9(4):525-545.

Porter, K. A., Beck, J. L., and Shaikhutdinov, R.V. (2002) "Sensitivity of building loss estimates to major uncertain variables." Earthquake Spectra 18 (4), 719–743.

Ryan, K. L., and Polanco, J. (2008) "Problems with Rayleigh damping in base-isolated buildings." J. Struct. Eng., 134(11), 1780-1784.

Scott, M. H., and Fenves, G., L. (2006). "Plastic hinge integration methods for force-based beam-column elements." J. Struct. Eng., 132(2), 244-252.

Shen, J., Kitjasateanphun, T., and Srivanich, W. (2000). "Seismic performance of steel moment frames with reduced beam sections." Engineering Structures, 22(8), 968-983.

Shenton, H.W. III., and A. N. Lin (1994). "Relative performance of fixed-base and base-isolated concrete frames." Journal of Structural Engineering (ASCE), 119(10):2952-2968.

Somerville, P., Anderson, D., Sun, J., Punyamurthula, S., and Smith, N. (1998). "Generation of ground motion time histories for performance-based seismic engineering." *Proc. 6th U.S. National Conf. of Earthquake Engineering*, Seattle,

Washington.

Taghavi, S., and Miranda, E. (2003) "Response assessment of nonstructural building elements." *PEER Report No. 2003-05*. Pacific Earthquake Engineering Research Center, Univ. of California, Berkeley, Calif.

Tsai, K. C., and Popov, E. P. (1988) "Steel beam-column joints in seismic moment resisting frames." Report No. UCB/EERC-88/19, Earthquake Engineering Research Center (EERC), University of California at Berkeley, Calif.

Zhang, J., and Huo, L. (2009). "Evaluating effectiveness and optimum design of isolation devices for highway bridges using the fragility function method." Engineering Structures, In Press.

CHAPTER 5

COMPARATIVE LIFE CYCLE PERFORMANCE ASSESSMENT OF LOW-RISE BASE-ISOLATED AND CONVENTIONAL STEEL MOMENT RESISTING FRAME BUILDINGS

Introduction

The principal benefit of seismic isolation for buildings, to offer far superior performance in a design level earthquake, is generally accepted and recognized by structural engineers. With seismic isolation, flexible devices installed at the base lengthen or shift the building's natural period to the low acceleration region of the spectrum. Consequently, an isolated building accommodates the lower design forces elastically, and structural damage is eliminated or greatly reduced relative to a conventional building that accommodates the design forces through inelastic response. However, only 10-20% of the value in a typical U.S. building is apportioned to the structural system, while at least 80% is apportioned to nonstructural components and building contents (ATC 2008; Taghavi and Miranda 2003). Post-earthquake observations (Kircher *et al.* 1997; Porter *et al*. 2002; Comerio and Stallmeyer 2002) suggest that on average, losses in nonstructural components far outweigh the costs of damage to structural elements. Fortunately, lower accelerations experienced in isolated buildings lead to greatly reduced damage in acceleration-sensitive nonstructural components.

In the U.S., seismic performance objectives, which differ for isolated and conventional systems, are only implicitly embedded in code design standards (BSSC 2004; ASCE 2005; ICC 2006), and the performance benefits generally are not recognized by building owners and decision makers. The business culture cultivates an emphasis on

initial rather than lifetime costs of structural systems. Design performance objectives are rarely discussed with stakeholders, and a typical building owner expects that a code compliant building will retain operability following an earthquake. Even sophisticated owners that initially require or are convinced to choose higher performance are constrained by initial costs. When faced with additional complexities of seismic isolation design, such as analysis procedures, involved device testing requirements, and a lengthy design review process, these owners, in consultation with design professionals, often opt for alternative systems. However, performance approaches based on stiffening, strengthening, or even energy dissipation, are not nearly as effective as seismic isolation in eliminating acceleration related damage. Seismic isolation has the potential to be routinely adopted if reliable analysis tools are available to predict economic outcomes, and cultural transformation leads to routine discussion of lifetime economics as a basis for making design decisions.

Methodologies for performance evaluation and life cycle cost estimation have been under development for many years, with major investment by the earthquake engineering research centers (Moehle and Deierlein 2007; MAE 2009). Several comprehensive, structure specific examples have been developed that demonstrate alternative details in carrying out the methodology (Comerio 2005; Krawinkler 2005; Haselton *et al*. 2007). The Pacific Earthquake Engineering Research (PEER) Center approach is currently being adapted for practice by ATC-58, wherein partial guidelines (ATC 2007) and a loss estimation tool have been released. The PEER approach measures performance in terms of probabilistic decision variables, such as repair costs, downtime, indirect profit loss, and casualties (Miranda and Aslani 2003). The consequence analysis

is deconstructed into four basic stages: hazard analysis, structural response analysis, damage analysis, and loss analysis. The analyses are combined by integration over each random variable to determine the expected annual losses according to the total probability theorem.

To our knowledge, conventional and seismic-isolated buildings thus far have not been comparatively evaluated using the PEER loss estimation methodology. However, closely related techniques have been applied to evaluate seismic protection strategies applied to buildings (Bruno and Valente 2002) and bridges (Hahm *et al*. 2004). A number of studies have developed fragility functions – probabilistic functions relating damage measures to metrics of response or ground motion intensity – for isolated structures (Karim and Yamazaki 2007; Mezzi and Comodini 2008; Zhang and Huo 2009), but stopped short of predicting economic consequences.

Thus, the overarching objective of our study is to comparatively evaluate the life cycle performance of code-designed 3-story conventional and base-isolated steel moment resisting frame buildings using the PEER loss estimation methodology. The overall cost versus benefit of seismic isolation will be analyzed through comparison of initial design costs and expected economic losses (repair cost) over the life of the buildings. A steel moment frame has been selected to address whether a substantial benefit can be provided by applying isolation to a relatively flexible lateral system compared to an ideal stiff system. The hazard analysis and structural response analysis results have already been presented in detail (Sayani *et al*. 2009), while the actual cost/benefit study, including initial and life cycle cost estimation through damage and loss analysis, are presented in this paper. The initial cost of these buildings was computed with the help of Peter Morris,

a professional cost estimator. Probabilistic repair cost is estimated for nine discrete earthquake scenarios representing various annual probabilities of exceedance on the seismic hazard curve and annualized repair cost is determined integrating repair cost of all nine scenarios.

Building Description

Hypothetical three-story conventional and base-isolated moment resisting frame buildings were designed by Forell/Elsesser Engineers Inc. for use in this study. These office buildings (occupancy category II and importance factor I = 1.0) were designed by the Equivalent Lateral Force Method based on 2006 International Building Code (ICC 2006), ASCE 7-05 (ASCE 2005), and AISC 341-05 (AISC 2005). The buildings were designed for Los Angeles, CA location (Latitude: 34.50 N, Longitude: 118.2 W) on stiff soil (site class D with reference shear wave velocity = 180 to 360 m/s). The mapped spectral accelerations for this location are Ss = 2.2g for short periods and S1 = 0.74g for a 1 second period (g = acceleration due to gravity).

The conventional building was detailed for high ductility as a special moment resisting frame (SMRF), and uses reduced beam section (RBS or "dogbone") connections, which are the only pre-qualified welded connections permitted by AISC 341-05 (AISC 2005). However, the isolated building, which has lower ductility requirements, was detailed as an intermediate moment resisting frame (IMRF) utilizing welded unreinforced flange, welded web (WUF-W) beam-column connections. As such, design force reduction factors were R = 8 for the SMRF and RI = 1.67 for the isolated IMRF – assuming a design yield strength of 345 MPa (50 ksi) for structural steel – while

design drift limits were 2.5% for the SMRF and 1.5% for the isolated IMRF. The design of both buildings was drift controlled.

The building configurations are based on the plan layout for the 3-story SAC steel buildings (FEMA 2000a) with modifications (Fig. 5.1). The buildings are 55 m by 36.6 m (180 ft by 120 ft) in plan, with story heights of 4.57 m (15 ft) and column spacing of 9.15 m (30 ft) in each direction. Lateral resistance is provided by two 5-bay perimeter moment frames in the X-direction, and two 3-bay perimeter and two 2-bay interior moment frames in the Y-direction; moment-resisting bays are indicated by bold lines in Fig. 5.1. The steel sections selected for the moment-resisting frame members are listed in Table 5.1. The design displacement D_D of the isolators in the design earthquake and the maximum displacement D_M in the MCE at the center of rigidity are computed as (ASCE 2005):

$$D_D = \frac{gS_{D1}T_D}{4\pi^2 B_D} \quad , \quad D_M = \frac{gS_{M1}T_M}{4\pi^2 B_M} \tag{1}$$

where T_D, T_M are effective isolation periods; B_D, B_M are coefficients that modify the spectrum for damping; and S_{D1}, S_{M1} are the 1 second spectral accelerations for the corresponding events. Target values of T_M = 3.07 sec and effective damping ratio β_M = 16% were chosen for the MCE, while design values T_D and β_D were determined by iteration (Table 5.2). The total isolator displacement in Table 5.2 accounts for displacement amplification due to accidental torsion (Eq. 17.5-5 and 17.5-6 of ASCE 2005). The isolation devices have not been designed in detail so as to keep the study neutral with respect to isolation system.

Loss Estimation Procedure

The PEER loss estimation methodology provides a robust, probabilistic framework that extends first-generation performance-based earthquake engineering procedures (FEMA 2000c). The methodology measures performance in terms of probabilistic losses, wherein decision variables (DV), which include direct repair costs, downtime, business interruption losses, and casualties, are determined through a four step consequence analysis. The assessment problem is deconstructed into four basic elements or stages with introduction of three intermediate variables: hazard analysis (characterized by intensity measure IM), structural analysis (characterized by engineering demand parameters EDP), damage analysis (characterized by damage measures DM) and loss analysis (characterized by DV). In the hazard analysis, ground motions are selected to represent earthquake hazard ranging from frequent lower magnitude earthquakes with high probability of occurrence to higher magnitude earthquakes with low probability of occurrence. A hazard curve representing ground motion intensity (IM) versus frequency is defined and ground motions are selected for discrete events along hazard curve. In the second step, structural analysis, building models are created and analyzed to determine engineering demands (EDPs) for use in the damage analysis. The damage analysis step utilizes fragility function which relates computed demands (e.g. story drift, and roof acceleration) to physical description of component damage (DM) through probabilistic distributions. The final step of this methodology which gives estimates of decision variable of interest (e.g. median repair cost, downtime, or number of casualty) is called loss analysis. Loss analysis is the probabilistic estimation of structural performance conditioned on the damage state of all components. Considered all interim variables

Table 5.1. Member Sizes for the Conventional SMRF and Isolated IMRF

Frame	Story	Columns	Beams
SMRF	Roof	W14x211	W27x102
	2	W14x370	W33x130
	1	W14x370	W33x141
IMRF	Roof	W14x109	W18x60
	2	W14x176	W24x76
	1	W14x176	W24x84

Table 5.2. Design Parameters for the Isolation Systems

Isolator Properties	DBE	MCE
Effective Period	T_D = 2.77 sec	T_M = 3.07 sec
Effective Damping	B_D = 24.2 %	B_M = 15.8 %
Isolator Displacement	D_D = 32.1 cm (12.7 in.)	D_M = 61.7 cm (24.3 in.)
Total Displacement	D_{TD} = 38.8 cm (15.3 in.)	D_{TM} = 74.6 cm (29.4 in.)

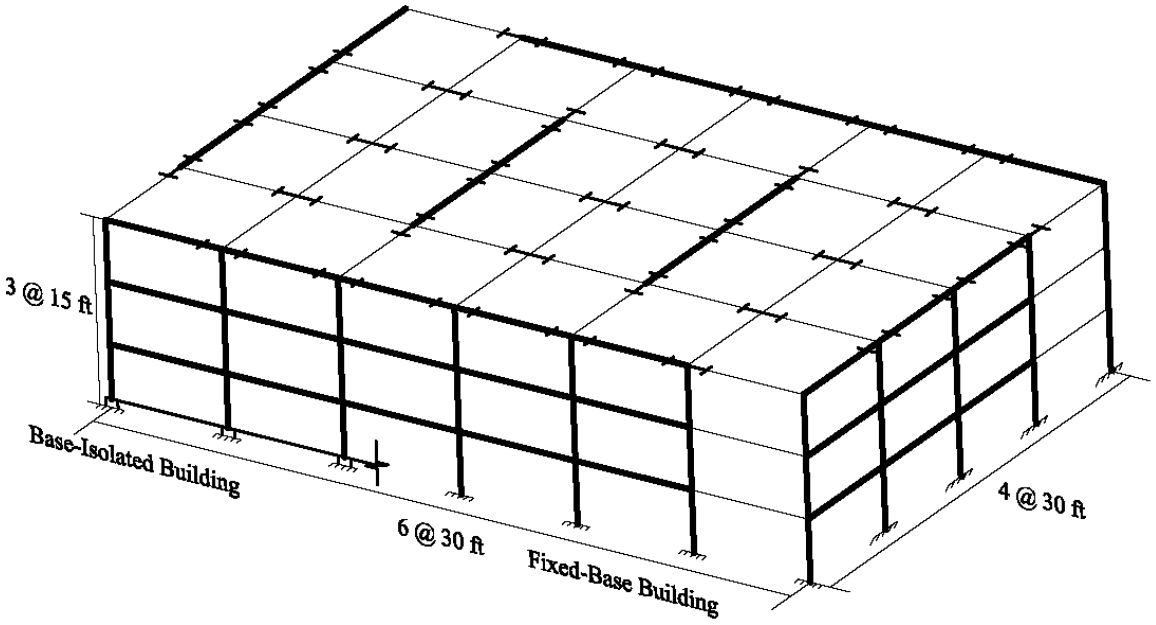

Fig. 5.1. D view of the building elevation and plan layout.

(IMs, EDPs, and DMs) as discrete random variables, loss analysis estimates the expected mean annual frequency (MAF) of the DV, i.e., λ(DV), according to the total probability theorem

$$\lambda(DV) = \iiint G\langle DV / DM \rangle / dG\langle DM / EDP \rangle / dG\langle EDP / IM \rangle / d\lambda(IM) \quad (2)$$

All the uncertainties inherent in this process can be tracked through this formula.

As such, three types of assessment procedures, namely, intensity, scenario, and time-based assessment are currently being considered in ATC guidelines (ATC 2007) for next generation PBEE. The intensity based assessment provides distribution of losses given that building experiences a ground motion of specific intensity, i.e. deterministic earthquake intensity. The scenario based assessment is similar to intensity based assessment except building experiences earthquake (rather than specific intensity) of specific magnitude and distance (e.g. 1994 Northridge earthquake or 1906 San Francisco earthquake). The time based assessment estimates probable loss, given all potential earthquakes that can occur in a given time period, and the mean probability of occurrence of each. There are various different ways to characterize earthquake shaking depending on type of assessment. The intensity based assessment uses response spectrum, the scenario based assessment utilizes median spectrum and its period dependent dispersion, and time-based assessment uses a mean seismic hazard curve. In the present study, scenario and time based assessment are used for performance assessment.

Various tools are available that can perform damage and los analysis (Mackie *et al*. 2006; Mitrani-Reiser 2007). For example, a program, the MATLAB Damage and Loss Analysis (MDLA) toolbox, was developed to integrate the hazard and structural analysis results and perform the damage and loss analyses (Mitrani-Reiser 2007). The inputs for

the toolbox are: a database of fragility and cost distribution functions, a table of the damageable components of the benchmark building, and the hazard and structural analysis results. The tool is divided into various modules which collects information for use in the damage and loss analyses, and to perform numerical integration (equation 2) using Simpson's method. The output of the damage and loss analysis include the average probability of damage for the mean design variants, the mean and variance of repair costs at each hazard level, the repair-cost vulnerability functions, the expected annual losses, the probability of safety tagging and associated downtime for damage assessments and repairs, the probability of fatalities and the mean losses associated with these deaths, and some modeling and design comparisons of the various design and modeling variants of the benchmark building.

Mackie *et al*. (2006) developed a program called Fourway which is a simple graphical tool for estimating the conditional dependence of decision variables *DVs*. The tool was consistent with the Pacific Earthquake Engineering Research Center's performance-based earthquake engineering framework (equation 2). The fourway tool simplifies the development of decision fragilities by exact determination of first moments and approximate determination of second central moments (variance) of the corresponding probability distributions, without the need for numerical integration of intermediate random variables as presented by equation 2.

For this study, a Matlab code is developed by authors to perform the damage and loss analyses. Rather than integrating integral (equation 2) explicitly, ATC (ATC 2007) uses Monte Carlo type procedures to develop mean estimates of casualties, direct economic losses and downtime. The same approach is also used in the Matlab code

developed for this study. A large set (hundreds) of simulations is required per intensity level to generate a loss curve using Monte Carlo procedures. Each simulation represents one possible outcome of the building experiencing the given intensity of motion. The Monte Carlo simulation sampling technique is used to sample from the distribution functions for seismic response, seismic fragility, and consequence functions. The discrete demand parameters determined from response history analysis (RHA) to individual ground motions are converted to distributions by computing the mean, standard deviation, and correlation matrix of the natural log of the demand vectors. Correlated demand vectors are generated by passing random variables sampled from a uniform distribution through a linear transformation based on the mean and correlated standard deviation (ATC 2007). By repeating the simulations and calculations many times, a distribution of loss (e.g. repair cost) is constructed for the chosen intensity of earthquake shaking. Sorting the losses in ascending or descending order enables the calculation of the probability that the total loss will be less than a specific value for a given intensity of shaking, producing a loss curve.

To summarize, PEER performance based loss estimation procedure involves following steps:

- Characterize earthquake shaking (hazard analysis)
- Simulate building response (structural analysis)
- Assess building damage (damage analysis)
- Compute building losses (loss analysis).

The damage analysis and loss estimation are the focus of this paper and described in detail in the following sections. The hazard analysis and structural analysis steps are presented in the first phase of this study (see Chapter 4) and summarized next.

Hazard Analysis and Ground Motion Selection

The following general procedure was used to select ground motions for loss estimation (ATC 2007). First, a hazard curve was defined that quantifies ground motion intensity versus frequency of occurrence. Individual points along the hazard curve represent various earthquake scenarios ranging from frequent small events to large rare events. For several distinct earthquake scenarios, target spectra were generated and ground motions were selected and amplitude scaled to best match the target spectra.

USGS national seismic hazard maps (Frankel *et al*. 2000) were consulted to generate uniform hazard spectra (target spectra) for nine selected events: which correspond to 10, 40, 72, 200, 475, 975, 1500, 2475, and 5000 year return periods. To modify the target spectra, spectral site modification factors that depend on both ground motion intensity and period were developed from next generation attenuation (NGA) relations (e.g. Campbell and Bozorgnia 2008; Chiou and Youngs 2008).

Three bins of ground motion were developed to represent three of the nine scenarios (72, 475, and 2475 year return period events). Using USGS seismic deaggregation data (Frankel *et al*. 2000), ground motions were selected according to the percentage contribution of magnitude and distance pairs to the seismic hazard for a given scenario. For each hazard level, 20 recorded natural ground motions that conform to the magnitude, distance and site class were selected from the PEER NGA database (Chiou *et al*. 2008), and amplitude scaled to match the target spectrum. Each bin was then

amplitude scaled again to match the two remaining nearest earthquake scenarios, as summarized in Table 5.3.

Table 5.3. Scale Factors for Each Earthquake Scenario Considered in this Study

Return Period (year)	Earthquake Bin	Bin Scale Factor
10		0.37
40	Bin 1	1
72		1.38
200		0.73
475	Bin 2	1
975		1.27
1500		0.84
2475	Bin 3	1
5000		1.21

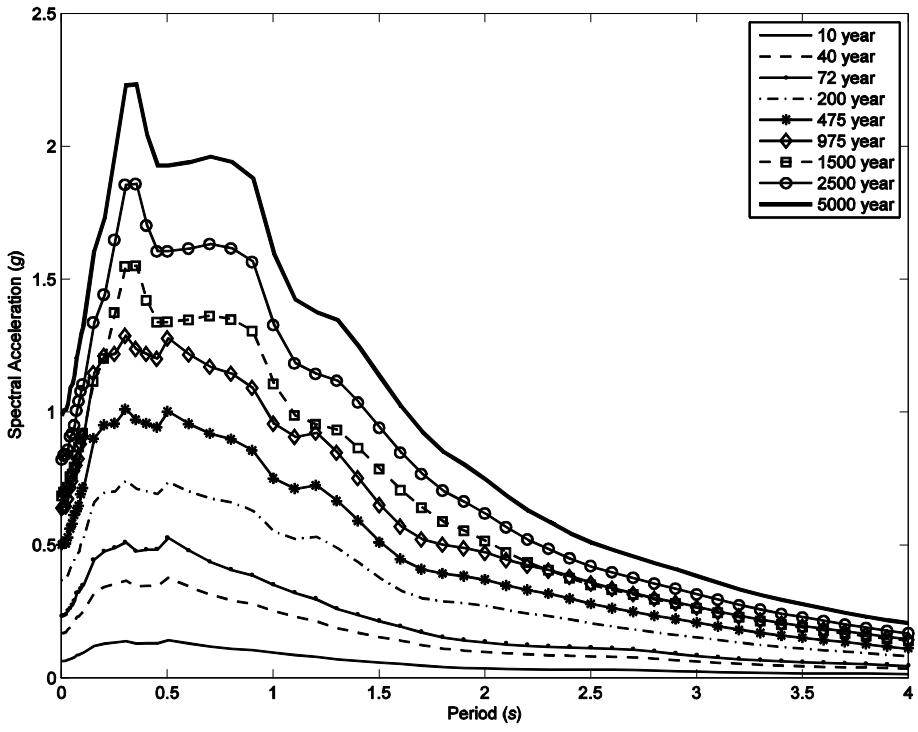

Fig. 5.2. Median response spectra of the scaled motions for all 9 earthquake scenarios.

While using recorded ground motions was considered to be ideal, we replaced some of the recorded motions with frequency modified motions to obtain a better match between the target hazard spectra and the median response spectra in the long period range. Hence, 10 pairs of ground motions in Bins 2 and 3, selected for the 475 and 2475 year hazard levels, were replaced by the corresponding SAC steel project – Los Angeles (SAC-LA) ground motion sets. These SAC motions were originally selected for similar location and site conditions, and frequency modified to match the target spectra (Somerville *et al*. 1998). These three ground motions bins are listed on the NEES TIPS project website (NEES TIPS 2009). Figure 5.2 compares the median response spectra for each bin scaled to the corresponding hazard level.

Model Development and Structural Analysis of the Buildings

For the structural analysis step, models for evaluation were developed using the guidelines of ASCE 7 (ASCE 2005) for design of new buildings and ASCE 41 (ASCE 2007) for evaluation of existing buildings. Detailed three-dimensional (3D) numerical models of both the conventional SMRF and isolated IMRF buildings were developed in the OpenSees computational environment. More information about modeling and design assumptions are presented in Chapter 4, and focusing on hazard and structural analysis results.

All columns and moment resisting beams were modeled using force-based nonlinear beam-column elements that combine finite length “plastic hinge” regions at the element ends with an interior elastic region (Scott and Fenves 2006). All columns were modeled using *fiber* sections, while moment resisting beams were modeled using stress

resultant section behavior. The steel stress-strain relationship for fiber sections and moment-curvature relationship for stress resultant models were both assumed to be bilinear with a strain hardening ratio of 3%. Gravity beams were modeled using elastic frame elements with moment releases at both ends. In the conventional SMRF, moment resisting and gravity columns were fixed and pinned at the base, respectively, while in the isolated IMRF, fixed connections were assumed at all beam-column joints at the base level. Energy dissipation was applied to the conventional structure and the isolated superstructure using tangent stiffness proportional damping calibrated to give 2.5% damping at their respective first mode frequencies.

In the RBS configuration, portions of the beam flanges at a section away from the beam end are tapered. Three frame elements were used to model beams with RBS connections for the conventional building, with elastic elements on the ends and the plastic hinge model described above in the middle to represent the region between the flange cutouts. Panel zone flexibility was explicitly modeled for the buildings, using a rotational spring that simulates the shear force/deformation behavior of the panel zone.

A model was developed for the behavior of isolation devices that incorporates a composite force-deformation relation in each direction that could represent either elastomeric or friction pendulum devices. An elastic column element and an elastic-perfectly plastic spring were assembled in parallel to obtain the composite bilinear lateral force-deformation behavior for a single isolator. The column element ensures transfer of the moments that arise due to the lateral deformation of the isolator. The elastic-perfectly plastic spring is a bidirectionally coupled element with a circular yield surface that exhibits identical resistance in any direction in the *x*-*y* plane. A nonlinear elastic spring

represented the vertical stiffness: with compressive stiffness to match a vertical frequency of 10 Hz, and a tensile stiffness of 1% of the compressive stiffness. The energy dissipation in the isolator model is provided by hysteresis in the lateral directions and viscous damping in the vertical direction (using a damping coefficient of 5% at the vertical frequency of 10 Hz).

Nonlinear response history analyses (RHA) were carried out to comparatively evaluate the structural response of the conventional SMRF and isolated IMRF when subjected to the ground motion suites described previously. Furthermore, incremental dynamic analysis (*IDA)* is carried out to evaluate collapse fragility for both building models. The results of these analyses are discussed in the following section.

Damage Analysis and Loss analysis

For the damage analysis step, the expected distribution of damage to structural and nonstructural building components is calculated based on the structural response determined from analysis together with data on the building configuration. This step utilizes component fragility curves, which relate qualitative descriptions of damage (DM) in structural and nonstructural components to the overall building response. For each component, one or more damage states are described, and fragility functions for each damage state are provided. The fragility functions are cumulative distribution functions relating the probability of being in each damage state to the most relevant EDP (e.g. story drift, floor acceleration). The probability density functions are lognormal distributions completely defined by median and dispersion. The EDPs associated with each fragilities are specified as directional (i.e. most lateral resisting systems) or non-directional (i.e. most acceleration sensitive nonstructural components).

Each structural and nonstructural component in a building is assumed to have a unique probability of sustaining damage in an earthquake, based on its construction characteristics, location in the building, and the response of the building to earthquake shaking. However, it is impractical to calculate losses for individual building components. Therefore, to make loss estimation manageable, components are assembled into collections of components called performance groups. Each performance group is statistically likely to experience the same damage, and thus is characterized by the same fragility functions in an earthquake. In this study, drift sensitive performance groups were differentiated not only by story, but also by plan location to account for the variation in observed story drifts across the plan of the building. For example, all the beam column connections in the first story of an exterior frame are identified as one performance group. Each structural analysis produces a vector of response quantities that can be applied as EDPs to one or more performance groups in the building. Component-specific fragility functions can then be used to characterize damage at the component level for the demands computed by the structural analysis.

Associated with each damage state is a repair action as well as consequence function, or loss function that describes the probabilistic repair cost associated with repairing a unit (sq. ft. of area, etc.) of the component in the given damage state. The consequence functions describe the median repair cost, and associated cost dispersion.

The structural and nonstructural components of the building shown in Fig 5.1 were determined from the building drawings provided by Forell-Elsesser Engineers. These basic structural plans were used to estimate quantities of building nonstructural components (e.g. exterior glazing, interior walls and finishes, and selected mechanical,

electrical, and plumbing features that would be damaged). In the absence of architectural drawings, quantities were based on the experience of our cost estimator. The building structural and nonstructural components considered for the damage and loss analyses, including brief descriptions and quantities, are summarized in Table 5.4. Assembly types numbering system is based on the Uniformat II classification system (ASTM 1996).

Table 5.5 summarizes the component fragility and consequence functions that were used in the study. Damage states and repair actions are described for each class of performance group. The fragility and consequence functions are represented as lognormal distributions, with given median (x_m) and dispersion (β) values. Whenever possible, fragility functions were selected from sources that documented their development.

Table 5.4. Table of Damageable Components

Assembly Type	Assembly Description	Unit	Quantity per Floor
B1035.000 a	Reduced Beam Section Connections	each	40
B1035.000 b	WUF W Connections	each	40
B2022.001	Aluminum Framed Windows	pane	6840
C1011.009a	Interior partitions & finish, 2 sided	sq. ft.	27100
C1011.009b	Interior finish only	sq. ft.	9000
C3032.001	Suspended Acoustical Tile Ceiling System	sq. ft.	23397
D1011.002	Traction Elevators	each	2
D4011.002	Automatic sprinklers (braced)	12 lf	595
E2022.011	Desktop computers	each	108
E2022.011a	Servers and Network equipment	each	1

Table 5.5. Performance Groups, and Fragility and Consequence Functions Used in Analysis

Performance Group	Fragility Functions				Consequence Functions			Source
	EDP^	Damage Description	x_m	β	Repair Action	x_m ($)	β	
RBS Connections	IDR* (%)	Flange and web buckling	2.2	0.22	Heat straightening	8000/each	0.3	Engelhardt *et al.* 2000 ; C. Gilton *et al.* 2000; and Yu *et al*. 2000
		Beam lateral torsional buckling	3.6	0.16	Heat straightening; replacement	15000 each	0.3	
		Tearing/fracture through beam flanges	5.6	0.17	Replace large portion of beam with shoring	60000 each	0.4	
WUF-W Connections	IDR (%)	Beam flange buckle; panel zone yielding	2.5	0.22	Add stiffener plate on web	8000/ each	0.3	Ricles *et al.* 2002
		Severe local buckling; weld cracking	3.7	0.14	Back gouge and reweld repair	15000 each	0.3	
		Beam bottom flange fracture	5.5	0.09	Replace large portion of beam with shoring	60000 each	0.4	
Aluminum Framed Windows	IDR (%)	Minor damage	1.6	0.29	Realignment	70/ pane	0.2	Krawinkler 2005
		Cracking without fallout	3.2	0.29	Replace glass panel	348/ pane	0.2	
		Panel falls out	3.6	0.27	Replace glass panel	696/pane	0.2	
2-sided Interior Partitions	IDR (%)	Small cracks	0.39	0.17	Patch	.67/sf	0.2	Porter 2000; and Mitrani-Reiser 2007
		Extensive cracking; crushing	0.85	0.23	Replace	3.90/ sf		

Table 5.5 Continued

Performance Group	Fragility Functions				Consequence Functions			Source
	EDP^	Damage Description	x_m	β	Repair Action	x_m ($)	β	
Interior Finish (Opposite Exterior Wall)	IDR (%)	Small cracks	0.39	0.17	Patch	.42/sf	0.2	Porter 2000; and Mitrani-Reiser 2007
		Extensive cracking; crushing	0.85	0.23	Replace	2.48/ sf	0.2	
Suspended Acoustical Tile Ceilings	PFA* (g)	Wires exposed, some panels fall	0.27	0.4	Fix wires, replace fallen panels	0.23	0.2	Krawinkler 2005
		Main runners & tee bars damaged	0.65	0.5	Replace bars and fallen panels	0.95	0.2	
		Grid tilts; near collapse	1.28	0.55	Replace ceiling and panels	3.16	0.2	
Traction Elevators	PGA* (g)	Failure	0.36	0.6	Inspection and repair	55000	0.2	
Automatic Sprinklers (braced)	PFA (g)	Fracture	32	1.4	Replace	1000	0.5	Mitrani-Reiser 2007
Servers and Network Equip.	PFA (g)	Overturning; Inoperable	0.8	0.5	Repair	50000	0.4	ATC 2007
Desktop Computers	PFA (g)	Falling; Inoperable	1.2	0.6	Repair/replace	3000	0.4	ATC 2007

* IDR = story drift, PFA = peak floor acceleration, PGA = peak ground acceleration

^ EDP = engineering demand parameter, x_m = median EDP for fragility or median repair cost for consequence, β = associated dispersion

Because documented fragilities for damage in moment connections could not be found, we developed fragilities separately for RBS and WUF-W connections from tests that were conducted as part of the SAC steel program (Engelhardt *et al.* 2000; Yu *et al*. 2000; Ricles *et al*. 2002). All test specimens utilized standard loading history developed for the SAC steel project and damage states were reported at discrete story drift values. Varied descriptions of damage in the connections were condensed to a total of three ordered damage states (DS1 precedes DS2, etc.) for each type of connection. Repair actions for all damage measures were obtained from FEMA guidelines (FEMA 2000b).

The fragility curves and damage states for RBS connection were developed from 18 tests on bolted and welded connection as shown in Table 5.6. Data from over twenty tests was reviewed and specimens with weak panel zones were excluded. The 18 test data set contains tests on welded and bolted connections, tests with strong panel zones, deep column specimen tests, and tests of connections with composite floor slab. During experimental testing, several tests were stopped prematurely due to damage in the test assembly and therefore, the third damage state (DS3) was observed in only 8 out of 18 test specimens. From test results, median story drift and dispersion in test data were determined for each damage state. Since the number of suitable tests for each case was limited, and due to the use of an identical loading protocol for each test, the observed variance in the test results is likely to be reality lower bound to the actual dispersion.

Similarly, the fragility curves for WUF-W connections were developed from seven test data developed for SAC steel project (Ricles *et al.* 2002). The third "failure" damage state was observed in six out of seven test specimens as shown in Table 5.7. Repair costs for structural beam/column connections were obtained from ATC guidelines

(ATC 2007). The fragility curves for nonstructural components and contents for this study were taken from best available sources and are discussed next. Repair costs for nonstructural elements and contents were evaluated by combining relative repair costs, denoted as a fraction of the replacement cost (Krawinkler 2005), with the unit replacement cost, evaluated from RSMeans (2008).

Table 5.6. Data Used to Develop Fragility Curves for RBS Moment Frame Connections

Type of connection	Test	DS1	DS2	DS3	Source
Welded	1	2.0%	4.0%		Engelhardt *et al.* 2000
	2	3.0%		7.0%	
	3	2.0%	4.0%		C. Gilton *et al.* 2000
	4	2.0%	4.0%		
	5	2.0%	4.0%		
	6	2.0%	5.0%		
	7	2.0%	3.0%	4.0%	
	8	1.5%	3.0%		Yu *et al.* 2000
	9	1.5%	3.0%		
Bolted	10	2.0%	3.0%		Engelhardt *et al.* 2000
	11	3.0%	4.0%	6.0%	
	12	2.5%	3.0%		
	13	2.0%			
	14	2.50%	3.50%	5%	Ricles *et al.* 2004
	15	2.50%	3.50%	5%	
	16	2.50%	3.50%	6%	
	17	2.50%	3.50%	6%	
	18	3.50%	4.50%	6%	
	Median	2.22%	3.61%	5.56%	
	Dispersion	0.22	0.16	0.17	

Table 5.7. Data Used to Develop Fragility Curves for WUF-W Moment Frame Connections

Test	DS1	DS2	DS3	Source
1	3.0%	4.0%	6.0%	Ricles *et al*. 2002
2	3.0%	4.0%		
3	3.0%	4.0%	5.0%	
4	2.0%	4.0%	6.0%	
5	2.0%	3.0%	5.5%	
6	2.0%	3.0%	6.0%	
7	3.0%	4.0%	5.0%	
Median	2.52%	3.68%	5.56%	
Dispersion	0.22	0.14	0.09	

Fragility curves for aluminum framed windows were obtained from Krawinkler (2005). Fragility curved for interior partitions (both 2 sided and 1 sided) as well as for automatic sprinklers were taken from Mitrani-Reiser (2007). Fragility curves for suspended ceilings were based on Krawinkler (2005). Fragility functions for desktop computers and network servers were obtained from ATC guidelines (ATC 2007).

The loss analysis, which is the final step of the PEER methodology, uses the *DMs* calculated in the damage analysis. The output of the loss analysis can be any decision variables that are in the interest of stake holders of the building such as direct economic loss. Performance metrics that have been generally considered include 3D's, i.e. dollar (repair cost), downtime (repair duration), and death (loss of life). Each metric provides unique and valuable information for stakeholders. Only repair cost is considered as decision variable (*DV*) in this study. However this framework can be easily modified to include other decision variables of interest as well. This final step of the methodology gives estimates of median repair cost for various scenario earthquakes as well as

annualized repair cost and these can be used to make variety of risk-management decisions.

Results

Initial Design and Construction Cost Estimates for the Buildings

Construction costs of the buildings were estimated were carried out to determine the initial cost premium for the isolated building (IMRF) relative to the conventional building (SMRF). The total cost of assembled structural elements, including materials and labor, was based on an assumed cost per unit quantity of raw materials using mid-2008 market values. For instance, concrete was priced at $350/cubic yard and steel was priced at $4000/ton. The cost of a moment connection was estimated from representative connection details, and is based on materials and labor per unit length of weld. Unit costs were also assumed for most assembled nonstructural components; for instance floor slabs, exterior walls, interior partitions, windows, roofing, ceilings, and wall finishes were all priced using a unit cost per square ft. Reasonable quantities for architectural elements that were not included in the structural plans were proposed based on Morris's professional experience.

The total building and site costs are broken down by category to illustrate the major contributing factors to the cost premium for seismic isolation (Table 5.8). The total building and site cost is US$16.8 million for the conventional SMRF and US$18.37 million for the isolated IMRF, which can be interpreted as a 9.3% cost premium for isolation. The additional costs for the foundation in the isolated building (Table 5.8) are primarily due to basement excavation, offsite disposal, and structural backfill. Added

costs associated with the seismic isolation layer include the isolation devices ($15000/each or $525K), the additional floor above the isolators ($710K), isolation pedestals ($28.8K), moat retaining wall ($170.6K) and moat covers ($47.4K) (Table 5.9). These additional costs are offset to some extent by reduced superstructure costs as a result of the substantially reduced section sizes of the moment frame elements in the isolated building. The small increase in the cost of nonstructural elements is due to waterproofing at the basement level ($139.3K), and the increase in utilities are due to line item add-ons such as suspended elevator shafts ($100K) and flexible piping

Table 5.8. Summary of Basic Building Cost

Component	Isolated IMRF	Conventional SMRF	% Increase for Isolation
Foundation	$487,288	$362,908	34.3%
Structural Elements (excluding the base level)	$1,506,050	$2,161,750	-30.3%
Isolation Layer	$1,482,192	-	NA
Nonstructural elements	$6,931,885	$6,792,605	2.1%
Elevators/mechanical and electrical systems	$7,965,112	$7,485,408	6.4%
Total Building and site cost	$18,372,527	$16,802,671	9.3%

Table 5.9. Component of Isolation Layer and Their Cost

Component of Isolation Layer		IMRF
Moat cover (sacrificial)		$47,400
Moat retaining wall, 8"		$170,640
Floor at lowest level		$669,832
	WF Structural steel	$428,000
	Metal deck with concrete fill	$177,632
	Fireproofing to steel	$64,200
Base isolator pedestals		$28,720
	Formwork	$11,760
	Concrete	$11,200
	Reinforcing	$5,760
Moment connections		$40,600
Isolators		$525,000

Table 5.10. Summary of Cost by Category

Category	Isolated IMRF	Conventional SMRF	% Increase for Isolation
Total building & site	$18,372,527	$16,802,671	9.3%
Planned construction cost	$21,027,527	$19,230,671	9.3%
Recommended budget	$23,130,527	$21,153,671	9.3%
Total soft cost package	$4,859,000	$4,231,000	14.8%
Total budget	$27,989,527	$25,384,671	10.3%

across the isolation interface ($105K), and lighting, sprinklers, and basement drainage in the isolation crawl space ($264.7K).

The total budget for the project is amplified by about 50% relative to the basic building and site cost, as reflected in Table 5.10. These various compounded surcharges are for the most part estimated as a percentage of the basic building and site cost, and are therefore unaffected by whether the building is isolated or not. The site cost portion generally includes site preparation and demolition, site paving and landscaping; however, the cost estimates for these buildings have been predicated on the assumption of a clean site with no site acquisition fee. The planned construction cost includes construction surcharges such as general conditions (9%) and contractor's overhead and profit (5%). The recommended construction budget is a fixed percentage of planned construction cost (usually 10%) to account for contingency for development of design, Soft costs (typically 18-20% of the construction budget) include items that are not considered in the direct construction cost such as architect and engineering design fees (8-10%), and legal fees. The only difference in the assumed surcharges for these buildings is an increased design fee for the isolated building (2% versus 1% for the conventional building), which is reflected in the soft cost package.

Structural Analysis

Eigenvalue analysis was carried out on both the building models to evaluate their elastic dynamic properties. The fundamental periods of the conventional SMRF and isolated IMRF are 0.89 and 3.23 sec, respectively. The fundamental period for the superstructure of the isolated building was found to be around 1.5 seconds, and thus isolation lengthens the period by less than a factor of 2. Nonlinear static analysis (or pushover analysis) was carried out under an inverted triangle load pattern to determine the base shear capacity and post-yield behavior based on the various building models. Capacity curves for both the conventional SMRF and superstructure of IMRF (without isolators) are plotted in Fig. 5.3. The conventional SMRF has a base shear capacity $V \approx 0.65W$, while the isolated IMRF has a base shear capacity $V \approx 0.25W$. Thus, the conventional SMRF is computed to be more than twice as strong as the isolated IMRF. While the SMRF model has positive incremental stiffness out to large deformation limits, the IMRF capacity curve essentially flattens after complete yielding. Thus, the isolated IMRF may be more prone to large inelastic excursions in yielding events.

The structural analysis step of the PEER PBEE methodology results in structural responses, or *EDPs*. The statistical distributions of various EDPs used by the fragility analysis are presented for 72, 475, and 2475 year events. The selected EDPs include peak story drift, and peak total floor acceleration. The EDPs were fit to lognormal distributions. One such fitted cumulative distribution function for story drift on the first and third floor is shown in Figure 5.4 [(a) and (b)]. Similarly, Figure 5.5 shows the fitted cumulative distribution functions from the raw data for peak floor and roof acceleration.

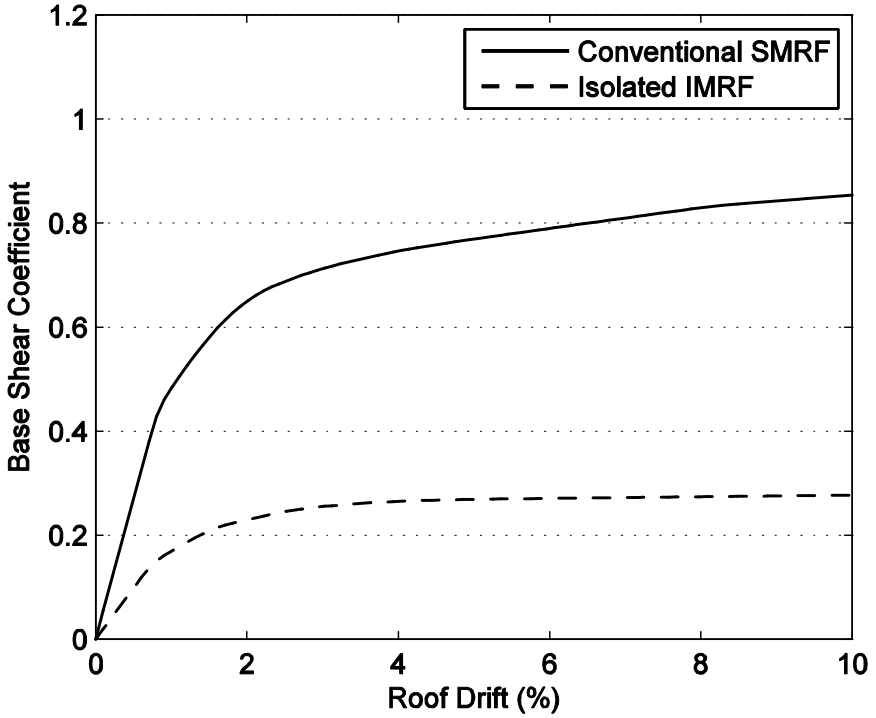

Fig. 5.3. Capacity curves.

Also shown in Figure 5.4 are the median damage state demands for various fragilities considered in this study. For example, interior partitions and connections are considered drift sensitive and their median values for different damage states are shown (Fig. 5.4). The median interstory drift demands for DS1 and DS3 (damage state 1 & 3) for interior partition are 0.39% and 0.85%. This means that interior partitions at first story can get damage in a frequent level earthquake (72 year) for both conventional and isolated buildings [Fig 5.4 (a)]. Thus, damage to interior partitions is likely in frequent level earthquake. Similarly, damage to the connections is unlikely in the isolated building in design event [Fig. 5.4 (b)]. However, damage to the connections is expected in both the buildings in design level (475 year) and rare earthquake events (2475 year) (Fig. 5.4).

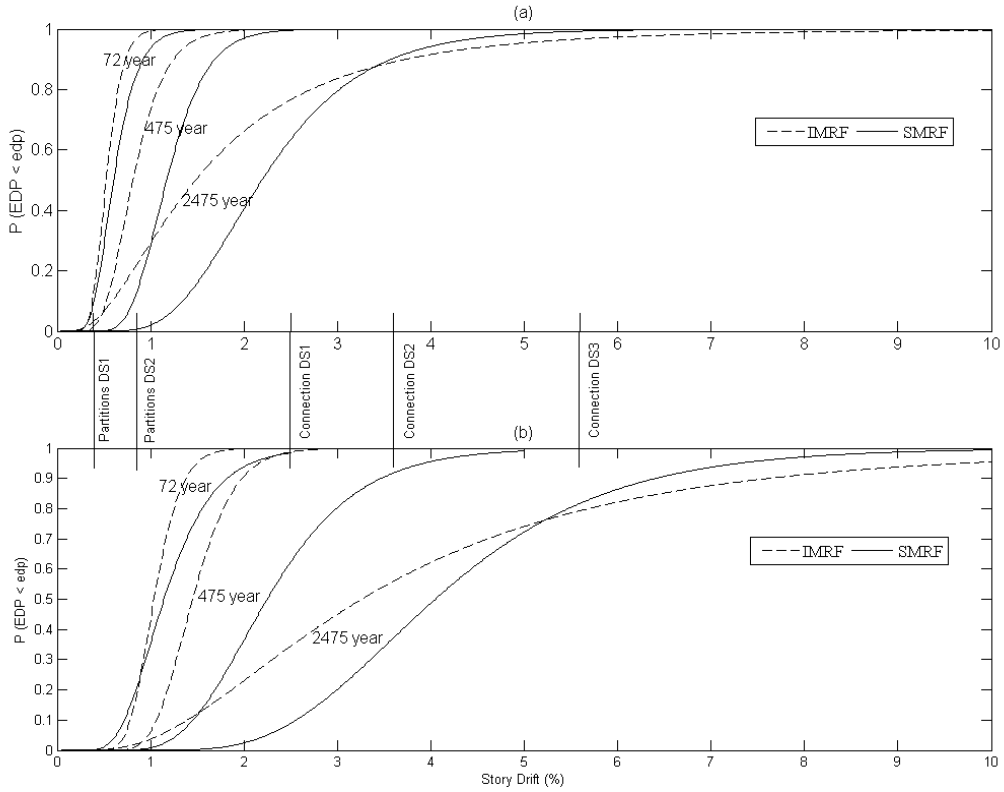

Fig. 5.4. Fitted cumulative distribution function for (a) 1st story drift, and (b) 3rd story drift.

As shown in Fig 5.5, damage to the acoustical ceiling is unlikely in the isolated building but likely in the conventional building for frequent level earthquake (72 year) as damage state 1 for ceiling (DS1) can occur at lower acceleration demands [Fig. 5.5 (a) and (d)]. However, further damage states are generally not observed in the isolated building since accelerations are attenuated from the ground. For the conventional building, damage is likely in acoustical ceilings [Fig. 5.5 (b), (c), (e), and (f)] as higher damage states (DS2 and DS3) are observed. Moreover, damage to servers and network equipment is expected in design (475 year) and rare (2475 year) events in the conventional building only (Fig. 5.5 (e)).

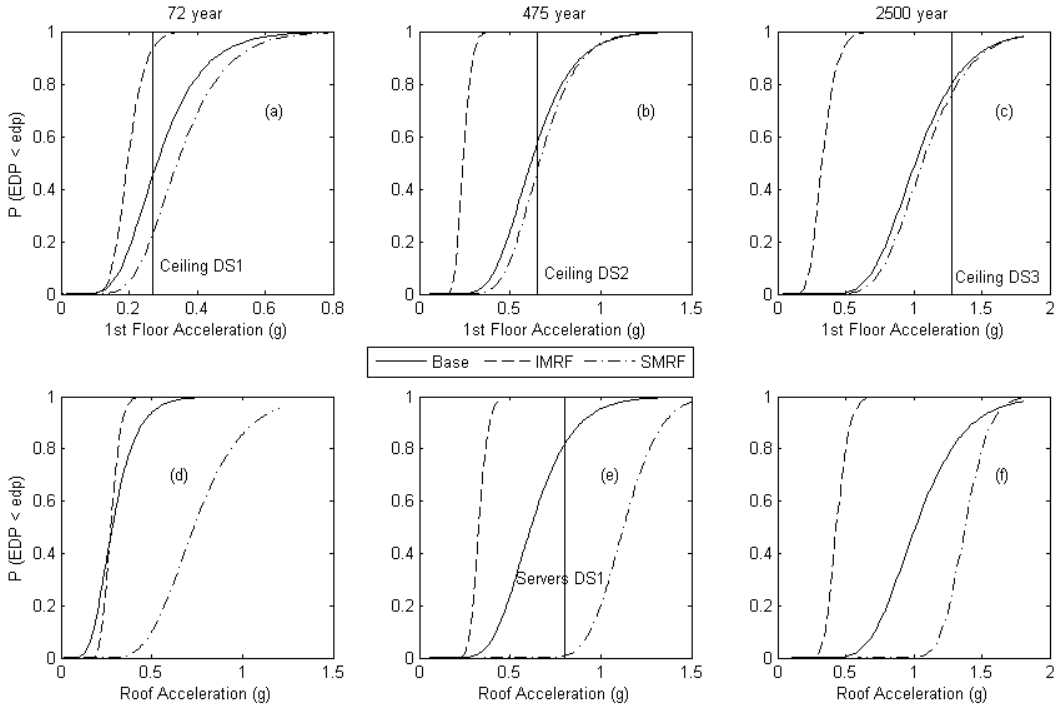

Fig. 5.5. Fitted cumulative distribution function for peak floor and roof acceleration.

Collapse Analysis

Incremental Dynamic Analysis (*IDA*) was carried out to predict collapse capacity of ground motion intensity measure *IM* (e.g. peak ground acceleration, S_a (T1)) of both the conventional and isolated IMRF buildings. Out of several methods to determine collapse capacity of a structure, incremental dynamic analysis (*IDA*) remains popular choice among engineers. In this analysis, for a representative ground motion record, a response history analysis is performed on a mathematical model of the structure and the response parameter (e.g. maximum interstory drift) is obtained (Villaverde 2007). The ground motion record is then incrementally increased and the analysis is repeated. This process of incrementing the strength of the record and re-performing the dynamic analysis is repeated until structural instability (large increment in response parameter for

a small increment in ground motion intensity) produced. The relationship between observed response parameter versus intensity measure (e.g. PGA, Sa (T1)) for each analysis is then plotted to determine collapse capacity. The collapse capacity of intensity measure *IM* is taken as the lesser of that intensity measure at which the slope of IDA becomes flat or at which confidence is lost in the validity of the analysis (Vamvatsikos and Cornell 2004).

For *IDA*, two-dimensional (2D) mathematical models were created using deterioration properties of beam sections for both the buildings. Analytical models use "clough material model" which are developed with stiffness and strength deterioration properties determined by the following model parameters, cap strength and deformation, post capping stiffness, and residual strength. Lignos and Krawinkler (2007) developed an extensive database on deterioration properties of steel beams and columns subjected to cyclic bending moments. This database is based on monotonic and cyclic component experiments for steel beams and columns performed over the last forty years. The parameters of the deterioration model used in this study were created with the help of this database and incremental dynamic analysis was performed using suite of twenty ground motions to predict the collapse capacity of intensity measure of both the buildings. The peak ground acceleration (*PGA*) was chosen as intensity measure (*IM*). The collapse fragility curve is then created and plotted in Fig 5.6. The median probability of collapse for the conventional SMRF and isolated IMRF is PGA of 2.39 *g* and 1.93 *g*, respectively.

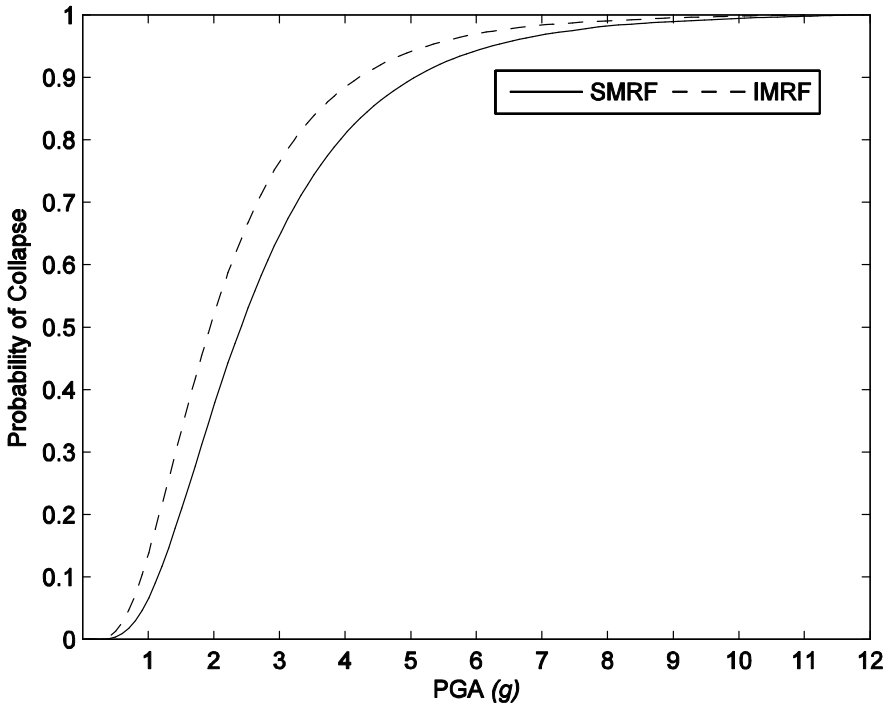

Fig. 5.6. Collapse fragility function.

Repair cost

In this study, loss estimation was carried out using a Matlab code developed by the authors for this purpose. A total of nine scenarios- ranging from 10 year to 5000 year event (10, 40, 72, 200, 475, 975, 1500, 2475, and 5000 year) are considered for loss estimation. Direct repair cost is selected as a measure of decision variable (*DM*). Total expected losses in the building is obtained using following equation,

$$E(L_T / IM = im) = E(LT \setminus NC, IM = im).P(NC \setminus IM = im) + E(LT \setminus C, IM = im).P(C \setminus IM = im) \quad (3)$$

where $E(LT \setminus NC, IM = im)$ is the expected losses in the building provided that collapse does not occur, $P(NC \setminus IM = im)$ is the probability of non-collapse, $E(LT \setminus C, IM = im)$ the expected losses in the building provided that collapse occurs, and

$P(C \setminus IM = im)$ is the probability of collapse. Thus, expected losses due to non-collapse scaled by probability of non-collapse is added to the expected losses due to collapse scaled by probability of collapse to obtain expected value of total repair cost for a given scenario.

Based on total repair cost results from equation 3, cumulative distribution function which shows -probability of exceeding certain dollar loss in a given earthquake scenario, P (total repair cost <= $C) - is plotted [Fig 5.8 (a) and (c)]. This measure of seismic performance can also provide dollar losses associated with certain probabilities of being exceeded in a given earthquake scenario. Out of nine scenarios considered for this study, the cumulative distribution function of the total building repair cost for only three different scenarios (72 year, 475 year, and 2475 year) are presented [Fig 5.8 (a) and (c)] for the purpose of brevity.

Numerous issues were encountered while calculating median repair cost for non-collapse case. In non-collapse losses distribution, when there are a lot of zeros present (more than 70% of data points) the median repair cost comes very close to zero while dispersion is very large. It was also noticed that few zeros (less than 10%) in the distribution has large impact on median values as median value was observed to be less than the average value. The underlying problem is that data does not fit lognormal distribution. In order to avoid this dilemma, zeros in non-collapse distribution were replaced by nonzero number which is defined by maximum number in the distribution multiplied by the cost factor. The cost factor is taken as 0.01 (for number of zeros in non-collapse distribution less than 10%) or 0.0001 (for number of zeros in non-collapse distribution less than 50% of the non- collapse distribution) depending on number of

zeros present in the non-collapse distribution. For number of zeros between 10% and 50% of non-collapse distribution, following expression is used (equation 4).

$$cost\ factor = e^{(-0.1151(\%\ of\ zeros)\ -3.4539)} \quad (4)$$

Cumulative distribution curves (Fig. 5.8 (a) and (c)) can be used to quantify the annual frequency of the total repair cost exceeding a given threshold. The resulting curve is called annualized loss curve which present the probability of loss considering all earthquakes that might occur in the period of a year. Fig. 5.8 [(b), (d)] presents annualized loss curve for both the buildings considering all nine scenarios and can be obtained as follows: First, a seismic hazard curve (ATC 2007), which plots the relationship between earthquake intensity, *e*, and the mean annual frequency of exceedance of *e*, is developed (Fig. 5.7) representing earthquake events ranging from frequent level earthquake to rare events (e.g. from 10 year event to 5000 year event). Second, the complement of each CDF (cumulative distribution function) curve presented in Fig. 5.8 [(a), (c)] is multiplied by the change in the mean annual frequency of exceedance of *e*, at the corresponding IM level; the resulting curves are integrated (summed over) across IM levels to construct an annualized loss curve of the type shown in Fig. 5.8 [(b) and (d)]. The accuracy of the annualized loss curve is a function of the number of intervals of earthquake intensity used in the computation. In this study, nine earthquake intensities (nine scenarios) are considered to develop an annualized loss curve.

Fig. 5.8 [(b) and (d)] shows the annual rate of exceeding total repair cost for all the IM levels for the conventional and the isolated buildings, respectively. Furthermore, the mean annual total loss can be obtained by integrating area under the loss curve which

is around $U.S 32,577 and $U.S 24,528 for the conventional and the isolated building, respectively.

The breakdown of median repair cost along with their probabilities for all the nine earthquake scenarios are presented next (Table 5.11). Note that collapse does not occur in any of the buildings (conventional SMRF and isolated IMRF) for 10 year and 40 year scenario earthquakes. However, small probability of collapse is observed for 72 year event in the isolated building. It is obvious that probability of collapse increases, as earthquake intensity increases. The total median repair costs for the isolated building are about 37% of the conventional building in the design earthquake. In the MCE, damage in the isolated building is about $1.4 million, which is about 58% of damage to the conventional building ($2.4 million).

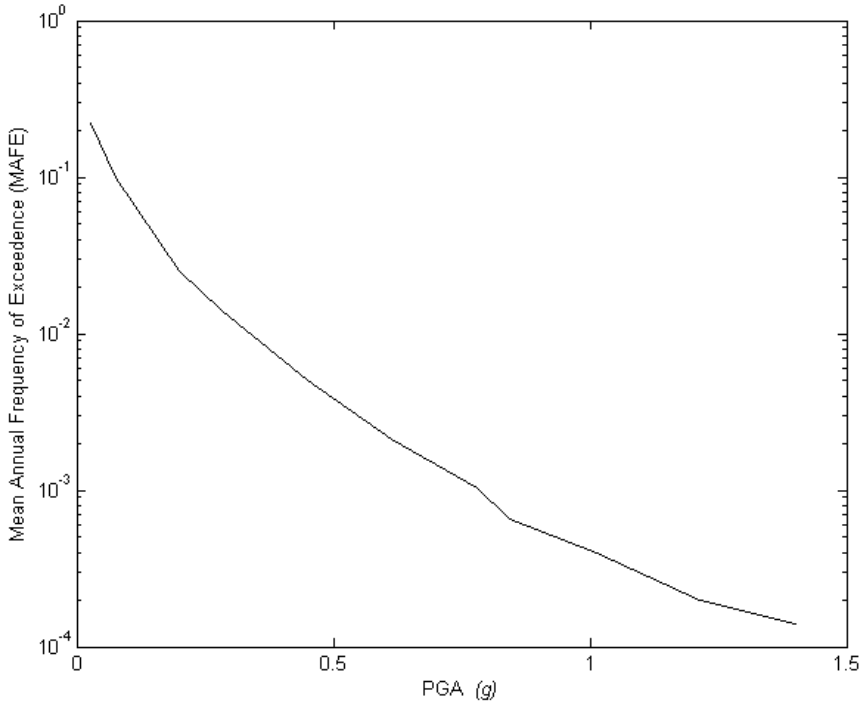

Fig. 5.7. Seismic hazard curve.

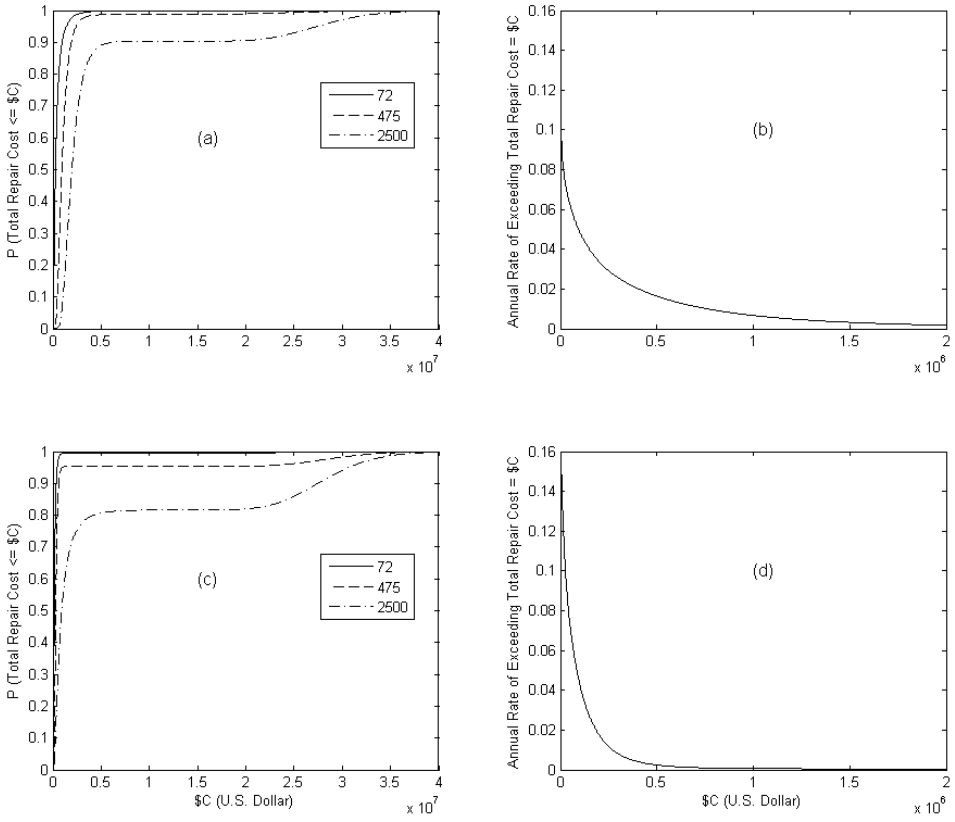

Fig. 5.8.CDF for P(Total Repair Cost <= $C/IM) for (a) Conventional Building, (c) Isolated building, Loss curve for (b) Conventional Building and (d) Isolated building.

Table 5.11. Summary of Total Median Repair Costs of Buildings

Scenario	Building	P (No Collapse)	P (Collapse)	Median Loss ($K)		
				NC	C	Total
10 year	SMRF	1	0	1.8	N.A.	1.8
	IMRF	1	0	20.1	N.A.	20.1
40 year	SMRF	1	0	131.7	N.A.	131.7
	IMRF	1	0	99.1	N.A.	99.1
72 year	SMRF	1	0	263.5	N.A.	263.5
	IMRF	0.996	0.004	136.9	27914	139.6
200 year	SMRF	0.996	0.004	622.7	28492	631.7
	IMRF	0.984	0.016	197.4	24984	213.5
475 year	SMRF	0.988	0.013	917.6	24848	956.2
	IMRF	0.954	0.046	283.9	28653	351.5
975 year	SMRF	0.959	0.041	1249	27765	1419.4
	IMRF	0.908	0.093	376.7	28321	561.8
1500 year	SMRF	0.958	0.043	1520.7	26897	1718.2
	IMRF	0.900	0.100	501.1	28485	750.6
2500 year	SMRF	0.904	0.096	1844.9	27657	2394.1
	IMRF	0.818	0.183	708.2	28023	1385.7
5000 year	SMRF	0.833	0.168	2412.9	27968	3637.3
	IMRF	0.781	0.219	1114.2	28307	2260.9

Conclusions

PEER loss estimation methodology is applied to 3 story conventional fixed-base SMRF and isolated IMRF building. For the design earthquake event, results suggest that the isolated building can save up to $605K USD. Loss estimation results suggests that seismic isolation of a steel moment frame building will save up to US$1.1 million or more in repair costs in an earthquake that equals or exceeds the design intensity. This is less than the estimated premium for seismic isolation for the building, which is more than US$2 million based on the recommended budget. Furthermore, annualized repair cost for the conventional SMRF and the isolated IMRF building is about $32,577 and $24,528 USD. Therefore, if the investor of the building opts for isolation design over conventional

design, saving of only $8000 per year can be realized. Considering initial cost premium of $2 million for isolation design over conventional design, it will take 250 years for any investor to recover his investment. This observation certainly does not provide any motivation to the investor to opt for isolation design alternative over conventional fixed-base design. However, the total economic impact of the earthquake, considering a more complete set of component fragilities, downtime, profit loss, and possible collapse of the building, could be much greater and can change the results observed in this study.

References

American Society for Testing and Materials (ASTM) (1996), "E1557-96 Standard Classification for Building Elements and Related Sitework – UNIFORMAT II." 1997 Annual Book of ASTM Standards, Section 4, Construction, Volume 04.11 Building Constructions, West Conshohocken, Penn.

American Institute of Steel Construction (AISC) (2005). *AISC 341-05 Seismic Provisions for Structural Steel Buildings*, Chicago, Ill.

American Society of Civil Engineers (ASCE) (2005). ASCE 7-05 Minimum Design Loads for Buildings and Other Structures, Reston, Va.

American Society of Civil Engineers (ASCE) (2007). ASCE 41, Seismic Rehabilitation of Existing Buildings, Reston, Va.

Applied Technology Council (ATC) (2007) "Guidelines for Seismic Performance Assessment of Buildings 35% Complete." *Draft prepared for Department of Homeland Security*, Washington, D.C.

Applied Technology Council (ATC) (2008). Reducing the Risks of Nonstructural Earthquake Damage, ATC-69 Project Report – State of the Art and Practice. Prepared for Federal Emergency Management Agency, Washington, D.C.

Building Seismic Safety Council (BSSC) (2004). FEMA 450, NEHRP Recommended Provisions and Commentary for Seismic Regulations for New Buildings and Other Structures, Washington, D.C.

Bruno, S., and Valente, C. (2002). "Comparative response analysis of conventional and innovative seismic protection strategies." Earthquake Engineering and Structural Dynamics, 31(5):1067-1092.

C. Gilton, B. Chi, and C. M. Uang., (2000) "Cyclic response of RBS moment connections: weak-axis configuration and deep column effects." SAC/BD-00/23, SAC Joint Venture.

Campbell, K. W., and Bozorgnia, Y. (2008). "NGA ground motion model for the geometric mean horizontal component of PGA, PGV, PGD and 5% damped linear elastic response spectra for periods ranging from 0.01 to 10 s." Earthquake Spectra, 24(1):139-171.

Chiou, B., Darragh, R., Gregor, N., and Silva, W. (2008). "NGA project strong-motion database." Earthquake Spectra, 24(1):23-44.

Chiou, B. S.-J., and Youngs, R. S. (2008). "An NGA model for the average horizontal component of peak ground motion and response spectra." Earthquake Spectra, 24(1):173-216.

Comerio, M. C., and Stallmeyer, J. C. (2002). "Nonstructural loss estimation: the UC Berkeley case study." *PEER Report No. 2002/01*, Pacific Earthquake Engineering Research Center, University of California at Berkeley.

Comerio, M. C., (ed.) (2005). "PEER testbed study on a laboratory building: exercising seismic performance assessment." *PEER Report No. 2005/12*, Pacific Earthquake Engineering Research Center, University of California at Berkeley.

Engelhardt, M. D., Fry, G., Jones, S., Venti, M., and Holliday, S. (2000) "Behavior and design of radius cut reduced beam section connections." SAC/BD-00/17, SAC Joint Venture.

Federal Emergency Management Agency (FEMA) (2000a) FEMA 355-C State of the Art Report on Systems Performance of Steel Moment Frames Subjected to Earthquake Ground Shaking, Washington, D.C.

Federal Emergency Management Agency, FEMA 352 (2000b) Recommended Postearthquake Evaluation and Repair Criteria for Welded Steel Moment-Frame Buildings, Washington, D.C

Federal Emergency Management Agency (FEMA) (2000c) FEMA 356 Prestandard and Commentary for the Seismic Rehabilitation of the Buildings, Washington, D.C.

Frankel, A. D., Mueller, C.S., Barnhard, T.P., Leyendecker, E.V, and Wesson, R.L. (2000). "USGS national seismic hazard maps." Earthquake Spectra, 16(1):1-19.

Hahm, D., Koh, H-M., Shin, J-H., and Park, Y.-S. (2004). "Life cycle cost analysis for the seismic isolation of bridges in a region of low to moderate seismicity." *Proc. 13th World Conference on Earthquake Engineering*, Paper No. 2844, Vancouver, Canada.

Haselton, C. B., Goulet, C.A., Mitrani-Reiser, J., and Beck, J.L. (2007). "An assessment to benchmark the seismic performance of a code-conforming reinforced concrete moment frame building." *PEER Report 2007/12*, Pacific Earthquake Engineering Research Center, University of California at Berkeley, Calif.

International Code Council (ICC) (2006). *International building code (IBC).* Falls Church, Va.

Karim, K. Z., and Yamazaki, F. (2007). "Effect of isolation on fragility curves of highway bridges based on simplified approach." Soil Dynamics and Earthquake Engineering, 27(5):414-426.

Kircher, C., Reitherman, R., Whitman, R., and Arnold, C. (1997). "Estimation of earthquake losses to buildings." Earthquake Spectra, 13(4):703-720.

Krawinkler, H. (ed.) (2005). "Van Nuys hotel building testbed report: exercising seismic performance assessment." *PEER Report No. 2005/11*, Pacific Earthquake Engineering Research Center, University of California at Berkeley, Calif.

Lignos, D.G., and Krawinkler, H. (2007), "A Database in Support of Modeling Component Deterioration for Collapse Prediction of Steel FrameStructures." ASCE Structures Congress, Long Beach, CA, Sei Institute.

Mackie, K., and B. Stojadinovic. (2006) "Fourway: Graphical Tool for Performance-Based Earthquake Engineering." ASCE Journal of Structural Engineering, August 2006, Vol. 132, No. 8, pp. 1274-1283

Mezzi, M., and Comodini, F. (2008). "Comparative economic assessment of R/C buildings with innovative seismic protection systems." *Proc. 14th World Conference on Earthquake Engineering*, Innovation Practice Safety, Paper No. 10-0017, Beijing, China, October 12-17.

Mid America Earthquake Center (MAE) (2009). "Research projects and goals." http://mae.cee.uiuc.edu/projects/research_projects.html [Feb. 6, 2009]

Miranda, E., and Aslani, H. (2003) "Probabilistic response assessment for building specific loss estimation." *PEER Rep. 2003-03*, Pacific Earthquake Engineering Research Center.

Miranda, E., and Aslani, H. (2003). "Probabilistic response assessment for building specific loss estimation." *PEER Report No. 2003-03*. Pacific Earthquake Engineering Research Center, Univ. of California, Berkeley, Calif.

Mitrani-Reiser, J. (2007) "An Ounce of Prevention: Probabilistic Loss Estimation for Performance-Based Earthquake Engineering." PhD Dissertation, California Institute of Technology, Los Angeles, Calif.

Moehle, J. P., and Deierlein, G. G. (2007). "The Pacific Earthquake Engineering

Research Center, a 10 year perspective." Final Report 2007, http://peer.berkeley.edu/publications/ annual_report.html [Feb. 6, 2009].

NEES TIPS: Tools for Isolation and Protective Systems (2009). http://www.neng.usu.edu/cee/faculty/kryan/NEESTIPS/PBEE_study.html [13 July, 2009].

Porter, K. A., Beck, J. L., and Shaikhutdinov, R.V. (2002). "Sensitivity of building loss estimates to major uncertain variables." Earthquake Spectra 18 (4), 719–743.

Porter, K. A, Kiremidjian, A.S., and Legrue, J. S. (2001)"Assembly-based vulnerability of buildings and its use in performance evaluation." Earthquake Spectra, 17 (2), 291-312.

Porter, K. A. (2007) "Fragility of elevators for use in performance-based earthquake engineering." Earthquake Spectra, 23(2), 459-469.

Ricles, J. M., Mao, C., Lu, L. W., and Fisher, J. W. (2002) "Development and evaluation of improved details for ductile welded unreinforced flange connections." SAC/BD-00/24, SAC Joint Venture.

Ricles, J. M., Zhang X., Lu, L., and Fisher, J. (2004) "Development of seismic guidelines for deep-column steel moment connections." ATLSS Report No. 04-13.

RS Means Co. (2008) Assemblies Cost Data, 34th ed., Construction Publishers & Consultants, Kingston, Mass.

Scott, M. H., and Fenves, G. L. (2006). "Plastic hinge integration methods for force-based beam-column Elements." J. Struct. Eng., 132(2), 244-252.

Somerville, P., Anderson, D., Sun, J., Punyamurthula, S., and Smith, N. (1998). "Generation of ground motion time histories for performance-based seismic engineering." *Proc. 6th U.S. National Conf. of Earthquake Engineering*, Seattle, Washington.

Taghavi, S. and Miranda, E. (2003). "Response assessment of nonstructural building elements." *PEER Report No. 2003-05*. Pacific Earthquake Engineering Research Center, Univ. of California, Berkeley, Calif.

Vamvatsikos, D., and Cornell C. A. (2004). "Applied incremental dynamic analysis." Earthquake Spectra 20 (2), 523–553.

Villaverde, R., (2007). "Methods to Assess the Seismic Collapse Capacity of Building Structures: State of the Art." J. Struct. Eng., 133(1), 57-66.

Yu, Q. S., Gilton, C., and Uang, C. M. (2000) "Cyclic response of RBS moment connections: loading sequence and lateral bracing effects." SAC/BD-00/22, SAC Joint Venture.

Zhang, J., and Huo, L. (2009). “Evaluating effectiveness and optimum design of isolation devices for highway bridges using the fragility function method.” Engineering Structures, In Press.

CHAPTER 6

CONCLUSION

Various approaches to characterize nonlinear isolation systems for design have been evaluated. The normalized strength approach characterizes the isolation system in terms of an isolation frequency, a characteristic strength, and a ground motion intensity measure. The equivalent linear approach characterizes the isolation system in terms of an effective period and effective damping ratio. For both approaches, intensity independent response measures were proposed: normalized deformation for the normalized strength characterization and deformation ratio (peak deformation divided by spectral displacement) for the equivalent linear characterization; and were evaluated in their ability to reduce dispersion compared to the actual deformation. For the normalized strength characterization, three measures of intensity were evaluated: peak ground velocity, spectral velocity, and peak ground displacement; wherein peak ground velocity was judged to be the most effective.

The normalized strength characterization is based on physically meaningful parameters of the isolation system that can be easily determined, while the equivalent linear characterization uses an effective period and effective damping ratio that are generally determined by iteration.

For the normalized strength characterization, the dispersion of normalized deformation is reduced somewhat compared to the dispersion of the actual deformation, indicating that peak ground velocity is an effective measure of ground motion intensity for this approach. For the equivalent linear characterization, the dispersion of the deformation ratio is reduced substantially compared to the dispersion of the actual

deformation, indicating that spectral displacement, which has long been used as the estimated deformation, is an effective starting point to obtain the actual deformation considering system nonlinearity.

The possibility of allowing the superstructures of isolated buildings to respond inelastically – with deformation ductilities comparable to those of fixed-base buildings – has been investigated. Response history analysis results have demonstrated that given comparable ductility, force reduction factors *R* in base-isolated buildings are smaller than in fixed base buildings, but superstructure design forces in isolated buildings can still be reduced considerably. Also, at the same superstructure ductility, isolated buildings showed greatly enhanced performance with respect to superstructure deformation and total acceleration demands. Thus, isolated buildings designed to reduced strength, which is expected to correlate to reduced design costs, still outperform fixed-base buildings.

Force reduction factors for isolated buildings tend to decrease with increasing isolation period shift, which limits the benefit of reducing forces by allowing superstructure inelasticity, but increase with increasing isolation system strength, which somewhat counteracts the larger superstructure force demands associated with increased strength. In general, the inelastic superstructure response is less sensitive to the isolation system properties than an elastic superstructure.

The seismic performance of code compliant 3 story low rise steel moment frame buildings – both conventional SMRF and base-isolated IMRF – has been compared. The design objectives for the isolated IMRF have been met, i.e., structural yielding is eliminated for both the design (10/50 year) and frequent (50/50 year) events and floor accelerations are reduced considerably – by factors of 3 or 4 – relative to the

conventional SMRF.

Demands in an isolated building can be predicted with high confidence for ground motion intensities at or below the design intensity, as the dispersions in response parameters are reduced to a fraction of those in the conventional building.

The flexibility of the moment frame leads to non-negligible structural participation in the first modes of the isolated IMRF, and larger relative story drifts compared to idealized (stiff) structural systems. This phenomenon is exacerbated in a frequent/small event where the isolation system is not fully activated. Even though the isolated IMRF does not yield in the design event, damage to drift-sensitive nonstructural components would not be prevented. However, steel moment frames provides reliable, stable performance, and floor accelerations are attenuated to values that would unequivocally safeguard acceleration sensitive nonstructural components and contents.

Given these conclusions, a knowledgeable stakeholder must determine whether protecting a steel moment-resisting frame building with seismic isolation is a good decision, knowing that performance might not be improved in the MCE. However, the composite probability that (a) an event like the MCE is experienced over the life of the building, and (b) the event induce an outlier response that puts the building in danger of collapse is extremely small. In our judgment, from the perspective of performance, choosing seismic isolation for a moment frame is still a wise investment, if it can be shown to effectively limit losses and interruptions in design events, which remains to be seen in the complete loss estimation study.

VITA

PRAYAG J. SAYANI

EDUCATION:

- Doctor of Philosophy (**Ph.D.**) October 2009
  Structural Engineering, Utah State University, Logan, Utah

- Master of Engineering (**M.E.**) July 2005
  Structural Engineering, Gujarat University, India

- Bachelor of Engineering (**B.E.**) July 2003
  Civil Engineering, Gujarat University, India

PROFESSIONAL SUMMARY:

- Analysis and Design of Steel Structures
- Base-Isolation Systems
- Design of RCC and Steel Bridges using AASHTO LRFD Bridge Design Specifications
- Performance Based Earthquake Engineering
- Nonlinear Dynamic Analysis
- Risk-Assessment Methodology

AWARDS AND HONORS:

- Distinguished Service Award, Graduate Student Senate, Utah State University, April 2009
- Outstanding Graduate Student Award, 2008-2009, Utah State University, March 2008
- 2nd in Master of Engineering (M.E.) Examination, Gujarat University, June 2004
- 1st in Bachelor of Engineering (B.E.) Examination (of 130 Students), Gujarat University, July 2003

- Awarded a Gold Medal and Certificate of Merit for Outstanding Academic Performance in Bachelor of Engineering (B.E.) Examination, Gujarat University, August 2003

RESEARCH EXPERIENCE:

Research Assistant at Utah State University August 2005-Current

- Consistent relative cost and performance comparison of seismic isolated and fixed-base building for various performance objectives.
- Evaluation of approaches to characterize seismic isolation systems for design
- Relative performance assessment of low-rise steel base-isolated and conventional moment resisting frame buildings for loss estimation
- Life cycle cost analysis of low-rise steel moment and braced frame buildings using PEER loss estimation techniques (Next Generation of Performance Based Design Methodology)

Research Assistant at Gujarat University August 2003-June 2005

- Comparative study of international codes for design of RC beam-column connections under seismic conditions
- Development of computer package to design RC beam-column connections using ACI-318, Eurocode-8, and IS-1893 Design Codes
- Response assessment and damage evaluation of a 10 story building against all kinds of loading (including earthquake and wind loadings)

TEACHING EXPERIENCE:

Teaching Assistant at Utah State University

- Structural Steel Design, Fall 2005
- Experimental Methods in Structural Engineering, Spring 2006
- Mechanics of Materials, Fall 2006

Teaching Assistant at Gujarat University

- Structural Analysis, Fall 2003
- Design of Reinforced Concrete Structures, Spring 2004

ACADEMIC PROJECTS

- A Design of RCC and Steel Bridges using AASHTO LRFD Bridge Design Specifications.
- A Design of 3 story Steel Frame Building by LRFD Method Using AISC Manual (13th edition).
- A Design of Elementary School Building by NDS Manual (2005 edition).
- Loss Based Evaluation of Seismically Isolated and Fixed-base Buildings using Performance Assessment Calculation Tool (PACT).

RELEVANT COURSEWORK:

Dynamics of Structures and Earthquake Engineering, Nonlinear Structural Analysis, Structural Steel Design, Bridge Engineering, Finite Element Analysis of Structures, Advanced Reinforced Concrete Structures, Experimental Methods in Structural Engineering, Computational Linear Algebra, Constitutive Modeling of Engineering Materials, Engineering Risk Assessment

TECHNICAL SKILLS:

Platform : Windows 95, 98, 2000, XP, Vista, UNIX

Engineering Tools : OpenSees, SAP, STAAD, @RISK, MATLAB, AutoCAD

Languages : C & C++, Visual Basic, VBA

Packages : MS Word, Excel, PowerPoint, LaTex

Code Provisions : AISC Manual for Steel Construction, ASCE 7-05, ACI 318-05, IBC 2006

PROFESSIONAL AFFILIATIONS:

- Member, American Society of Civil Engineers (ASCE)
- Member, Earthquake Engineering Research Institute (EERI)

ARCHIVAL JOURNAL PUBLICATIONS:

- **Sayani, P. J.** and Ryan, K. L. "Comparative Evaluation of Base Isolated and Fixed-Base Buildings using a Comprehensive Response Index", ASCE Journal of Structural Engineering, Vol. 135 (6), 698-707, June 2009.

- **Sayani, P. J.** and Ryan, K. L. "Evaluation of Approaches to Characterize Seismic Isolation Systems for Design", Journal of Earthquake Engineering, Vol.13 (6), 835-851, July 2009.

- **Sayani, P. J.,** Erduran, E., and Ryan, K. L. "Comparative Performance of Low-rise Base-Isolated and Conventional Steel Moment Resisting Frame Buildings for Loss Estimation", submitted to ASCE Journal of Structural Engineering

- **Sayani, P. J.** and Ryan, K. L., "Comparative Life cycle Performance Assessment of Low-rise Base-Isolated and Conventional Steel Moment Resisting Frame Buildings", in preparation

CONFERENCE PROCEEDINGS:

- **Sayani, P. J.** and Ryan, K. L., "Evaluating Performance in Seismic Isolated Buildings using Performance Indexes", Proceedings, Structures Congress, 18th Analysis and Computation Specialty Conference, Vancouver, BC, 2008.

- Ryan, K. L., Morgan, T. A., and **Sayani, P.**, "Consistent Performance Comparison of Seismic-Isolated and Fixed-Base Buildings." Proceedings, 8th U.S. National Conf. of Earth-quake Engineering, Paper No. 1617, San Francisco, CA, 2006.